UNIVERSITY OF CALIFORNIA,

IRVINE

Mechanisms and Treatments for Reperfusion Injury of the Brain During Cardiac Arrest and Resuscitation

DISSERTATION

Submitted in partial satisfaction of the requirements for the degree of

DOCTOR OF PHILOSOPHY

in Biomedical Sciences

by

Sangwoo Han

Dissertation Committee:
Associate Professor Yama Akbari, Chair
Professor Bernard Choi
Professor John Weiss

2023

TABLE OF CONTENTS

List of Figures

Acknowledgements

I would like to thank firstly my wife, Anuradha, who has been with me since even before my MD-PhD journey and has continued to support me throughout. Doing a PhD, especially during the time of COVID was much more difficult than I imagined. It would have been an arduous task for me to have to undergo this whole process alone without her continuous emotional support and encouragement.

Secondly, I'd like to thank my family who've raised me to work hard and persist in all that I do. They've had my back and helped push me forward up to this point. I know they will continue to do so throughout the rest of my career.

Thirdly, I'd like to thank all my committee members: Drs. John Weiss, Bernard Choi, Robert Wilson, and Oswald Steward. This dissertation was very multidisciplinary, covering more topics than I had anticipated, from neuroanatomy, cellular and molecular mechanisms, systems physiology, biomedical engineering, and physics. Without their knowledge, guidance, and inspiration, this work would not have been possible.

Fourthly, I am very grateful to my mentor and advisor, Dr. Yama Akbari. Although initially I was more interested in mechanisms underlying memory and cognition, the Akbari lab has broadened my mind to the neuro ICU and especially ischemia-reperfusion injury which I find fascinating. As a truly multidisciplinary lab, I've learned more than I thought I would starting my PhD, sometimes as a necessity and sometimes out of desire to learn more. There were certainly ups and downs, happy and hard times, but at the end of it all, I am more prepared for the world of research because of it.

Lastly, I want to give a thank you to our lab members: Afsheen Bazrafkan, Dr. Masih Rafi, Alex Liu, Justin Yi, as well as the undergraduate students who helped with all the experiments. I learned lots about animal surgery from Afsheen and Masih, histology from Alex, and data analysis from Justin. The experiments were very complex requiring assistance from generally multiple people. These experiments wouldn't have been possible without everyone's combined efforts.

I would like to thank my funding sources including Arnold and Mabel Beckman Foundation, the Roneet Carmell Memorial Endowment Fund (Dr. Akbari), the US National Institutes of Health (P41EB015890), Stanley Behrens Fellowship Award (Sangwoo Han), the National Center for Research Resources and National Center for Advancing Translational Sciences, NIH, through these grants: TL1TR001415-01 (Dr. Wilson), R21 EB024793 (Dr. Akbari), and a ICTS/CTSA Pilot Grant (Dr. Akbari) via UL1 TR001414 .

Chapter 2 of this dissertation is a reprint from a manuscript titled 'Cortical anoxic spreading depolarization during cardiac arrest is associated with remote effects on peripheral blood pressure and post-resuscitation neurological outcome' published in Neurocritical Care with permission from Springer Link, and was in collaboration with Mayra Contreras, Afsheen Bazrafkan, Masih Rafi, Shirin Dara, Ani Orujyan, Anais Panossian, Christian Crouzet C, Beth Lopour, Bernard Choi, Robert Wilson and Yama Akbari.

VITA

Sangwoo Han

EDUCATION

University of California, Irvine, School of Medicine M.D., Medicine	Expected May 2025 Irvine, CA
University of California, Irvine, School of Medicine Ph.D. in Biomedical Sciences, Department of Neurobiology and Anatomy	Aug. 2019-May 2023 Irvine, CA
The University of Iowa B.S. Human Physiology with Distinction B.S. Biology (Neurobiology Track) with Distinction	May 2016 Iowa City, IA

RESEARCH

Graduate Student in Akbari Lab Department of Anatomy and Neurobiology	Oct. 2019-May 2023 Irvine, CA
Narayanan Lab Student Research Assistant Department of Neurology, The University of Iowa Hospitals and Clinics	Apr. 2014-Jul. 2017 Iowa City, IA
Honor's Thesis Department of Human Physiology, The University of Iowa	Aug. 2014-May 2015 Iowa City, IA
Recober Lab Student Research Assistant Department of Neurology, The University of Iowa Hospitals and Clinics	May. 2013-Jun. 2014 Iowa City, IA

TEACHING EXPERIENCE

TA for Bio93 University of California, Irvine School of Medicine	Aug. 2020-Dec. 2020 Irvine, CA
Mentor for GATI BEAM Summer Program University of California, Irvine School of Medicine	Jul. 2020-Jul. 2020 Irvine, CA
Physiology Tutor for 1st year medical students University of California, Irvine School of Medicine	Aug. 2018-Aug. 2019 Irvine, CA

HONORS AND AWARDS

Stanley Behrens Fellowship in Medicine	Aug. 2022-May 2023
CLAS Undergraduate Scholarship Fund ($2,000)	Aug. 2015-May 2016
Old Gold Scholarship ($12,000)	Aug. 2012-May 2016
Iowa Center for Research by Undergraduates Fellowship ($2,500)	May 2015-Aug. 2015
Margaret Foster Hoff Memorial Scholarship ($3,000)	Aug. 2014-May 2015
Iowa Scholars Scholarship ($1,000)	Aug. 2012
National Honors Society	Aug. 2010-May 2012

PUBLICATIONS

1. **Han SW**, Contreras MI, Bazrafkan A, Rafi M, Dara SM, Orujyan A, Panossian A, Crouzet C, Lopour B, Choi B, Wilson RH*, Akbari Y*. 2022. Cortical anoxic spreading depolarization during

cardiac arrest is associated with remote effects on peripheral blood pressure and post-resuscitation neurological outcome. Neurocrit Care. 37:139-154.

2. **Han SW**, Yi J, Bazrafkan A, Rafi M, Liu A, Puppali V, Singh A, Yoo J, Zandihaghighi S, Nath A, Pham J, Wilson RH*, Akbari Y*. 2023. Blocking hyperemia with esmolol following resuscitation from cardiac arrest improves neurological outcome. *Manuscript in preparation*.
3. Han SW, Yi J, Bazrafkan A, Rafi M, Liu A, Naousri F, Suayngam K, Avilez A, McCluskey K, Vu M, Wilson RH*, Akbari Y*. 2023. Hyperemia following resuscitation from cardiac arrest may be a major contributor to the burst of ROS during reperfusion. *Manuscript in preparation*.
4. Yi J, Tian G, Han SW, Aguirre F, Bazrafkan A, Azadian M, Desai M, Wais T, Khan AA, Suri Y, Maki N, Steward O, Akbari Y. 2023. Activation of brain regions post-cardiac arrest coma and early recovery. *Manuscript in preparation*.
5. Justin D. Yi, Samuel Tincher, **Sangwoo Han**, Afsheen Bazrafkan, Yama Akbari, and Robert H. Wilson. 2023. Synaptic failure and partial restoration can be inferred from sudden 1/f slope changes in a rodent cardiac arrest model. *Manuscript in preparation*.
6. Heskje J, Heslin K, De Corte BJ, Walsh KP, Kim YC, **Han SW**, Carlson ES, Parker KL. 2020. Cerebellar D1DR-expressing neurons modulate the frontal cortex during timing tasks. Neurobiol Learn Mem. 170:107067.
7. **Han SW**, Kim YC, and Narayanan NS. 2017. Projection targets of medial frontal D1DR-expressing neurons. Neurosci Lett. 655:166-171.
8. Kim YC, Miller A, Lins CRFL, **Han SW**, Keiser M, Boudreau RL, Davidson BL, Narayanan NS. 2017. RNA-interference of human alpha-synuclein in mouse. Front Neurol. 8:13.
9. Kim YC, **Han SW**, Ruggiero R, Alberico S, Chen KH, and Narayanan NS. 2017. Optogenetic stimulation of frontal D1 neurons compensates for impaired temporal control of action in dopamine-depleted mice. Curr Biol. 27(1):39-47.
10. Han SS, Tompkins VS, Son DJ, **Han S**, Yun H, Kamberos NL, Dehoedt CL, Gu C, Holman C, Tricot G, Zhan F, Janz S. 2015. CDKN1A and FANCD2 are potential oncotargets in Burkitt lymphoma and multiple myeloma. Exp Hematol Oncol. 4:9
11. Han SS, **Han S,** Kamberos NL. 2014. Piperlongumine inhibits the proliferation and survival of B-cell acute lymphoblastic leukemia cell lines irrespective of glucocorticoid resistance. Biochem Biophys Res Commun. 452(3):669 -75

POSTERS/ABSTRACTSs

i. **Han S,** Kim Y, Narayanan N**.** (2016) Neural Circuitry of D1 Receptor Neurons in the PFC. *Iowa Center for Research by Undergraduates.*
ii. **Han S**, Wilson RH, Crouzet C, Bazrafkan A, Maki N, Rafi M, Choi B, Akbari Y. (2020) Cerebral blood flow, oxygenation, and metabolism immediately prior to cardiac arrest can predict neurological recovery after resuscitation. *Neurocritical Care Society Conference*
iii. **Han S,** Bazrafkan, Wilson R, Akbari Y. (2020) Rate of Physiologic Shutdown During Ischemia May Modulate Neuroprotection and Recovery. Anatomy and Neurobiology Department Seminar.
iv. **Han S,** Bazrafkan, Wilson R, Akbari Y. (2021) Reperfusion Targets Immediately After CPR for Improved Recovery Following Different Etiologies of Cardiac Arrest. Annual Lake Arrowhead MSTP Conference.
v. **Han S,** Bazrafkan A, Rafi M, Maki N, Dara S, Avilez A, Nath A, Yun H, McCluskey K, Baghbaninogourani R, Agrawal S, Wilson R, Akbari Y. (2021) Different cardiac arrest etiologies lead to differences in peripheral perfusion and neurological outcome post-resuscitation. *Neurocritical Care Society Conference*
vi. Yi J, Tincher S, **Han S**, Bazrafkan A, Rafi M, Dara S, Panossian A, Avilez A, Nath A, Yun H, McCluskey K, Akbari Y, Wilson R. (2021) EEG/ECoG metrics near-death during cardiac arrest

elucidate neurovascular coupling and correlate with neurological recovery post-resuscitation. *Neurocritical Care.*

vii. Khachatryan T, Rafi M, Chaudhari A, Aini A, Dara S, Irani T, **Han S**, Wei K, Keys M, Hsu F, Golshani K, chen J, Suzuki S, Yuki I, Warren R, Ueda Y, Wilson R, Akbari Y. (2021) Continuous Non-Invasive Monitoring of Vasospasm in Subarachnoid Hemorrhage Using Next-Generation Optical Spectroscopy. *Society of Vascular and Interventional Neurology.*

viii. **Han S**, Bazrafkan A, Rafi M, Maki N, Dara S, Liu A, Martin J, Akbari Y. (2022). Greater hyperemia immediately following resuscitation from cardiac arrest is associated with worse neurological outcome. *Society for Neuroscience*. *Distinguished Poster Award

ix. Yi J, Do-Tran K, Weiss-Hung E, Tincher S, Wang S, Sandhu R, Gorham M, Luong D, Baghbaninogourani R, Ramachandran G, Mogul A, Bazrafkan A, **Han S**, Dara S, Rafi M, Wilson R, Akbari Y. (2022). Cardiac arrhythmias coincide with anoxic spreading depolarization and predict altered cerebral perfusion and worse cardiac arrest outcomes in a rodent model. *iCSD COSBID Conference.*

x. Rafi M, Khachatryan T, **Han S**, Do-Tran K, Dara S, Chaychian A, Chavarria Y, Chaudhari A, Wong S, Aini A, Irani T, Wei K, Keys M, Yoshimoto K, Wada H, Ohmae E, Hsu F, Golshani K, Chen J, Suzuki S, Yuki I, Groysman L, Stern-Nezer S, Warren R, Ueda U, Wilson R, Choi B, Akbari Y. (2022), Time-resolved spectroscopy as a continuous, noninvasive method to monitor vasospasm in aneurysmal subarachnoid hemorrhage in the ICU and during endovascular treatment. *Neurocritical Care Society Conference.*

Abstract of the Dissertation

Mechanisms and Treatments for Reperfusion Injury during Cardiac Arrest and Resuscitation

By

Sangwoo Han

Doctor of Philosophy in Biomedical Sciences

University of California, Irvine, 2023

Associate Professor Yama Akbari, Chair

Cardiac arrest is a major public health concern affecting over half a million people per year in the US. Furthermore, many survivors have brain injury that worsen their quality of life and increases mortality in the long term. However, medical advances have failed to develop good treatments to improve outcome and survival rates in the recent decades. The pathophysiology of cardiac arrest is very complex, involving multi-system processes, that makes it difficult to find a single simple treatment. In this dissertation, we split the process of cardiac arrest and resuscitation into two parts to better understand the pathophysiological process of cardiac arrest and recovery: Induction of cardiac arrest and reperfusion.

Chapter 2 describes the role of spreading depolarizations in the induction of cardiac arrest. Cardiac arrest induces global ischemia that produces cortical spreading depolarizations SD, self-propagating waves of neuronal and glial depolarizations, that is traditionally thought to be harmful and worsens ischemic injury. While asphyxia-induced cardiac arrest leading to a severe drop in blood pressure may affect cerebral hemodynamics and is widely known to cause anoxic SD, the effect of anoxic SD on peripheral blood pressure in the extremities has not been investigated. This relationship is especially important to understand for conditions such as circulatory shock and cardiac arrest that directly affect both peripheral and cerebral perfusion in

addition to producing anoxic SD in the brain. In this study, we used a rat model of asphyxial cardiac arrest to investigate the role of anoxic SD on cerebral hemodynamics and metabolism, peripheral blood pressure, and the relationship between these variables in 8-12 weeks old male rats. We incorporated a multimodal monitoring platform measuring cortical DC current simultaneously with optical imaging. We found that during anoxic SD there is decoupling of peripheral BP from cerebral blood flow and metabolism. We also observed that anoxic SD may modify cerebrovascular resistance. Furthermore, shorter time difference between anoxic SDs measured at different locations in the same rat was associated with better neurological outcome based on the recovery of electrocorticography activity (bursting) immediately post-resuscitation and neurological deficit scale 24 hours post-resuscitation. To our knowledge, this is the first study to quantify the relationship between peripheral blood pressure, cerebral hemodynamics and metabolism, and neurological outcome in anoxic SD. These results indicate that the characteristics of SD may not be limited to cerebral hemodynamics and metabolism but rather may also encompass changes in peripheral blood flow, possibly through a brain-heart connection, providing new insights into the role of anoxic SD in global ischemia and recovery.

Chapter 3 describes the role of hyperemia in reperfusion injury post-CA. After resuscitation from cardiac arrest, patients often suffer from secondary injury of post-cardiac arrest syndrome, caused by the ischemic and reperfusion injury. Post cardiac arrest care focuses on minimizing this secondary injury, which has increasingly been shown to be a critical determinant of neurological outcome. In the first 30 min post resuscitation from cardiac arrest (CA), there is a brief hyperemia phase where blood pressure rises significantly, followed by a prolonged hypoperfusion phase in which blood pressure remains below baseline levels. Most of these studies focused on a broad time range in the span of hours post cardiac arrest and mainly treated the hypoperfusion phase. Because of this, the only current American Heart Association guideline for blood pressure is to simply treat hypotension, but states that there is no evidence

for an optimal blood pressure target. However, the very dynamic hyperemia phase that occurs during the first 30 min post resuscitation has been neglected. It may be that hyperemia contributes to reperfusion injury, worsening neurological outcome. In this study, we analyzed the role of hyperemia in eventual neurological recovery using two different rodent models of cardiac arrest to investigate the role of hyperemia post-CA and the effects of using a cardioselective beta blocker to blunt hyperemia on neurological outcome. Overall, we found that a high hyperemia was associated with worse outcome which could be improved by blocking hyperemia with a cardio-selective beta blocker. In addition, we found that esmolol may be protective of vessels and maintain a certain level of cerebral autoregulation.

In Chapter 4, we followed up on possible mechanisms of hyperemia related reperfusion injury. As we saw injury could be reduced by blunting hyperemia, we specifically investigated the role of the concentration of oxygen inspired during hyperemia and how it may contribute to an increase in reactive oxygen species. Reactive oxygen species is a known contributor of reperfusion injury and so we tested the effects of 100% oxygen vs room air concentration of oxygen inspired during hyperemia and saw that reducing the inspired oxygen levels during hyperemia reduced oxidative injury and improved outcome. All of these studies provides support towards the injurious of role of hyperemia in reperfusion injury and warrants further investigation of hyperemia as a therapeutic target for improving recovery post-CA.

Chapter 1

Introduction

I. Significance and Background

Cardiac arrest is when the heart stops beating and blood flow to the body ceases. Cardiac arrest can occur from external causes (drowning, trauma, asphyxia, or drug overdose) or medical causes (arrhythmia, heart failure, coronary artery disease)[1]. Roughly every 40 seconds, an American will suffer from a cardiac arrest[1], and more than 800,000 people/year suffer from cardiac arrest (CA) in the US[2] and are treated with cardiopulmonary resuscitation (CPR). But in-hospital survival is only around ~15% and out-of-hospital survival is even lower[3], making CA a large burden to society and a public health concern. However, injury from CA does not stop after successful resuscitation and many survivors suffer secondary complications which reduce quality of life and increase mortality for survivors. Despite 40 years of advancements in medicine and care, survival for CA patients have not improved[4]. One of the large contributing factors is the debilitating long-term neurological impairments[5]. Neurological recovery is a major determinant of outcome for CA survivors[6], however, therapeutic temperature management, the only current treatment for neurological recovery after CA, has been recently called into question[7]. Therefore, there are no reliable treatments targeting neurological recovery after CA, a continuing unmet clinical need.

II. Different etiologies of cardiac arrest

The chance of successful resuscitation in patients with cardiac arrest is highly associated with the etiology of cardiac arrest[8]. Cardiac arrest patients with shockable rhythm (ventricular fibrillation or

ventricular tachycardia) have better survival than those without it[8,9], such as asystole or pulseless electrical activity, which can occur from respiratory illness, drug overdose, drowning, etc. Ventricular fibrillation is an arrhythmia, or irregular beating of the heart, that causes the heart to fail to pump blood properly. Asystole is the absence of heart movements and no detectable pulse or electrical activity of the heart, while pulseless electrical activity (PEA) is the lack of heart movements, no detectable pulse, but presence of electrical activity in the heart. For shockable CAs, an automatic electronic defibrillator (AED) can be used to shock the heart into proper rhythm. In the non-shockable rhythm CAs, an AED cannot be used to help jumpstart the heart. However, the trend is moving towards there being less shockable rhythm CAs and more asystole or pulseless electrical activity CAs[9], with these two accounting for more than 70% of in-hospital CAs[10]. As the ratio of these CAs with poor survival increases, it is becoming more important to not understand how differences in asystole and PEA CAs affect outcome[11].

III. Anoxic Spreading Depolarization

Cortical spreading depolarizations (SDs) are self-propagating waves of transient or persistent[12] loss of neuronal transmembrane ion gradients leading to neuronal and glial depolarizations[13]. SD is an extremely energy-demanding process[13] and causes neurovascular decoupling[13–15]. SDs can occur during ischemia, such as in stroke[16]. In such cases, SDs are thought to worsen ischemic injury by diverting blood flow and worsening ischemia[17]. It can also worsen inflammation [18], uncouple blood flow response[19], and cause vasoconstriction leading to prolonged hypoxemia[20]. Experimentally, in healthy tissue, vessels respond to SD to produce transient hyperperfusion, but severe hypoperfusion (spreading ischemia) in tissue at risk for progressive injury, which contributes to ischemic lesions growing larger[21]. Interestingly, despite SDs being associated with many deleterious effects, there are still studies that show beneficial effects of SD. One study showed that SD increased neurogenesis[22]. However, anoxic SD, a

type of SD caused by anoxia or asphyxia is a little different than traditional SDs as these do not have single foci. In addition, the SD is persistent until return of blood flow or oxygen, after which repolarization occurs[12]. Anoxic SD is also seen in global ischemia produced by cardiac arrest and has been recently found by our lab to be related to outcome[23]. Specifically, in that study, an earlier anoxic SD during cardiac arrest was correlated with better outcome post resuscitation[23,24]. Therefore, anoxic SD may be of widespread clinical importance and interest.

Anoxic SD's effect on cerebral hemodynamics has been studied, but its effects on peripheral hemodynamics are poorly understood. The potential effects of anoxic SD on both peripheral and cerebral hemodynamics has garnered more interest as recent studies have shown that the vagus nerve, which controls cardiac activity, can also modulate SD[25–28]. This brain-heart coupling via the vagus nerve raises the possibility that anoxic SD may be able to affect the heart through the vagus nerve.

IV. Reperfusion Injury in Cardiac Arrest and Ischemic Injuries

It has become increasingly known that secondary brain injury that occurs from ischemic and reperfusion injury is a critical determinant of neurological outcome following successful return of spontaneous circulation (ROSC) after cardiac arrest[29]. Many studies have investigated targeting blood pressure during periods post-ROSC[30–34], but there have been overall contradictory results, and the American Heart Association (AHA) has stated that there is insufficient evidence to determine an optimal blood pressure target in post resuscitative care, besides treating hypotension[35]. So far, the only treatment recommended post-CA, therapeutic temperature management, has been called into question very recently for its effectiveness[7]. Thus, there is a strong need for post-ROSC treatments targeting neurological recovery.

In the moments following ROSC, reperfusion occurs in two phases: there is a brief hyperemia phase where blood pressure spikes and is very high[36], followed by a prolonged hypoperfusion phase, where the blood pressure decreases below baseline levels[37]. Due to hypoperfusion, there may be a lack of blood supply to the brain and resulting in a mismatch of supply vs metabolic demand, leading to further injury. This has sparked much investigation in treating the hypoperfusion state post-ROSC by raising the blood pressure[30–34]. In fact, a rat CA study that used norepinephrine to raise CBF during hypoperfusion to baseline levels showed reduced hippocampus apoptosis[34].

However, the brief period of hyperemia prior to hypoperfusion has been left largely unexplored. In rats, the hyperemia phase occurs in the few minutes post-resuscitation and can last 10-20 min with systolic pressure rising into the 200s and mean arterial pressure (MAP) into the high 100s[38]. This hyperemia phase may be a critical contributor to reperfusion injury. Reperfusion injury[39,40] is a broad category that refers to potentially avoidable injuries where cells that may be viable end up dying from causes other than the initial ischemia[41]. Blood brain barrier disruption, edema, mitochondrial injury[41,42], and ROS production[43,44], among several other disruptions in homeostasis may contribute to the overall reperfusion injury. Additionally, a surge in perfusion during a state of low cellular activity in the brain may result in a flow-metabolism mismatch (supply and demand), exacerbating reperfusion injury.

With blood pressure reaching over 200 mmHg systolic, there is likely direct perfusion injury such as shear injury to the vessels and surrounding tissue. This suggests perhaps that blocking hyperemia may produce benefits to recovery. This could be achieved with blood pressure medications, such as the commonly used beta blockers. However, to target hyperemia without affecting unintended organs and the vasculature, a cardio-selective beta blocker such as esmolol is the better choice. Furthermore, esmolol has a short half-life of 9 minutes, allowing better control of the drug’s effects and not worsening the hypoperfusion that occurs after

hyperemia. Few studies have investigated the effects of esmolol in ischemia-reperfusion injury. These studies found that the small dose of esmolol improved outcome after ischemia-reperfusion[45–49] and one study even found that giving a small bolus of esmolol during CPR with epinephrine protected the endothelium of microvasculature of the brain[50,51]. However, these studies were not specific to hyperemia and mainly investigated how a small dose of a beta blocker may improve outcome after ischemia. The studies either gave too low of a dose in bolus or infusion to produce meaningful changes in blood pressure, pre-treated before injury, or infused for a time period much longer than hyperemia.

In addition to hyperemia, there are many other known contributors to reperfusion injury such as reactive oxygen species (ROS)[40,52–54], zinc[55–60], excitotoxicity[61–63], inflammation[64–68], etc. It is possible that hyperemia leads to increased circulation of these harmful substances, worsening reperfusion injury. The increased production of reactive oxygen species (ROS) leading to greater oxidative and overall injury in ischemia-reperfusion injury is well documented. Furthermore, in-vitro[44] and swine models[43] have shown a burst in ROS production within 30 min of reperfusion after ischemia. This timing coincides with hyperemia and may suggest that hyperemia may contribute to increased ROS production through increasing oxygen circulation. This is relevant to humans as after cardiac arrest, the current standard of treatment is hyperoxia on 100% oxygen, which may further increase oxygen circulation and worsen ROS mediated injury during reperfusion. Although there is still an ongoing debate regarding normoxia vs hyperoxia following resuscitation from cardiac arrest in human patients, dogs studies have shown a marked reduction in ROS as well as improved neurological outcome with normoxic ventilation after cardiac arrest compared to hyperoxic ventilation[69–71]. However, similarly, these studies did not target hyperemia and grossly observed the effects of normoxia on post-CA outcome.

V. Current Treatments and Guidelines

Currently, the most recent AHA guidelines[72] for post-CA care is just route critical care support such as mechanical ventilation, intravenous vasopressors, and targeted temperature management, which has recently been called into question as mentioned earlier. The most recent AHA hemodynamic guidelines[35] cite insufficient evidence for a defined blood pressure target following CA, except to avoid hypotension. Despite contradictions regarding optimal blood pressure targets, the resulting consensus from the AHA is that treating hypotension and maintaining a mean arterial pressure (MAP) of at least 65 mmHg is associated with good neurological outcome[73]. However, there are no guidelines on the hyperemia phase.

>94% O_2 is still recommended by the American Heart Association for resuscitation and post-CA care in humans. Studies have suggested that hyperoxia following resuscitation after CA may lead to worse outcome [69–71,74–76] in animals, but there appears to be contradictory results in human patients[74,75,77,78]. In those animal studies, normoxic ventilation following resuscitation from CA led to improved neurological behavioral outcome, reduced ROS, and reduced neuronal death[70,71].

VI. Current Multimodal Monitoring Methods

Currently, hemodynamic status is typically monitored through the femoral artery. However, these measurements occur distant from the brain, and are often not informative of cerebral hemodynamic processes[79]. Methods for direct measurement of cerebral blood flow (CBF) or oxygen consumption in the brain are typically invasive[80] and generally cannot be used at the same time. Non-invasive CBF measurement can be achieved[81,82] but do not have the temporal resolution required to monitor rapid changes in CBF and metabolism as occurs during an ongoing hyperacute stroke or CA. However, we use our custom built platform, capable of surpassing those limitations, that includes high-speed multispectral spatial frequency domain imaging (SFDI)[83], laser speckle imaging (LSI)[79], and electrocorticography (ECoG), to monitor

CBF, brain oxygenation, cerebral metabolic rate of oxygen ($CMRO_2$), and cerebral electrical activity. This is in addition to femoral vessel cannulation, enabling us to get blood pressure and heart rate. The ratio between CBF and $CMRO_2$ quantifies the degree of mismatch between cerebral perfusion and metabolism and serves as a metric of neurovascular-coupling. The high temporal resolution of our device (~60 Hz for LSI, ~20 Hz for SFDI) enables observation of rapid changes in cerebral perfusion and metabolism during the dynamic periods of CA and immediately post-resuscitation. Additional innovative features of our platform include our ability to measure CBF and CMRO2 in physiological units (e.g., mm^2/s for CBF; uM oxygen consumed per minute for CMRO2). These are not changes relative to baseline, so allowing us to look at any time points during ischemia and reperfusion independently without needing to normalize to the data to a baseline state. This is critical as CA patients in out-of-hospital settings do not have baseline recordings.

Chapter 2

Cortical anoxic spreading depolarization during cardiac arrest is associated with remote effects on peripheral blood pressure and post-resuscitation neurological outcome

Authors: Han SW, Contreras MI, Bazrafkan A, Rafi M, Dara SM, Orujyan A, Panossian A, Crouzet C, Lopour B, Choi B, Wilson RH, Akbari Y*

* Corresponding author

Introduction:

Cortical spreading depolarizations (SDs) are self-propagating waves of transient or persistent[12] loss of neuronal transmembrane ion gradients leading to neuronal and glial depolarizations[13]. SD is an extremely energy-demanding process and has been shown to double the cerebral metabolic rate of O_2 consumption ($CMRO_2$)[13] and cause neurovascular decoupling[13–15]. SDs can occur during ischemia, in human pathological conditions such as stroke[16] and traumatic brain injury[84,85]. SDs in these conditions are believed to exacerbate injury by diverting blood flow and worsening ischemia[17]. Except at the ischemic core, the SDs produced in these conditions are transient, meaning repolarization occurs spontaneously[12]. In contrast, anoxic SD, a type of SD caused by anoxia or asphyxia, is persistent until return of blood flow or oxygen, after which repolarization may occur[12]. Anoxic SD is also seen in global ischemia produced by cardiac arrest and has been recently found by our lab to be related to outcome[23]. Specifically, in that study, an earlier anoxic SD during cardiac arrest was correlated with better outcome post resuscitation[23,24]. Therefore, anoxic SD may be of widespread clinical importance and interest.

While the effects of anoxic SD on cerebral hemodynamics has long been of interest, its effects on peripheral hemodynamics during brain injury are poorly understood. The potential effects of anoxic SD on both peripheral and cerebral hemodynamics has garnered more interest as recent studies have shown that the vagus nerve, which controls cardiac activity, can also modulate SD[25–28]. This brain-heart coupling via the vagus nerve raises the possibility that anoxic SD may be able to effect the heart through the vagus nerve. Currently, it is difficult in critical care settings to continuously monitor cerebral blood flow (CBF) and brain metabolism in parallel with peripheral perfusion, especially with the high temporal resolution required to quantify the dynamics of anoxic SD[23,79]. Furthermore, it is difficult to predict the timing of anoxic injury and begin invasive monitoring procedures in advance. Therefore, investigations using animal models are necessary. With our custom-built multimodal monitoring devices in our rodent model of cardiac arrest and resuscitation, we were able to continuously monitor DC electrocorticography, CBF, brain oxygenation, cerebral metabolic rate of oxygen ($CMRO_2$), and peripheral blood pressure, all simultaneously during anoxic SD.

Most studies investigate SD's effect on CBF[13,14,86,87] or $CMRO_2$[13,15], but almost no studies have compared the changes in CBF and peripheral blood pressure and their coupling during anoxic SD. To our knowledge, only one study has been conducted on the effects of anoxic SD during CA on peripheral hemodynamics and its coupling with cerebral hemodynamics[88]. This paper showed no changes in peripheral or cerebral hemodynamics during anoxic SD, but the time resolution they used for analysis was too low to capture rapid changes as they only used averaged signals at 7 selected time points over 3 minutes[88]. The most extensive investigations into SD in rodent models have been in non-pathological states[15,19,87,89,90], followed by conditions known to produce SD such as stroke, hemorrhage, and traumatic brain injury[17,85,88,91,92], rather than anoxic SD. Global ischemia, often caused by cardiac arrest, has been shown to produce

anoxic SD, but few studies have investigated SD in this setting or characterized its effects on cerebral and peripheral hemodynamics[23,79,88]. Thus, the effects of anoxic SD on peripheral hemodynamics are not well understood. Interestingly, in a prior study, we found that another measure of cortical activity during near-electrocerebral silence of impending cardiac arrest, namely phase coherence as measured by electrocorticography, coincided with a transient rise in peripheral blood pressure, suggesting neurovascular coupling during cardiac arrest[93]. However, it is unclear if anoxic SD, which occurs well after such phase coherence in our cardiac arrest model, shares such changes in peripheral hemodynamics. It is important to investigate what hemodynamic effects anoxic SD produces in a state of global ischemia and the ramifications of these effects so that we can better understand what is happening clinically in human patients with similar conditions. In this pilot study, we aimed to investigate the effects of anoxic SD on peripheral and cerebral hemodynamics and outcome. In particular, we found in our cardiac arrest model of global ischemia, blood flow to the brain shuts down, leading to anoxic SD throughout the brain. We observed that anoxic SD onset occurred at different times at different electrodes. Based on this observation as well as previous literature[94], we hypothesized that our observed anoxic SD is multifocal and the time delay between the anoxic SD onsets at different foci may be a signature of a broad connectivity-related metric while the brain shuts down during anoxia. We measured the time delay between anoxic SD onsets at two different electrodes, which we termed the "ΔSD1-2 period" to represent asynchronous depolarizations of different brain regions. We saw fluctuations in peripheral (femoral) blood pressure and CBF during this period. Based on our recent studies showing that post-cardiac arrest outcome is related to coupling of the neurovascular unit as well as dissociation between features of the peripheral blood pressure and CBF[41,43], we hypothesized that peripheral perfusion and CBF change during the ΔSD1-2 period may also affect outcome. We found that a shorter ΔSD1-2 period and a faster drop in peripheral perfusion during this period may be associated with better neurological outcome. This suggests that the consequences of anoxic SD

stretch further than just within the brain and may impact the overall pathological process and even potentially recovery in conditions such as cardiac arrest.

Methods:

In this study, we analyzed a naturally occurring anoxic SD during asphyxial cardiac arrest using Ag/AgCl DC electrodes, optical imaging, and femoral artery cannulation for peripheral blood pressure monitoring at a high temporal resolution. For optical imaging, we used laser speckle imaging to monitor CBF and multispectral spatial frequency domain imaging to monitor $CMRO_2$. For the purpose of simplicity in the methods and results, where only anoxic SD is mentioned, we will refer to anoxic SD as just SD.

Preclinical Rodent Model of Asphyxial Cardiac Arrest: Surgical Preparation

The animal model of asphyxial cardiac arrest and resuscitation used in this study has been described previously[23,83,95,96] [23,83,95,96] by our lab and is summarized in **Fig. 1**. Briefly, male Wistar rats (Charles River, Canada facility) of 8-12 weeks of age, weighing 300-400g were handled daily for at least 1 week prior to any experimentation. The night prior to cardiac arrest experiments, rats were calorically restricted (75% restriction) with 3 food pellets, as is standard with our model[95]. The next morning, rats were endotracheally intubated and received femoral artery and vein cannulation to enable arterial blood pressure monitoring and venous drug delivery, respectively. Temperature of the animals were maintained at 37 degrees Celsius using a temperature probe and heating pad.

Preclinical Rodent Model of Asphyxial Cardiac Arrest: Cardiac Arrest

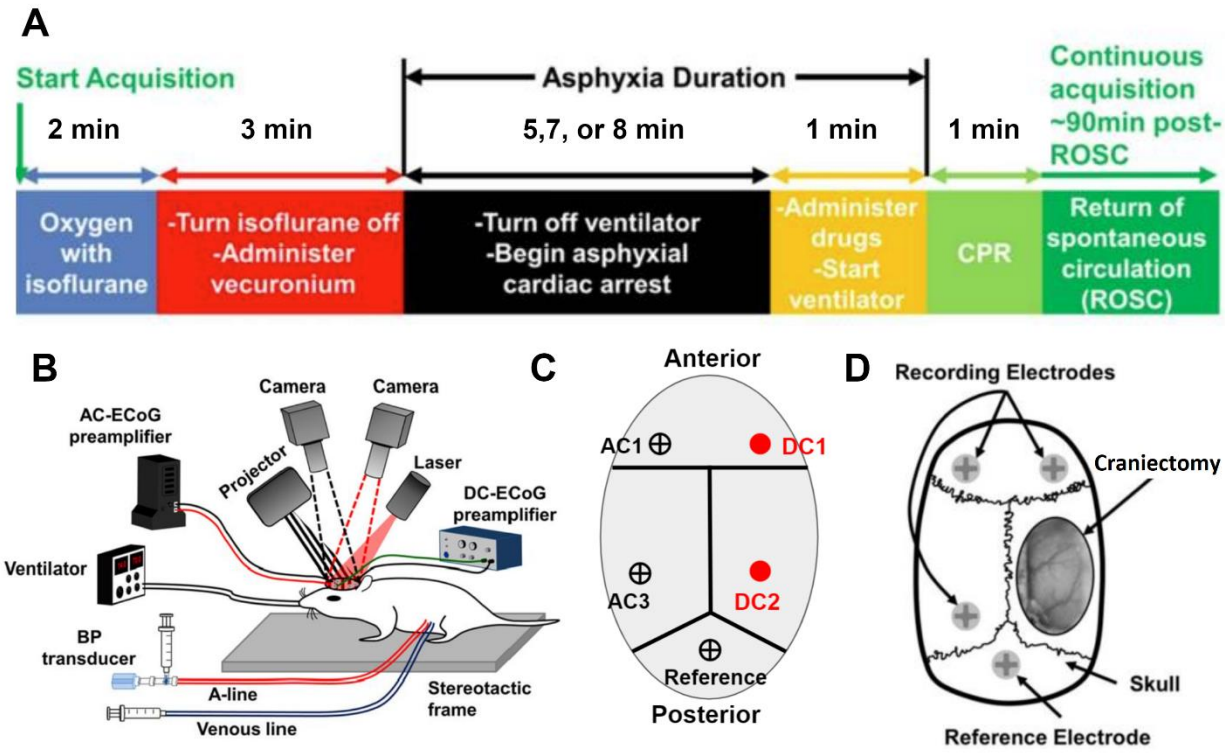

Fig 1. Experimental timeline and set up: **A)** Timeline of the asphyxial cardiac arrest experiment. **B)** Schematic of our multimodal monitoring platform during the experiment. **C)** Location of the AC and DC electrodes for Cohort 1. **D)** Location of the AC electrodes and craniectomy window for Cohort 2. [Reprinted/Adapted] with permission from [ref #15] © The Optical Society.

Before the experiment (**Fig. 1A**), the rats were on 50% O_2, 50% N_2; this was subsequently switched to 100% O_2 at the beginning of the experiment. Anesthetic (isoflurane) was washed out over a 3 min period, and a paralytic agent (vecuronium) was given. Following the washout period, cardiac arrest was induced by turning off the ventilator for 8 min. Subsequently, CPR was initiated by turning the ventilator back on with 100% O_2, giving epinephrine and sodium bicarbonate, and performing manual chest compressions. Chest compressions were continued until the return of spontaneous circulation, after which the rats were monitored continuously for an additional 2-4 hr. When the rat was able to breathe on its own, it was taken off the ventilator and breathed room air.

Preclinical Rodent Model of Asphyxial Cardiac Arrest: Post-Resuscitation Assessment

Staff assessing neurological outcome were blinded to the experimental groups. Neurological Deficit Scale, a behavioral test, was used to score neurological function at 24 hr post-resuscitation with a higher score representing better neurological function[97–99]. Burst suppression ratio, a quantification of suppression of AC-ECoG activity, was also used as an outcome measure at 40-60 min post-resuscitation, when the rat was neurologically recovering. Burst suppression ratio decreases as the rat regains consciousness. Time to burst is the time to resumption of electrical activity of the brain as measured by the first burst of activity in AC-ECoG signal and was used as another marker of neurological recovery.

Experimental Groups

In this study, two separate cohorts of rats, each with different multimodal monitoring techniques, were used **(Fig. 1B)**. Animals were randomized into these two cohorts. In Cohort 1 **(Fig. 1C)**, 14 rats underwent surgery to implant 3 screw electrodes for AC-ECoG recordings and 2 DC Ag/AgCl for DC-ECoG recordings 1 week prior to the asphyxial cardiac arrest experiment. All rats in this cohort underwent an 8 min asphyxial cardiac arrest. The Ag/AgCl electrodes were made by chloridizing silver wires (Stoelting 50880) in household bleach. The Ag/AgCl electrodes with diameter of 0.01 in were implanted 1 mm into the cortex in the right frontal hemisphere, and another one implanted in the right parietal cortex. Implanting and recording at the level of the cortex has better signal-to-noise ratio, higher spatial and temporal resolution, and is less prone to artifacts[100]. We did not find any histological signs of neurodegeneration in the implantation sites. The skin at the back of the neck for each rat was clamped onto with an alligator clip to serve as a reference for the DC electrodes. 10 rats in Cohort 2 **(Fig. 1D)** were monitored with optical imaging after performing a partial craniectomy over the right parietal lobe with the dura intact (not removed) on the day of the experiment. Rats in this cohort were monitored

continuously with AC-ECoG electrodes but did not have DC-ECoG monitoring. These animals were non-survival due to the craniectomy. DC electrodes were used to monitor SD in Cohort 1, and optical scattering changes were used to monitor SD in Cohort 2. For analysis of outcome in Cohort 1, 2 rats were excluded from analysis as statistical outliers because they had significantly higher post cardiac arrest blood glucose levels, which could have been due to additional surgical stress. However, these 2 rats were included in the analyses not pertaining to outcome, as only time periods before resuscitation were analyzed in those cases.

Data Acquisition and Post-Processing

Post-processing of arterial BP, AC-ECoG, DC-ECoG, and optical imaging data was performed using MATLAB (The MathWorks, Inc., Natick, MA). In this study, AC-ECoG data was primarily used for the analysis of ECoG burst onset and burst suppression ratio.

Burst Suppression Ratio

To calculate burst suppression ratio for each rat, the AC-ECoG signal was processed by down sampling by 6 to 254 Hz to reduce computational load, performing common average referencing for 2 AC-ECoG channels (AC1, AC3), notch 60 Hz filtering to remove electrical noise, and 1-150 Hz bandpass filtering. Afterwards, a threshold for the amplitude of the signal was calculated by taking the sum of the mean and standard deviation during a period of 20-30 min post-resuscitation. A burst suppression was calculated at an interval of at least 0.5s in which the amplitude of the AC-ECoG signal did not exceed the threshold. The ratio of the time in burst suppression was calculated over a period of 1 min with an overlapping window of 30s. This was calculated from 5 min prior to the onset of asphyxia to 100 min after. For this study, we used an

average of the burst suppression ratio during 40-60 min period after onset of asphyxia as one of the markers for neurological outcome.

Time to Burst (TTB)

Time to Burst was obtained by visually observing the first burst of AC-ECoG activity on our live stream of the AC-ECoG signal post-resuscitation and is another marker of recovery in animals waking from coma after cardiac arrest. This was double checked by plotting the AC-ECoG signal with MATLAB and confirming the first burst of activity.

Arterial BP and Arterial Blood Gas (ABG)

For both cohorts, BP was measured continuously at 191 Hz from an arterial line. Mean arterial pressure (MAP) was calculated using the formula MAP= (systolic blood pressure + 2*diastolic blood pressure)/3.

DC-ECoG

In Cohort 1, DC-ECoG data was acquired at 305 Hz with Duo 773 and Model 750 electrometers (World Precision Instruments, Saratosa, FL) with two DC leads, DC1 and DC2. A 1-Hz LP filter was used on the DC-ECoG signal post-acquisition to remove noise and identify SD. DC1 (located in right frontal cortex) and DC2 (located in right parietal cortex) both produced SD at different times, shown as DC potential shifts. SD was detected with DC electrodes by observing a DC potential shift and visually identifying the negative deflection in DC-ECoG to mark the SD onset.

Optical Imaging

Throughout the experiments, rats in Cohort 2 were monitored with two diffuse optical imaging technologies: Laser Speckle Imaging and multispectral Spatial Frequency Domain Imaging.

Laser Speckle Imaging measures blood flow, as previously established in both preclinical and clinical studies[101–103], including investigations into cardiac arrest[83,101,104]. Spatial frequency domain imaging[105,106] measures the tissue absorption coefficient (related to hemoglobin concentration and oxygenation[83,105,107]) and scattering coefficient (related to morphology and distribution of cells and organelles[108]). Tissue scattering has been shown to change during SD, likely due to cytotoxic edema[107]. The combination of Laser Speckle Imaging and Spatial Frequency Domain Imaging data can be used to calculate cerebral metabolic rate of oxygen ($CMRO_2$)[109]. In this study, Laser Speckle Imaging data were acquired with a frame rate of 60 Hz and Spatial Frequency Domain Imaging data were acquired with a frame rate of 14 Hz. However, to reduce computational load, we reduced the sampling rate to ~17 data points per min for SFDI and ~39 data points per min LSI, which was enough to capture the dynamic changes during SD.

Data Analysis

Laser Speckle Imaging Data: Relative cerebral blood flow

The Laser Speckle Imaging data was used to compute Speckle Flow Index, a measure of CBF, over a fixed spatial region of interest spanning the majority of the imaging window. Relative cerebral blood flow (rCBF) was normalized to the mean CBF calculated over the 30 second interval immediately prior to the onset of asphyxia.

Spatial Frequency Domain Imaging Data: Tissue scattering and oxygenation

For Spatial Frequency Domain Imaging data analysis, custom MATLAB code[83] calculated a best fit of a computational (Monte Carlo) model of light-tissue interaction to the measured data. These model fits provided tissue oxy-hemoglobin concentration ($ctHbO_2$), deoxygenated hemoglobin (ctHb), and scattering maps. The $ctHbO_2$ and ctHb data were combined to calculate

tissue oxygenation (StO_2) via the formula $StO_2 = 100*ctHbO_2/(ctHbO_2+ctHb)$. Time-resolved $ctHbO_2$, ctHb, StO_2, and tissue scattering curves were formulated by averaging the optical property maps over a fixed spatial region of interest.

Laser Speckle Imaging + Spatial Frequency Domain Imaging Data: $CMRO_2$

Time-resolved $CMRO_2$ was calculated using the formalism developed by Boas and Dunn[108,110], combining CBF data from Laser Speckle Imaging with $ctHbO_2$ and ctHb data from Spatial Frequency Domain Imaging. For the calculation of $CMRO_2$, the CBF data were analyzed using an ROI covering the majority of the imaging window (to represent overall perfusion into the brain), while ctHbO2 and ctHb data were analyzed using an ROI over a prominent vein (to more accurately probe the amount of oxygen consumed by the tissue).

Cerebrovascular Resistance (CVR) data

CVR is the ratio of cerebral perfusion pressure to cerebral blood flow. The relative CVR versus time [rCVR(t)] was defined as rCVR(t)=rMAP(t)/rCBF(t)[111–114], where rMAP and rCBF are values normalized to the mean over a 30s interval immediately before onset of asphyxia.

Multimodal Parameter Set

For each cohort, a multimodal set of parameters was extracted from the data around SD onset to analyze several associations. In Cohort 1, these parameters included: (i) time to DC-ECoG SD onset during asphyxial cardiac arrest for SD1 and SD2; (ii) average rate of change of MAP, systolic BP, diastolic BP, and heart rate 30s before and after SD onset at both DC leads, as well as in between the SD onsets in the two leads (ΔSD1-2 period).

In Cohort 2, the parameter set included quantities obtained from the optical measurements. In this cohort, SD onset was most reliably measured via spatial propagation of changes in tissue scattering. The parameters extracted from Cohort 2 included: (i) Scattering change onset during

asphyxial cardiac arrest (SD); (ii) percentage change in scattering during SD; (iii) AUC of scattering change during SD; (iv) Time to peak of CVR; (v) maximum relative increase in CVR compared to baseline; (vi) AUC and slope over the 30s before and after scattering change of MAP, systolic BP, diastolic BP, pulse pressure, and heart rate with the additional inclusion of CBF, $CMRO_2$, CBF/$CMRO_2$, and CVR; The ratio of CBF/ $CMRO_2$is a metric of cerebral flow-metabolism (supply and demand).[96,109]

Statistical Models and Tests

The personnel performing data analysis were not blinded to the experimental groups (cohort 1 and cohort 2). Statistical testing was performed with MATLAB. For each correlation analysis, Spearman correlations were performed when one of the parameters used was not normally distributed. When both parameters used for correlation were normally distributed, Pearson correlation was used. For each cohort, paired t-Tests were performed to compare between time points for AUC and slopes.

Results

Detection of anoxic SD during asphyxial Cardiac Arrest with DC electrodes

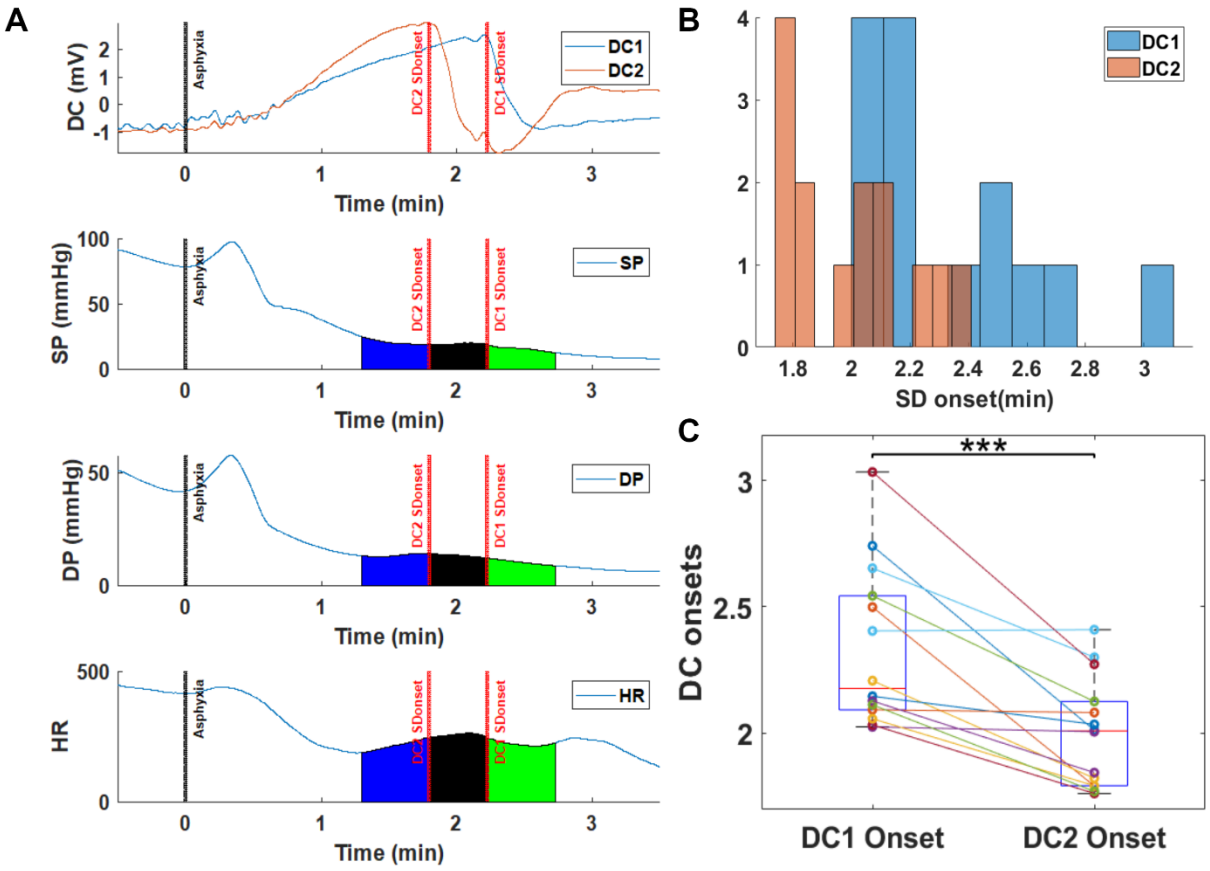

Fig 2. Detection of SD during asphyxial cardiac arrest with DC electrodes in Cohort 1. **A)** Example DC potential tracing for rat undergoing asphyxial cardiac arrest, showing DC1 and DC2 potential shifts, as well as the corresponding systolic (SP) and diastolic (DP) blood pressures and heart rate (HR) during this period. **B)** Distribution of SD onset times detected by DC1 and DC2 leads. SD occurs earlier in DC2 than DC1. **C)** Paired one tailed t-test showing DC1 SD onset is significantly later than DC2 SD onset (* is <0.05, ** is <0.01, *** is<0.001, **** is <0.0001)

In Cohort 1, using DC electrodes, detection of SD occurred between 1.7 and 3 minutes after the onset of asphyxia in our cardiac arrest model (Fig 2). For Cohort 1, DC channel 1 (DC1) and DC channel 2 (DC2) were used to separately detect SD onset (Fig 2) with DC2 detecting anoxic SD earlier than DC1. Due to this, SD detected first by DC2 will be referred to as SD1, while the SD

detected later by DC1 will be referred to as SD2. The SD was persistent until after successful resuscitation, at which point repolarization occurred. We refer to the period of delay in detection of anoxic SD between the two DC electrodes, located in different parts of the brain, as the "ΔSD1-2 period." In the first part of this study, we analyzed the peripheral hemodynamic changes that occurred during this period of depolarizations of the brain.

Diastolic BP drop accelerates during ΔSD1-2 period

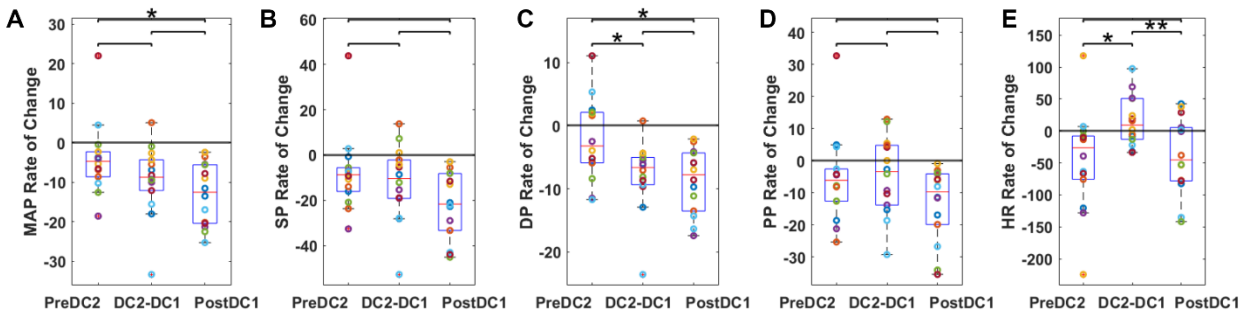

Fig 3. Diastolic BP drop accelerates between SD1-2 onsets: In Cohort 1, rate of change for (A) MAP (mean arterial pressure), (B) SP (systolic BP), (C) DP (diastolic BP), (D) PP (pulse pressure), and (E) HR (heart rate) during the 30 s period before SD1 onset, the ΔSD1-2 period, and the 30 s period after SD2 onset. A negative rate of change value represents the drop rate. After SD1 onset, DP drop rate steepens while SP drop rate remains stable and HR drop rate subsides and plateaus. (* is <0.05, ** is <0.01)

For Cohort 1, mean arterial pressure (MAP) dropped faster in 30s after the 2nd detected SD compared to the MAP drop during the 30s before the 1st detected SD (Fig. 3A). Systolic BP and pulse pressure dropped at a consistent rate as the rate of change was not significantly different between the three time periods (Figs. 3B,D). Of note, in contrast to other blood pressures, diastolic BP dropped faster within the same time frame (Fig. 3C). Fig. 3E shows that the rate of change of the heart rate curve actually plateaus during the ΔSD1-2 period. This indicates that heart rate was dropping before it stabilized and was maintained during the ΔSD1-2 period then dropped again afterwards.

Peripheral BP is transiently decoupled from heart rate during SD

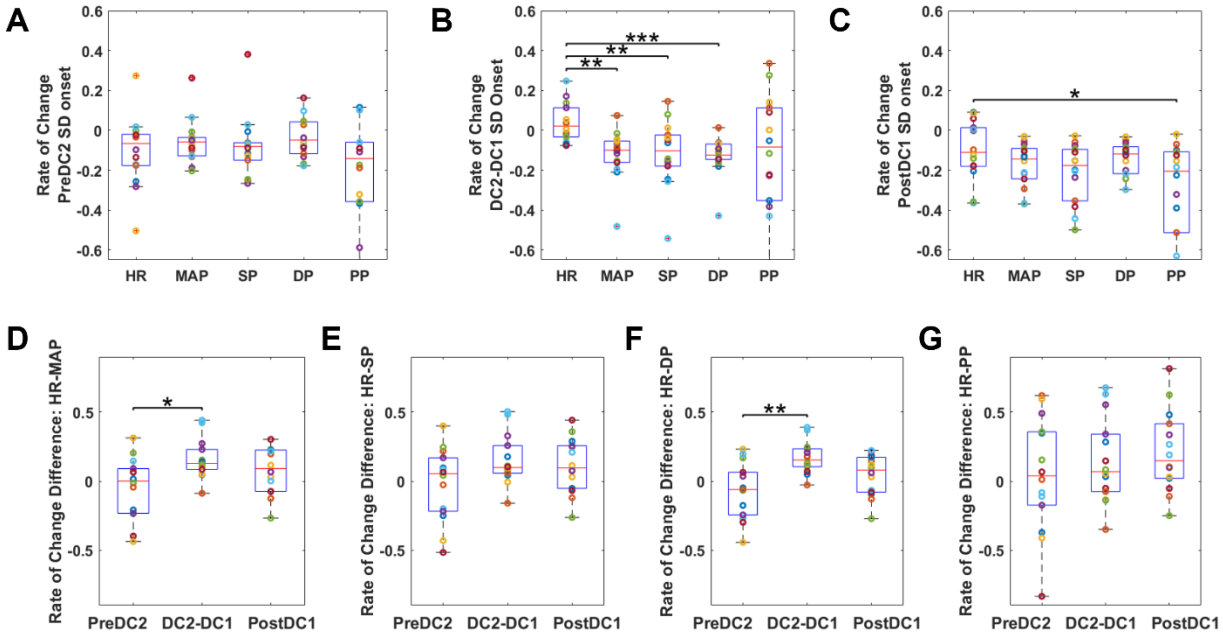

Fig 4. Heart Rate and BP become transiently decoupled during SD and partially re-coupled after SD. In Cohort 1 **A)** Average rates of change (slope) during the 30s period before SD1 (preSD1) of HR (heart rate), MAP (mean arterial pressure), SP (systolic BP), DP (diastolic BP), and PP (pulse pressure). Prior to calculating rates of change, each of these parameters was normalized to baseline so that the parameters could be compared with each other. There is no difference in the rate of change between HR and BP before SD1 onset. **B)** HR and BP metrics (as in (A)) during the ΔSD1-2 period. During SD, there is a significant difference between the average rate of change of HR and BP parameters. **C)** HR and BP metrics during the 30s after SD2 (PostSD2). **D,E,F,G)** Difference in rate of change (slope) between HR and MAP, SP, DP, PP: preSD1, ΔSD1-2, and postSD2. HR relative to MAP and DP show significant initial decoupling with a recoupling postSD2, while relative to SP and PP, HR shows no significant decoupling throughout. (* is <0.05, ** is <0.01)

Heart rate and BP were closely associated physiologically. Using values normalized to baseline (30s before asphyxia), rate of change (slope) in heart rate was compared to rate of change in normalized BP (Fig. 4) during the same time periods as in Fig. 3: pre-SD1, ΔSD1-2 period, and post-SD2 (Figs. 4A-C respectively). The values were normalized to obtain relative (percent) changes so that heart rate and BP could be compared individually and between each other because in a clinical setting, percent changes of these values are important for assessing disorders such as in heart failure. We saw that rate of change in heart rate was well coupled to

rate of change in all peripheral BP measures prior to the 1st SD onset as expected (Fig 4A). However, heart rate increased and/or plateaued during the ΔSD1-2 period while BP continued to drop (Fig. 4B). Thus, the rates of heart rate and BP drop became different, indicating decoupling of the heart rate and BP during this period. Figure 4C shows that after detection of the 2nd SD onset, the heart rate began to fall again and partially closed the 'gap' with the drop rates of the BPs. After detection of the 2nd SD onset, heart rate again became coupled with BP with the exception of pulse pressure. Fig. 4D shows the difference in rate of change of relative heart rate and MAP (heart rate-MAP) during the same time points. The difference between heart rate and MAP being close to zero before the 1st SD onset indicates how well-coupled they began prior to their significant decoupling during the ΔSD1-2 period. They became coupled once again after the 2nd SD onset as the change became non-significant in relation to before the 1st SD onset ($p>0.05$). A similar trend is shown with diastolic BP in Fig. 4F. However, a significant difference in coupling of heart rate with systolic BP and pulse pressure were not seen (Fig 4.E,G).

Shorter ΔSD1-2 period and faster drop in MAP are associated with better neurological outcome post-cardiac arrest

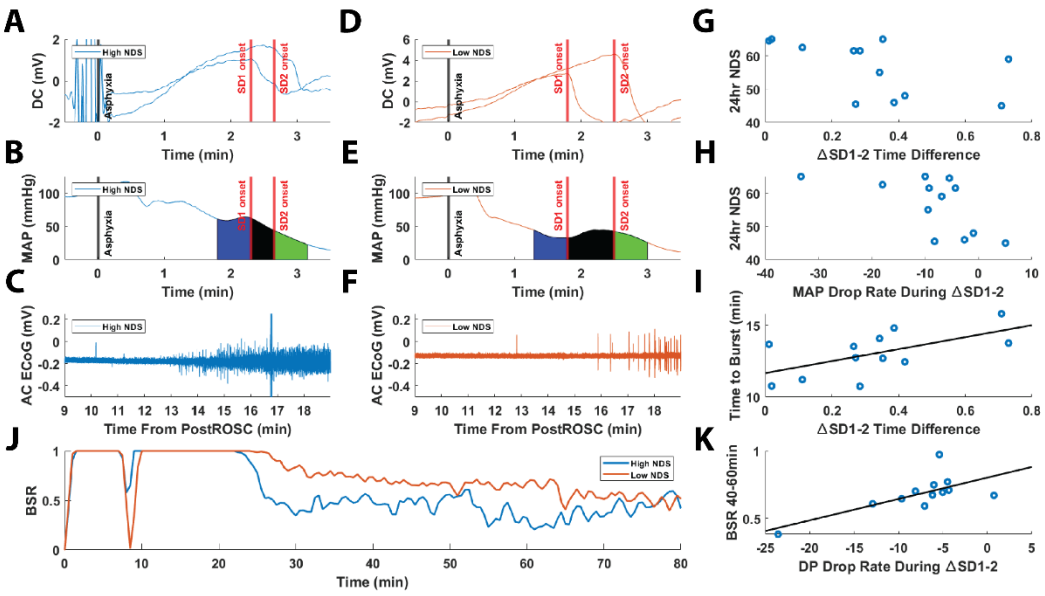

Fig 5. Shorter ΔSD1-2 period is associated with better neurological outcome post-cardiac arrest. In Cohort 1, **A,B,C** show SD onsets, MAP (mean arterial pressure), and AC ECoG respectively for an animal with good outcome (high 24hr neurological deficit scale, NDS). **D,E,F** show SD onsets, MAP, and AC ECoG respectively for an animal with a poor outcome (low 24hr neurological deficit scale). **C** shows an earlier time to burst (TTB), defined as the resumption in cerebroelectrical activity, in the AC ECoG signal post-resuscitation in a rat with good outcome while **F** shows a later time to burst in a rat with poor outcome. **J** shows corresponding rats from C and F with their burst suppression ratios (BSR), with the good outcome rat (C, blue tracing) having a lower burst suppression ratio and poor outcome rat (F, orange tracing) having a high burst suppression ratio. **G** shows that a shorter ΔSD1-2 period is associated with higher 24hr neurological deficit scale (Spearman $p<0.05$, $r=-0.60$). **H** shows that a faster drop rate in perfusion (as measured by slope of MAP) during ΔSD1-2 period is associated with higher 24hr neurological deficit scale (Spearman $p<0.05$, $r=-0.69$). **I** shows that a shorter ΔSD1-2 period is correlated with shorter time to burst (Pearson $p<0.05$, $r=0.60$). **K** shows a faster drop rate of DP (diastolic BP) during DC2-DC1 SD onset time period is associated with less burst suppression at 40-60min post-resuscitation, indicating a better outcome (Pearson $p<0.005$, $r=-0.77$).

The rats with a good outcome (blue tracing, Fig 5A) were seen with a shorter ΔSD1-2 period, a faster drop rate in MAP during the same time period (Fig 5H), an earlier time to first burst or time to burst (Fig 5C) and a lower burst suppression ratio (Fig 5J). The rats with poor outcome were seen to have a longer ΔSD1-2 period, slower MAP drop rate during that period, later time to burst, and higher burst suppression ratio (Fig 5 D,E,F,J respectively). Mean perfusion varied from rat to rat during ΔSD1-2 period (mean MAP: 21 +/- 10 mmHg, range from 7-40 mmHg.) The mean MAP for preSD1 and postSD2 were 23.05 +/- 9.07mmHg and 16.58 +/- 8.45mmHg

respectively. The mean values at any of these periods did not correlate with any of our outcome measures. The same was found for diastolic BP, systolic BP, and pulse pressure (not shown in the figure). However, we found that a faster drop in MAP during this period was associated with better neurological outcome as measured by behavioral neurological deficit score 24 hours post-resuscitation (fig 5H). We also found that a faster drop rate of diastolic BP during the ΔSD1-2 period was associated with faster recovery of electrical brain activity, indicated by lower burst suppression ratio or, more simply, an increase in ECoG bursting 40-60min post-resuscitation (Fig. 5K). Lastly, we found that a shorter ΔSD1-2 period was correlated with better 24hr neurological deficit score (Fig. 5G) as well as an earlier resumption of electrical activity in the brain, measured by time to burst (Fig. 5I). Clinically, this means that shorter duration of ΔSD1-2 in the brain and faster drop rate of peripheral BP during SD in global ischemia are associated with better outcome. This was only done for Cohort 1, as Cohort 2 were non-survival and were euthanized ~90min after resuscitation.

Magnitude of SD-dependent changes in tissue scattering associated with subsequent changes in cerebrovascular resistance (CVR)

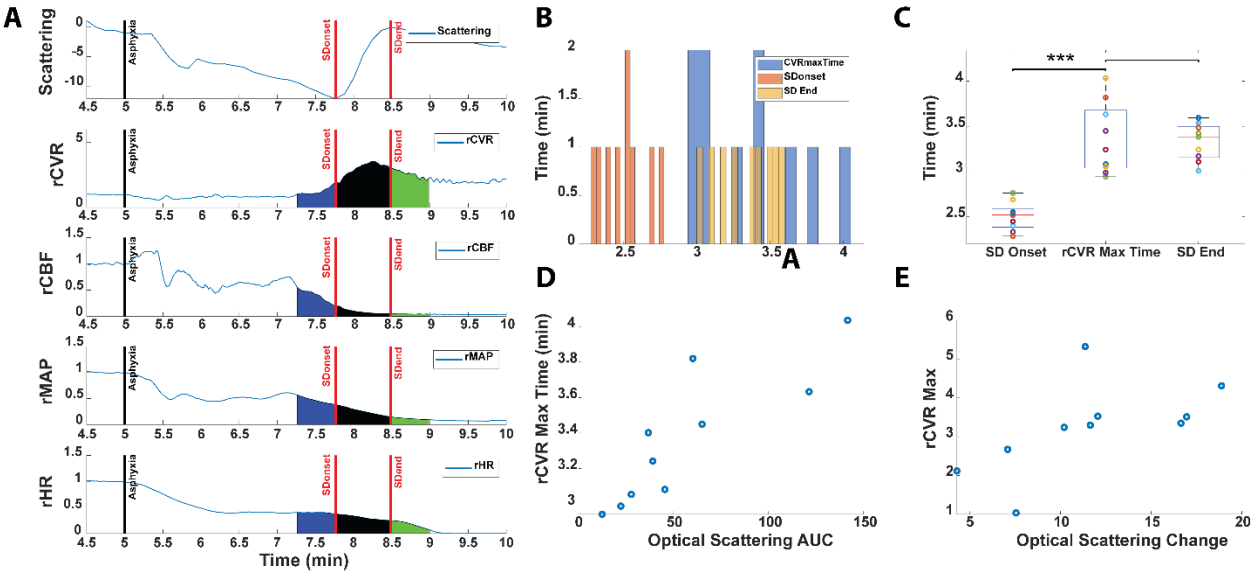

Fig 6. **SD, measured by optical scattering, is associated with changes in CVR:** In Cohort 2, **A)** Tracings of tissue scattering changes in the brain, along with rCVR (relative cerebrovascular resistance), rCBF (relative cerebral blood flow), rMAP (relative mean arterial pressure), and rHR (relative heart rate), in a representative rat, all normalized to baseline. **B)** Distributions of SD onset time, completion time, and time at which CVR peaks in Cohort 2 animals. **C)** Comparison of SD Onset and SD End times vs rCVR Max time, showing that rCVR Max time occurs significantly after SD onset and occurs around SD End time (*** is $p<0.0005$) **D)** Scatter plot showing positive correlation between optical scattering AUC during SD and rCVR Max time (spearman $p<0.0005$, $r=0.92$). **E)** Scatter plot showing positive correlation between magnitude of optical scattering change during SD and rCVR peak value (spearman $p<0.05$, $r=0.75$).

In Cohort 1, we analyzed how SD may affect peripheral dynamics, but did not measure any cerebral hemodynamic changes. In Cohort 2, we measured the cerebral hemodynamic changes in concert with peripheral hemodynamic changes during SD to determine if SD affected both the same way. SD in Cohort 2 was monitored with optical imaging and was measured via optical scattering changes in the brain (Fig. 6A). Due to the optical window taking the place of where DC2 lead would go, we could not analyze the exact same duration of SD utilizing the two DC leads as in Cohort 1. Also, because we observed scattering change through one cranial window, we were unable to spatially discern if the scattering changes were multiple or a single wave. The wave of scattering change we observed may be a composition of multiple waves, but it is unclear. Although, a different metric of SD from Cohort 1, this still provided cerebral hemodynamic changes to be compared with peripheral hemodynamic changes that occurred during SD. The onset of the scattering change (defined as the local minimum point on the scattering curve) was marked as the onset of SD. The maximum point at the end of the scattering change was marked as the end of SD. This period from the onset to the end simply indicates the time in which we observed scattering change in our window and likely does not represent the state of the entire brain. The changes in rCBF, rMAP, and rHR (Fig 6A) were more subtle during the scattering change (SD) compared to before and after SD, but the rise and peak in rCVR was apparent during this period. The peak rCVR occurred near the end of the SD-related optical scattering change (Fig. 6B,C). The time at which rCVR peaked was also strongly correlated with the AUC of optical scattering change (Fig. 6D). The peak value of rCVR

during this period correlated with the magnitude of optical scattering change (Fig. 6E). These findings indicate that the timing and magnitude of SD, as measured by optical scattering, is correlated to changes in CVR.

Significant transient rise of CVR coincides with perturbation in cerebral flow-metabolism coupling during SD

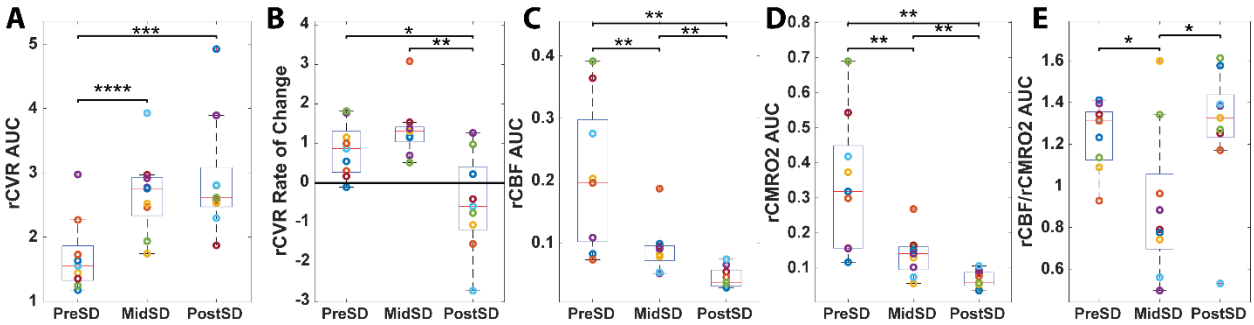

Fig 7. Rise in CVR coincides with perturbed flow-metabolism coupling: In Cohort 2, **A)** AUC of rCVR (relative cerebrovascular resistance) normalized to the 30s period before SD (PreSD), during the span of SD (MidSD, duration of scattering change), and the 30s period after SD (PostSD). Compared to before SD, there is a significant increase in the CVR MidSD and PostSD. **B)** Rate of change of rCVR through SD timepoints. The rate of change of CVR increases MidSD compared to PreSD, but decreases significantly PostSD. **C)** AUC of rCBF (relative cerebral blood flow) through SD timepoints. rCBF dramatically drops from MidSD onwards. **D)** AUC of r $CMRO_2$ (relative cerebral metabolic rate of O2) through SD timepoints. r $CMRO_2$ drops dramatically MidSD and PostSD. **E)** rCBF/r $CMRO_2$ is a metric of cerebral flow-metabolism (e.g.supply and demand). While the individual AUCs of both rCBF and r $CMRO_2$ decrease MidSD and PostSD, the ratio of rCBF to r $CMRO_2$ AUCs normalized to time shows significant reduction during MidSD only.

With the onset of SD, there was a rise in CVR that persisted through SD and after (Fig. 7A). However, with the end of SD, the rate of change of rCVR became negative, indicating a decrease in CVR (Fig. 7B). rCBF and $rCMRO_2$ consistently dropped throughout the course of SD (Figs. 7C,D). However, there was a noticeable SD-related change in the rCBF/$rCMRO_2$ ratio, which is a metric of cerebral flow-metabolism (supply and demand)[96,109]. The AUC of rCBF/$rCMRO_2$ ratio (AUC rCBF/AUC $rCMRO_2$ then normalized to duration) transiently but

significantly dropped during SD, indicating cerebral flow-metabolism decoupling, but returned to pre-SD values after SD (Fig. 7E).

After SD, the drop in peripheral BP is decoupled from cerebral perfusion and metabolism

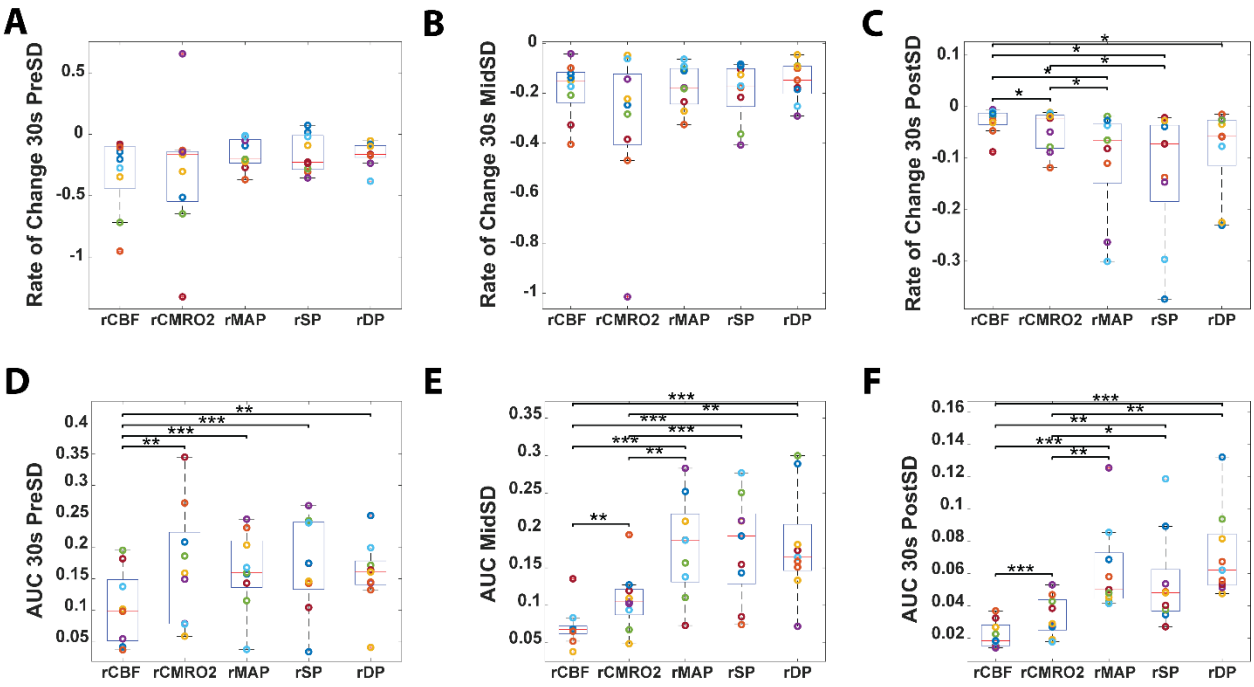

Fig 8. Decoupling of peripheral BP from cerebral perfusion and metabolism MidSD and/or PostSD. In Cohort 2, **A, B, C)** shows the rate of change of rCBF (relative cerebral blood flow), r $CMRO_2$ (relative cerebral metabolic rate of O2), rMAP (relative mean arterial pressure), rSP (relative systolic BP), rDP (relative diastolic BP) PreSD, MidSD, and PostSD respectively. There is no difference between rCBF and other parameters PreSD and MidSD, but there is a significant difference PostSD. **D, E, F)** AUC of rCBF, r $CMRO_2$, peripheral BPs PreSD, MidSD, and PostSD. rCBF is significantly lower than the other parameters PreSD, MidSD, and PostSD. r$CMRO_2$ is only significantly different from peripheral BP MidSD and PostSD.

PreSD and MidSD, the rates of change in CBF, $CMRO_2$, and peripheral BP were similar (Fig. 8A, B), signifying coupling between these parameters. PostSD, CBF became decoupled to both $CMRO_2$ and peripheral BP (Fig. 8C). During this period, the rate of drop in CBF was closer to zero than $CMRO_2$ and peripheral BP. This was likely due to the maximum CVR occurring at the same time, shutting off blood flow and causing decoupling between CBF and peripheral BP. Similarly, $CMRO_2$ was coupled with peripheral BPs PreSD (Fig. 8D), but became decoupled

from peripheral BPs at start of SD (Fig 8E,F). $CMRO_2$ dropped dramatically with SD onset, much greater than the relative drops in peripheral BPs (Fig 8E,F). However, CBF AUC was significantly lower than $CMRO_2$ AUC and peripheral BP AUC throughout all time points.

Discussion

In this study, we investigated the effects of anoxic SD on CBF, cerebral metabolism, and peripheral BP during global ischemia and its effect on neurological outcome after resuscitation. While most literature focuses on the effect of SD on local cerebral perfusion or the effect of ischemia/hypotension on induction of anoxic SD, here we focused on the reverse possibility: the potential for anoxic SD to invoke changes in peripheral BP. Moreover, to our knowledge, this is the first study to characterize the relationship between peripheral BP and CBF during anoxic SD. A previous study[88], using multi-modal imaging of anoxic depolarization, used voltage-sensing dye to measure SD, and investigated CBF with laser speckle imaging and peripheral BP during SD in a non-resuscitation cardiac arrest model, but their analysis concluded that SD did not affect either CBF or peripheral BP. However, the aforementioned study did not assess with a high temporal resolution during SD as they only used averaged signals at 7 selected time points over 3 minutes which was too low to capture rapid changes[88]. By contrast, our study measured ~17 data points per minute with Spatial Frequency Domain Imaging and ~39 data points per second with Laser Speckle Imaging. Additionally, the previous study did not characterize the relationship between CBF and peripheral BP, but rather looked at them independently, finding that anoxic SD did not affect the changes in CBF or peripheral BP. In contrast, we found that anoxic SD may affect peripheral BP, possibly by relaxing peripheral vasculature and decouple the peripheral BP from CBF and metabolism. Furthermore, in our resuscitation cardiac arrest model, we show for the first time, an association between the characteristics of peripheral BP during anoxic SD and neurological outcome.

In Cohort 1 animals, the ΔSD1-2 period, a time delay between detection of two anoxic SDs measured in two different locations, was analyzed. We found this period to be significant as we found the time delay varied from rat to rat and it may represent a broad connectivity metric across the brain while it is shutting down. Furthermore, we noticed blood pressure fluctuations during this period, and so we investigated the potential peripheral and cerebral changes occurring during this period. As mentioned in the results, although we cannot be certain that the detected SDs were from separate foci or from a single propagating SD, it is likely more than one anoxic SD based on the global ischemia model[94] and that the speed of propagation (if single SD) would be much too fast compared to what is known in literature. Using the distance between the two DC electrodes and the time delay between the two, the calculated speed of the anoxic SD ranged from 7-724 mm/min. Based on known SD speeds of 1.5-9.5 mm/min, these speeds were too fast which suggests that rather than a single propagating wave, there were likely multiple foci where SD originates, leading to, in some cases, near simultaneous detection at both DC electrodes. This may be because in this asphyxial cardiac arrest model, blood flow to the whole brain shuts down, leading to not a single, but likely multiple ischemic cores occurring at near simultaneous times, due to difference in ischemic thresholds in different regions of the brain based on possible proximity to blood vessels and the local blood flow and metabolic demand. Per prior studies, during global ischemia, anoxic SD is likely to occur at slightly different times in different brain regions, possibly reflecting small variations in tissue perfusion loss during ongoing ischemia and/or different regions having varying thresholds for triggering of anoxic SD[115–117]. In contrast, in focal stroke or other conditions where there is a single ischemic core, the SD propagates outward from the ischemic core.

Cortical anoxic SD transiently decouples peripheral blood pressure from heart rate

Effects of SD on cerebral hemodynamics and metabolism have been investigated[13], but the effects of SD on peripheral BP and heart rate remain largely unexplored. Our data showed that the rate of change of systolic BP was consistent from before the ΔSD1-2 period, during the ΔSD1-2 period, to after, while diastolic BP's drop rate increased throughout the same time periods. This contrasts with the transient rise and/or plateauing of heart rate we observed during the ΔSD1-2 period, which was accompanied by stronger systolic function that prevented the systolic BP from dropping at an accelerated rate. While these may appear to be compensatory cardiac functions in a state of circulatory shock, the diastolic BP drop rate continued to accelerate, supporting a possible relaxation of the peripheral vascular tone and/or changes in cardiac diastolic function. Since diastolic BP is closely associated with vascular tone and elasticity[118,119] more than cardiac function, it is possible that anoxic SD may be indirectly affecting peripheral vascular tone. Future studies will focus on direct assessment of peripheral arteries to assess for vasodilation and evaluation of cardiac function for changes in diastole. This is further supported by the changes in heart rate being coupled with changes in the peripheral BP before the 1st SD onset while during the ΔSD1-2 period the heart rate transiently rose, decoupling it from all the peripheral BP metrics, and after detection of the 2nd SD onset, becomes less decoupled. These data suggest that anoxic SD may possibly produce a transient brain-heart coupling effect which increases heart rate while relaxing vascular tone. One mechanism of such brain-heart coupling may be via the vagus nerve, which can modulate the parasympathetic activity of the heart, including regulation of both the sinoatrial nodes and atrioventricular nodes[120]. Interestingly, the vagus nerve has recently been shown to modulate SD[25–28], however our data suggests that the reverse directionality is plausible, namely that anoxic SD may also potentially modulate the heart through the vagus nerve or its related components.

Shorter ∆SD1-2 duration and faster drop in peripheral perfusion during the ∆SD1-2 period is associated with better outcome 24 hrs post-cardiac arrest

We found that a faster drop in peripheral perfusion (slope of MAP and diastolic BP) during the ∆SD1-2 period was correlated with a higher behavioral recovery 24 hrs later (neurological deficit scale scores) (Fig 5H). This suggests that faster drop in peripheral perfusion during the ∆SD1-2 period is associated with better neurological outcome. However, we also showed that a shorter ∆SD1-2 period was also associated with better outcome, as evidenced by shorter time to burst (Fig 5I), as well as increased behavioral recovery 24 hrs later (Fig 5G). We also saw that a faster drop in diastolic blood pressure during the ∆SD1-2 period was associated with better neurological outcome in quantitative ECoG parameters immediately post-resuscitation and better neurological outcome post-cardiac arrest (Fig 5K). This may appear counter-intuitive as faster depression of the brain with anoxic SD and a faster drop in perfusion may be expected to produce worse outcomes. However, in another recent study from our research lab, we again found that faster drop in perfusion before anoxic SD is associated with better neurological outcomes after cardiac arrest.[9] It is possible that there may be an unmeasured component related to SD and perfusion that produces a protective effect. Future studies will focus on teasing these complex mechanisms apart.

Magnitude of anoxic SD is associated with subsequent changes in cerebrovascular resistance (CVR) and transient decoupling of CBF and metabolism during anoxic SD

Our multimodal platform using optical imaging of the brain alongside peripheral blood pressure monitoring allowed us to simultaneously and continuously monitor CBF, brain metabolism, and peripheral BP throughout the cardiac arrest experiment. Using the measured CBF and MAP, we estimated a surrogate measure of the relative CVR (rCVR)[111–114]. We suspected that rCVR may be particularly sensitive to changes in CBF and BP during anoxic SD given that SD is known to

affect CBF while our data in this study support BP changing after anoxic SD onset. Interestingly, we observed a significant increase in rCVR starting with the onset of SD-associated changes in optical scattering. During SD, there were morphological changes in tissue that increased scattering of light, which could be detected by spatial frequency domain imaging and used to determine the onset of SD[23]. Under normoxic conditions, SD is known to induce vasodilation to increase CBF[13], but in pathological conditions (e.g. ischemic or hypoxic), it has been shown to reduce vessel diameter[88], thus increasing CVR. However, to our knowledge, the changes that occur in peripheral and cerebral hemodynamics as well as cerebral metabolism during time periods 30 s before, during, and 30 s after anoxic SD have not been analyzed with high temporal resolution. High temporal resolution was needed as it allowed us to separate the dynamics between these 30-60 s periods to provide insights into the physiology of cerebral and peripheral hemodynamics before, during, and after anoxic SD. In addition to the rise of CVR with anoxic SD onset, we also found that the peak of CVR coincided with the end of optical scattering changes (end of anoxic SD). After anoxic SD, the CVR interestingly began to decrease. The time at which CVR peaked was also strongly correlated with the AUC (a measure of total magnitude) of optical scattering change during anoxic SD ($p<0.0005$, $r=0.92$). Additionally, the peak CVR was also strongly correlated with the magnitude of optical scattering change during SD ($p<0.05$, $r=0.75$). Greater observed optical scattering changes may be related to anoxic SD-induced extracellular ion changes (i.e. increase K+ ions) and thus greater vasoconstriction. This aligns with findings from another study that found extracellular K+ to be the predominant vasoconstrictor in SD[13,121]. This may explain how CVR peaks at the end of anoxic SD and how the magnitude of anoxic SD or extracellular K+ ion change is correlated with magnitude of the CVR. Moreover, while immediately before, during, and after anoxic SD, the CBF and $CMRO_2$ continuously drop, the ratio of $rCBF/rCMRO_2$, a metric of cerebral flow-metabolism coupling, showed a different trend. Specifically, during anoxic SD, $rCBF/rCMRO_2$ dramatically dropped but then returned to its previous state after anoxic SD. We speculate that

rise in CVR was caused by CBF decreasing more than $CMRO_2$, thus producing the flow-metabolism imbalance during anoxic SD.

Anoxic SD is associated with decoupling of peripheral blood pressure from CBF and brain metabolism

Before and during anoxic SD, the rate of change in CBF was coupled with that of $CMRO_2$ and peripheral BP, suggesting that the changes in all these parameters are similar. After anoxic SD, CBF became decoupled from $rCMRO_2$ and peripheral BP. During this period, the rate of drop in CBF was closer to zero compared to $CMRO_2$ and peripheral BPs, indicating that it had likely fallen to a minimum and could not be reduced further. This is likely due to the CVR hitting its peak at this time, nearly shutting down blood flow and causing decoupling of CBF from $CMRO_2$ and peripheral BP. Similarly, $CMRO_2$ was coupled with peripheral BPs before anoxic SD, but became decoupled starting at anoxic SD onset. $CMRO_2$ dropped dramatically with anoxic SD onset with a magnitude much greater than that of the relative drops in peripheral BPs. This may be because anoxic SD is a highly energy consuming event, and with a lack of oxygen to begin with, cerebral metabolism consumes any remaining oxygen and shuts down quicker. This is in contrast to SD in normal condition with sufficient oxygen in which $CMRO_2$ increases to the point of potentially doubling compared to baseline. These data further show that unlike in a normal state, during an ischemic-hypoxic state, anoxic SD leads to a dramatic relatively greater drop in both CBF and $CMRO_2$, leading to a decoupling of both with peripheral BP during and after anoxic SD.

Limitations

Our study has several limitations that we hope to address in future experiments. A major limitation in our study is that some of our findings and relationships between factors are correlational. Future studies will require interventions during ongoing global ischemia to better

assess causality and the specific mechanisms that may tie anoxic SD with cardiovascular function and neurological outcome. Along these lines, this report does not characterize cerebral changes and neurological recovery data on a molecular, cellular, and histological level, which would help to better elucidate the mechanisms underlying our findings. In addition, our sample size was low and due to the high number of statistical comparisons, there is a concern for underpowering and type II error in this pilot study. The uncoupling effects seen in our results may also simply be due to cardiac dysfunction occurring at the same time as SD. It is unclear whether the cerebral dysfunction or cardiac dysfunction played a greater role, but due to some of the hemodynamic effects being transient just during SD, it seems less likely it is purely due to cardiac dysfunction. Furthermore, we only had two DC electrodes and we also did not test if these results would hold true if the electrodes were to be placed in different regions of the brain. Future experiments can include more DC electrodes and in different locations to test if the results still hold, and also to be able to better decipher the pattern of connectivity with greater spatial resolution. Another major limitation is that this study only used male animals. Sex differences are critical to a variety of neurological and cardiovascular functions, and future experiments should account for this by including both sexes. Furthermore, animals were divided into two cohorts with different surgical preparations, precluding us from obtaining behavioral outcome data (e.g., neurological deficit scale) 24 hrs later for animals in the optical imaging cohort, as they were euthanized after 2 hrs of monitoring following resuscitation due to the craniectomy. Additionally, a craniectomy can introduce its own confounding variable as it provides an outlet for intracranial pressure changes that may occur during ischemia. While this is a limitation, it also may indeed make our rCVR estimation more reliable since a craniectomy helps to mitigate major changes in intracranial pressure[111–114]. The craniectomy also may affect cerebral blood flow. Nevertheless, limitations with a craniectomy can be addressed in future studies by using either a chronic imaging window or a thinned skull procedure to enable survival studies out to 1 week post-resuscitation or beyond. Finally, the craniectomy was performed over

only a 6 mm × 4 mm area of the skull rather than the entire surface of the brain. Therefore, our measurements of SD onset in Cohort 2 were limited to the location and time the CBF and scattering changes first appeared within the craniectomy region. Another limitation of this study is that we did not measure PaCO2 or local pH continuously throughout asphyxia and anoxic SD, which may affect anoxic SD.

Conclusion

In this study, we used a rat model of asphyxial cardiac arrest with continuous and simultaneous multimodal monitoring, including optical imaging and electrophysiology to quantify changes in cerebral activity, blood flow, oxygen metabolism, as well as peripheral blood pressure and heart rate before, during, and after anoxic spreading depolarizations. We analyzed the effects of different stages of anoxic SD on CBF, $CMRO_2$, peripheral BP as well as the relationship between these three metrics. While the effect of hypoperfusion on anoxic SD has long been known, our study demonstrates for the first time that anoxic SD may in turn have effects on peripheral perfusion by not only affecting CBF and $CMRO_2$, but stretching further, leading to changes in the peripheral BP measured in the extremities and heart rate likely via a brain-heart connection. We show that there is a significant transient rise of cerebrovascular resistance during anoxic SD that is positively correlated with the magnitude of anoxic SD, and that the rise in this CVR coincides with perturbation in cerebral flow-metabolism coupling during anoxic SD. We also show that a faster drop of peripheral perfusion during anoxic SD is associated with better short-term (40-60 min) and longer-term (24 hr) neurological recovery after cardiac arrest. These results provide support for the likelihood that the influence of anoxic SD may not be limited to the brain but can likely reach the peripheral cardiovascular system. Peripheral BP is generally monitored in a critical care setting in the hospital, so characterizing the effects of anoxic SD on peripheral BP may have significant potential for clinical translation and potential interventions. Further investigation into the relationship between the peripheral cardiovascular

system and the brain during anoxic SD may provide new insights into understanding a potentially critical role for anoxic SD in global ischemia and recovery[23].

Chapter 2

Blocking Hyperemia With Esmolol Following Resuscitation From Cardiac Arrest Improves Neurological Outcome

Authors: Han SW, Yi J, Bazrafkan A, Rafi M, Liu A, Puppali V, Singh A, Yoo J, Zandihaghighi S, Nath A, Pham J, Wilson RH, Akbari Y.

Introduction:

Over half a million people suffer from cardiac arrest (CA) each year, making it a pressing public health concern.[122] Survival from CA in-hospital is only around ~15% [3] and those who survive often suffer from debilitating neurological impairments[5]. It has become increasingly known that secondary brain injury that occurs from ischemic and reperfusion injury is a critical determinant of neurological outcome following successful return of spontaneous circulation (ROSC) after cardiac arrest[29].

In the moments following ROSC, reperfusion occurs in two phases: there is a brief hyperemia phase where blood pressure spikes and is very high[36], followed by a prolonged hypoperfusion phase, where the blood pressure decreases below baseline levels[37]. This hypoperfusion was found to be associated with worse outcome[30–34] and thus the AHA recommended treating hypotension.[73]

However, most studies looked at hypoperfusion, and not the brief period of hyperemia. In rats, the hyperemia phase can last 10-20 min with systolic pressure rising into the 200s and mean arterial pressure (MAP) into the high 100s[38]. This hyperemia phase may be a critical contributor to reperfusion injury through direct shear injury from high perfusion, or through excess circulation of harmful metabolites. Reperfusion injury[39,40] is a broad category that refers to secondary injury post-ischemia where cells end up injured or die.[41]. Blood brain barrier disruption, edema, mitochondrial injury[41,42], and ROS production[43,44], among several other disruptions in homeostasis are known to contribute to reperfusion injury. Additionally, a surge in perfusion during a state of low cellular activity in the brain may result in a flow-metabolism mismatch (supply and demand), exacerbating reperfusion injury.

In this study, we targeted hyperemia using esmolol, a cardio-selective beta blocker, to assess if blocking hyperemia would improve outcome. Few studies have investigated the effects of esmolol in ischemia-reperfusion injury. These studies found that the small dose of esmolol improved outcome after ischemia-reperfusion[45–49] and one study even found that giving a small bolus of esmolol during CPR with epinephrine protected the endothelium of microvasculature of the brain[50,51]. However, these studies were not specific to the brief hyperemic period. Our study is the first to completely block hyperemia post-CA to investigate its role in reperfusion injury and recovery.

Methods:

In this study, we analyzed the hyperemia phase following CA with optical imaging of the brain and femoral artery cannulation for peripheral blood pressure monitoring at a high temporal resolution. For optical imaging, we used laser speckle imaging (LSI) to monitor CBF and

multispectral spatial frequency domain imaging (SFDI) to monitor cerebral oxygen levels, and combined them to obtain cerebral metabolic rate of oxygen consumption ($CMRO_2$).

Preclinical Rodent Model of CA

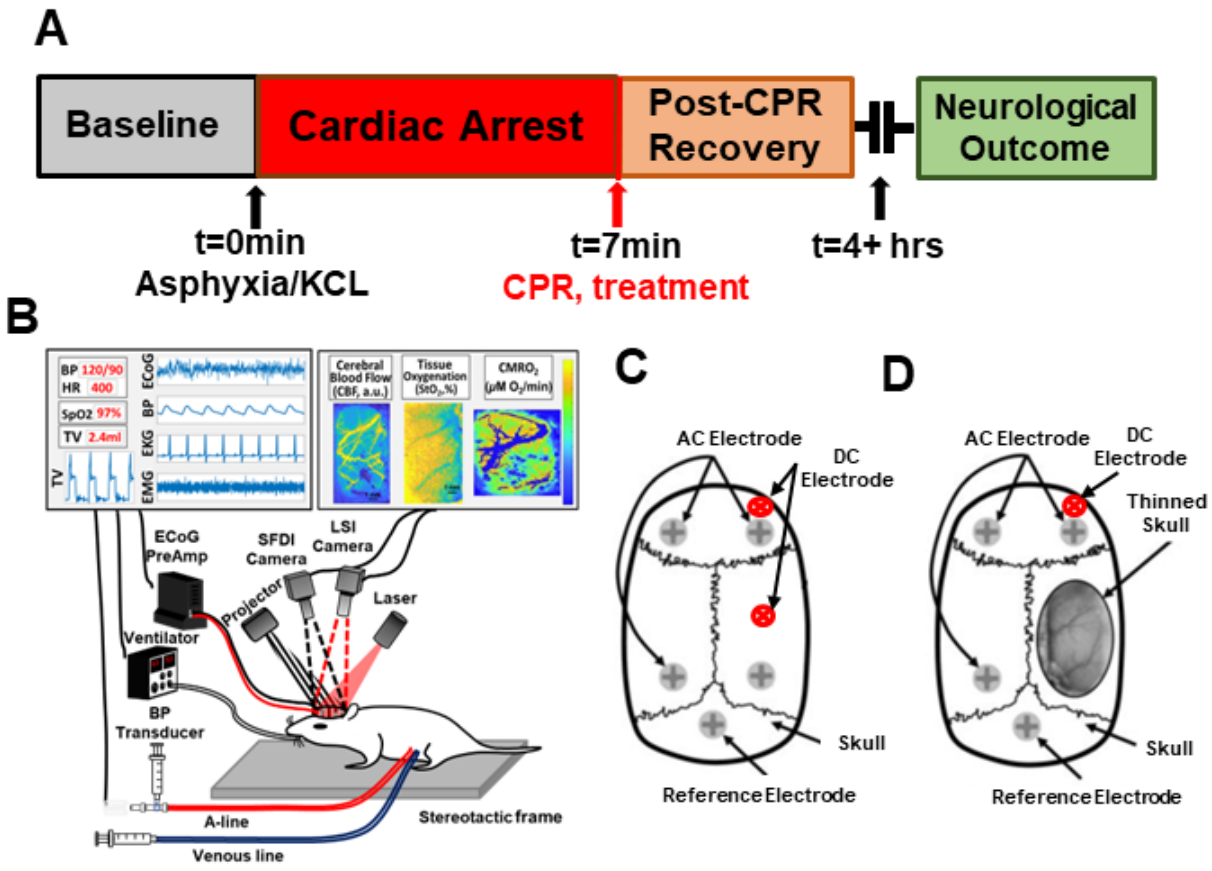

Figure 1. Experimental Timeline and Set Up. **A)** Brief timeline of the CA experiment. **B)** Schematic showing the multimodal monitoring system. **C-D)** Placement of electrodes and optical imaging window.

Cohort 1

The animal model of CA and resuscitation used in this study has been described previously by our lab and is summarized in **Figure 1**. This cohort had two different models of CA, an asphyxial (n=32) and KCL-induced CA (n=23), to analyze hyperemia in two different naturally occurring CAs. These rats did not have optical imaging. However, a separate set of 13 rats underwent asphyxial CA with optical imaging. In summary, male Wistar rats (Charles River, Canada facility) implanted with electrodes a week prior to the CA (**Fig. 1C-D)** depending on if they had optical imaging or not, were calorically restricted (75% restriction) with 3 food pellets, as is standard with our model, the night before the CA experiment. The next morning, rats were endotracheally

intubated and received femoral artery and vein cannulation to enable arterial blood pressure (BP) monitoring and venous drug delivery, respectively. At the beginning of the experiment (**Fig. 1A**), arterial blood gases were measured from the femoral artery to confirm normal blood gas levels. The animals were on 100% O_2 and the anesthetic (isoflurane) was washed out over a 3 min period. This was followed by administration of a musculo-paralytic agent (vecuronium or rocuronium). After the washout period, CA was induced by turning off the ventilator or intravenously administering KCl, depending on the experimental group. Then, 8 min later, CPR was initiated by turning the ventilator back on with 100% O_2, giving epinephrine and sodium bicarbonate, and performing manual chest compressions. Chest compressions were continued until the return of spontaneous circulation (ROSC) and 10-15 min post-ROSC arterial blood gases were measured once again from the femoral artery. The rats were monitored continuously for an additional 4hr until behavioral testing. The animals were kept on 100% O_2 until extubation from the ventilator, which occurred roughly 1hr post-ROSC. Neurological Deficit Scale (NDS), a behavioral test, was used to score neurological function at 4, 24, 48, and 72 hr post-ROSC, with a higher score representing better neurological function[97–99]. Burst suppression ratio (BSR), a quantification of suppression of AC-ECoG activity, was also used as an outcome measure at 60-80 min post-resuscitation, when the rat was recovering from coma and regaining consciousness. BSR decreases as the rat regains consciousness. Time to burst (TTB) is the time until electrical activity in the brain resumes as measured by the first burst of activity in AC-ECoG signal, and was used as another marker of neurological recovery. The rats were euthanized at 24hr or 72hr post-ROSC for immunohistochemistry of the brain. The animals' body temperatures were monitored with a rectal probe and maintained at 37 degrees Celsius using a heating pad during the entirety of the experiment.

Cohort 2

Cohort 2 was used in studies modulating blood pressure during hyperemia with esmolol infusion or vehicle. The CA model was the same as in Cohort 1, with some minor differences. These rats were implanted with electrodes the morning of the experiment, not a week before, and also had the right parietal bone thinned with an electric hand drill to enable a window for optical imaging (**Fig. 1D)**. These rats underwent a 7 min asphyxial cardiac arrest and received either vehicle or esmolol infusion after resuscitation. The vehicle (**Veh,** n=10) and esmolol from hyperemia (**EH**, n=10) groups received esmolol (10mg/ml) or vehicle (saline) infusion at the beginning of hyperemia (roughly 5 min post-ROSC). The infusion rates for EH group were adjusted on a rat to rat basis to maintain a mean arterial blood pressure (MAP) below 140 mmHg with vehicle groups receiving a similar rate of infusion of saline. MAP of 140 mmHg was selected due to our findings which suggested a potential threshold around MAP of 140 at which the rats seemed to have poor outcomes. This result is shown later in this paper. We had an additional esmolol group (**EC**, n=9) which received an infusion of esmolol from the beginning of CPR. The infusion rate during CPR was 0.01ml/min, then was increased post-ROSC to maintain MAP levels below 140. The infusions continued until end of hyperemia as determined by returning to baseline MAP or until 15 min post-ROSC to prevent too large of infusion volume. These rats were euthanized at 4hr post-ROSC, but their brains were not histologically analyzed as they were mainly used to collect dynamic physiological data for cerebral autoregulation.

ECoG and DC electrodes

Rats in Cohort 1 underwent surgery to implant 5 screw electrodes for AC-ECoG (alternating current) recordings and 2 DC (direct current) Ag/AgCl for DC-ECoG recordings 1 week prior to the CA experiment as shown in **figure 1C**. The Ag/AgCl electrodes were made by chloridizing silver wires (Stoelting 50880) in household bleach. The Ag/AgCl electrodes were implanted 1 mm into the cortex in the right frontal hemisphere, and another one implanted in the right

parietal cortex. In the rats with optical imaging, due to the optical window, the DC lead and ECoG electrode in the right parietal bone were not used.

Data Acquisition and Post-Processing

Post-processing of arterial BP, AC-ECoG, and optical imaging data was performed using MATLAB (The MathWorks, Inc., Natick, MA). In this study, AC-ECoG data was primarily used for the analysis of ECoG burst onset. DC-ECoG data was not analyzed for this study.

Burst Suppression Ratio (BSR)

To calculate BSR for each rat, the AC-ECoG signal was processed by down sampling by 6 to 254 Hz to reduce computational load, performing common average referencing for 3 AC-ECoG channels, notch 60 Hz filtering to remove electrical noise, and 1-150 Hz bandpass filtering. Afterwards, a threshold for the amplitude of the signal was calculated by taking the sum of the mean and standard deviation during a period of 20-30 min post-ROSC. A burst suppression was calculated at an interval of at least 0.5s in which the amplitude of the AC-ECoG signal did not exceed the threshold of 20mV. The ratio of the time in burst suppression was calculated over a period of 1 min with an overlapping window of 30s. This was calculated from 5 min prior to the onset of asphyxia to 60 min after. For this study, we used an average of the BSR during 30-40 min period after onset of asphyxia as one of the markers for neurological outcome.

Time to Burst (TTB)

Time to Burst was obtained by visually confirming the first burst of AC-ECoG activity on our live stream of the AC-ECoG signal post-ROSC and was used as another marker of recovery in

animals waking from up post-CA. The timing was confirmed by plotting the AC-ECoG signal with MATLAB and noting the first burst of activity.

Arterial BP

For both cohorts, BP was measured continuously at 191 Hz from an arterial line. Mean arterial pressure (MAP) was calculated using the formula MAP= (systolic blood pressure + 2*diastolic blood pressure)/3. Pulsatility was measured as the difference between systolic and diastolic blood pressure (pulse pressure).

Optical Imaging

Throughout the experiments, rats with optical imaging were monitored with two diffuse optical imaging technologies: Laser Speckle Imaging (LSI) and multispectral Spatial Frequency Domain Imaging (SFDI). LSI measures blood flow, as previously established in both preclinical and clinical studies [96,111], including investigations into CA[83,101,104]. SFDI [96,106] measures the tissue absorption coefficient (related to hemoglobin concentration and oxygenation[83,105]) and scattering coefficient (related to morphology and distribution of cells and organelles[108]). The combination of LSI and SFDI data can be used to calculate cerebral metabolic rate of oxygen ($CMRO_2$)[109]. In this study, Laser Speckle Imaging data were acquired with a frame rate of 60 Hz and Spatial Frequency Domain Imaging data were acquired with a frame rate of 14 Hz. However, to reduce computational load, we reduced the sampling rate to ~17 data points per min for SFDI and ~39 data points per min LSI, which was enough to capture the dynamic changes during hyperemia.

Data Analysis

LSI Data: relative cerebral blood flow

The Laser Speckle Imaging data was used to compute Speckle Flow Index, a measure of CBF, over a fixed spatial region of interest spanning the majority of the imaging window. Relative cerebral blood flow (rCBF) was normalized to the mean CBF calculated over the one-minute interval immediately prior to the onset of asphyxia.

LSI Data: Vessel Diameter

The laser speckle images were processed in Matlab where a vessel was selected and the full-width-half-max of the vessel width calculated over the time course of the experiment.

SFDI Data: Tissue scattering and oxygenation

For SFDI data analysis, custom MATLAB code[83] calculated a best fit of a computational (Monte Carlo) model of light-tissue interaction to the measured data. These model fits provided tissue oxy-hemoglobin concentration (ctHbO2), deoxygenated hemoglobin (ctHb), and scattering maps. The ctHbO2 and ctHb data were combined to calculate tissue oxygenation (StO2) via the formula StO2 = 100*ctHbO2/(ctHbO2+ctHb). Time-resolved ctHbO2, ctHb, StO2, and tissue scattering curves were formulated by averaging the optical property maps over a fixed spatial region of interest (ROI).

LSI + SFDI Data: CMRO2

Time-resolved CMRO2 was calculated using the formalism developed by Boas and Dunn[108,110], combining CBF data from LSI with ctHbO2 and ctHb data from SFDI. For the calculation of

CMRO2, the CBF data were analyzed using an ROI covering the majority of the imaging window (to represent overall perfusion into the brain), while ctHbO2 and ctHb data were analyzed using an ROI over a prominent vein (to more accurately probe the amount of oxygen consumed by the tissue).

Multimodal Parameter Set

For each cohort, a multimodal set of parameters was extracted from the data around the hyperemia phase to analyze several associations. In all cohorts, these parameters included: (i) absolute and relative hyperemic peak post-ROSC; (ii) area under the curve (AUC) of the hyperemia (post-ROSC to 20 min after). These were done for MAP, systolic blood pressure (SBP), cerebral blood flow (CBF), $CMRO_2$, as well as ctHb and ctHbO2.

Statistical Models and Tests

Statistical testing was performed with MATLAB. For each correlation analysis, Spearman correlations were performed when one of the parameters used was not normally distributed. When both parameters used for correlation were normally distributed, Pearson correlation was used. Unpaired or paired T-Tests were used for comparison between two groups while one-way anovas were performed to compare between multiple groups or parameters.

Immunohistochemistry and Quantification

Cohort 1: Immunohistochemistry

Based on different time points, 24 hours or 72 hours after cardiac arrest, animals were subjected to euthanization via sodium pentobarbital and perfused transcardially by injection of 0.9% saline followed by 4% paraformaldehyde (PFA), made at pH 7.6. Animals' brains were post-fixed in 4% PFA for 3 days and then they were transferred into 30% sucrose to cryo-protect. Following that, brains were hemisected, and hemispheres were frozen in optimal cutting temperature (OCT) solution to cryo-cut and stored in - 80°C freezer. For each animal, the left hemisphere was coronally sectioned at 30 µm intervals using a cryostat (Microm HM 505N). The Sections were stored in a 8 96-well plates filled with 1xPBS with sodium azide and were stored at 4°C. Within the regions of interest (bregma -2.04 to -3.24), which includes the hilus, the stratum lacunosum moleculare (SLM), and the thalamic reticular nucleus (TRN) regions,desired sections were chosen from each plate at 360 µm intervals. For fluorojade-b (FJB), mounted sections were stained with 0.0008% FJB in 0.1% acetic acid. To immunostain, all sections within the cohort were stained at once and immunostaining was done on all subjects from a cohort on one run to ensure the uniformity of the immunohistochemistry processes for all subjects. On the first day of the experiment, sections were washed thrice in 1xPBS in 10 minutes intervals and then blocked in a solution of 3% normal donkey serum (NDS), 1xPBS, and 0.3% Triton x-100 for an hour. Incubations of sections in the primary antibody were done using Rabbit α IBA1 (1:1000) [Wako 019-19741] and Mouse α GFAP (1:1000) [Sigma G-3893] antibody diluted in a blocking buffer. Plates were left overnight on a shaker at room temperature. On the second day of immunostaining, sections were washed thrice in 1xPBS in 10 minutes intervals and incubated for secondary antibody in 1:250 Donkey α Rabbit Alexa Fluor 488 and 1:250 Donkey α Mouse cy3 in a solution of 1xPBS +3% NDS + 0.3% TritonX-100 for two hours. Following incubation, sections were washed thrice with 1x PBS for ten minute intervals and mounted on gelatin-subbed slides using weak mounting solution. To ensure accurate visualization of brain structures, slides were hydrated, stained in 0.5 µg/mL DAPI for 5

minutes, rinsed and put away for air drying. Lastly, slides were cover slipped under Vectashield and stored in 4°C temperature within a dark box.

Cohort 1: Imaging and Quantification

Stained slides were imaged using the Keyence BZ-x800 light microscope. To ensure consistency within imaging runs, all parameters of imaging such as exposure were pre-set for all subjects with a cohort. Imaged sections were stitched together by Keyence software and channels were separated based on different stains. To analyze images, trained members were each assigned to a specific region in which each region was quantified by measuring the fluorescence intensity with ImageJ by least two members. Each person used DAPI staining to identify the region of interest and quantified the mean integrated density of GFAP and IBA1 three times after subtracting background. Integrated density values from the three quantifications were averaged, and the resulting values were averaged between quantifiers.

For FJB quantification, at least two quantifiers counted FJB cells in the hilus and TRN using the Cell Counter Tool in ImageJ. Positive FJB signal was defined as brightly fluoresced GFP signal compared to tissue background with the same morphology as DAPI-marked cells. Counts were averaged across sections per animal and then averaged between quantifiers.

Cohort 2: Immunohistochemistry

Animals followed the same euthanization and tissue processing methods as Cohort 1, except animals were sacrificed at 4 hours post-ROSC and whole brains were sectioned and stored in 12-well plates in cryoprotectant at -20C. For each animal, three 30 µm tissue sections (Bregma -

2.92mm to -3.48mm), which includes the hilus, were chosen from each plate at approximately 360 µm intervals.

For FJB neurodegeneration staining, mounted sections on slides were warmed on a hotplate for 30 minutes at 55°C. In a dipping rack, slides were rehydrated in nanopure water for 5 seconds, dehydrated in an ethanol series, then incubated in: 0.3% Triton X-100 for 3 min, 0.06% $KMnO_4$ for 15 min on an orbital shaker, nanopure water for 1 min, then 0.001% FJB in 0.1% acetic acid with 100µg/mL DAPI for 30 min. Next, sections on slides underwent three washes of nanopure water 1 min each, dried on a hotplate for 10 min at 55°C, cleared in xylenes three times 2 min each, then coverslipped with DPX mounting medium.

For aquaporin-4 (AQP4) and endothelial cell (CD31) immunostaining, free-floating sections were stained at once in 48-well plates to ensure the uniformity of the immunohistochemistry processes for all animals. Two rounds of primary and secondary antibody incubations were performed to allow tyramide signal amplification of both AQP4 and CD31 following similar methods done with microwave treatment[123]. Before each of the following steps, sections were washed in new wells of 1xPBS thrice at 5 min each. On the first day of the experiment, sections quenched with 3% H_2O_2 in 1xPBS twice at 10 min each and blocked in blocking buffer (5% normal donkey serum, 1xPBS, and 0.3% Triton x-100) for an hour. The first round of primary antibody incubations was done using Goat α CD31 (1:50) [R&D Systems; #AF3628] and Mouse α GFAP (1:1000) [Sigma; G-3893] antibody diluted in blocking buffer. Plates were left overnight on a shaker at room temperature. On the second day of immunostaining, sections were incubated in secondary antibodies for direct fluorescence and amplification using Donkey α goat HRP-conjugated (1:500) [ThermoFisher Scientific; #A16005] and Donkey α Mouse Cy3 (1:500)

in blocking buffer for 1 hour. Following incubation, CD31 was visualized using tyramide-Cy5 (1:250) [Akoya Biosciences; #SAT705A001EA] for 25 min. Next, sections were quenched again with 3% H_2O_2 in 1xPBS once for 20 min and rebound with primary antibody Rabbit α AQP4 (1:250) [Sigma-Aldrich; #AB3594] for 45 min. A second round of secondary antibody was performed using Donkey α rabbit biotin-conjugated (1:500) [Fisher Scientific; #PI31821] with 100µg/mL DAPI (1:1000) in blocking buffer for one hour—followed by ABC-peroxidase incubation using 10µL/mL of Solution A in 1xPBS with 0.1% Triton X-100 [Vector Laboratories; #PK-6100] for 30 min. AQP4 was visualized using tyramide-FITC (1:250) [Akoya Biosciences; #SAT701001EA]. Lastly, sections were mounted on gelatin-covered slides and coverslipped under Vectashield [Vector Laboratories; #H-1900] and stored in 4°C temperature within a dark box.

Cohort 2: Imaging and Quantification

Imaging and quantification of Cohort 2 is the same as that for Cohort 1 above using the Keyence BZ-x800. Briefly, imaging settings (exposure, excitation light, magnification) for all sections were kept consistent for intensity quantification. To analyze images, at least two trained quantifiers measured the fluorescence intensity using ImageJ of the hilus and whole hippocampus. For each of the three sections per animal, each quantifier used DAPI staining to identify the region of interest and quantified the mean integrated density of GFAP, AQP4, and CD31. Tissue background was subtracted using the ImageJ rolling ball method. Integrated density values from the three sections were averaged, and the resulting values were averaged between quantifiers.

FJB quantification is the same as described in Cohort 1

Results:

Different etiologies of CA have different hyperemia profiles and outcomes post-ROSC

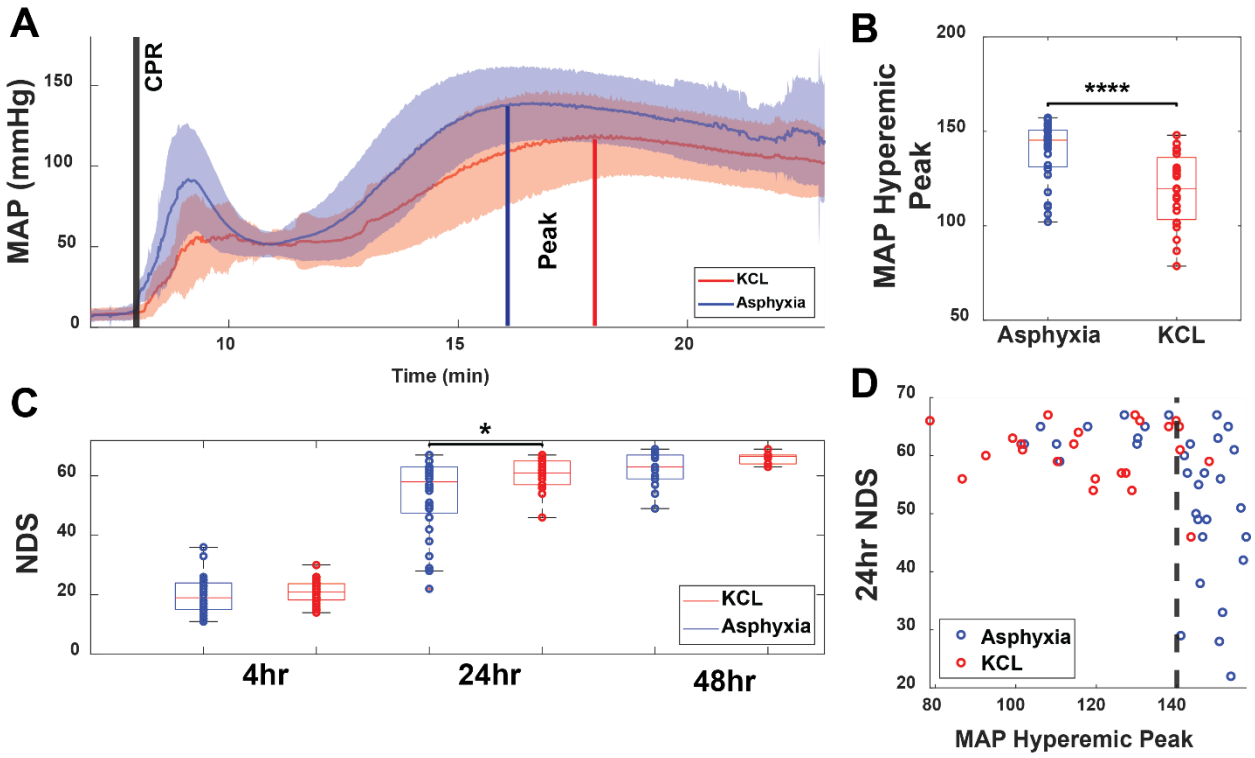

Figure 2. Different etiologies of CA have different hyperemia profiles and outcomes post-ROSC. **A)** shows MAP tracings from CPR for asphxyia and KCL-induced CA rats. The shaded regions show the standard deviation with the solid line indicating the mean. **B)** Unpaired T-test comparing MAP hyperemic peak between asphyxia and KCL groups. **C)** Neurological deficit scale (NDS) at 4hr, 24hr, 48hr post-ROSC for asphyxia and KCL rats. **D)** Scatter plot of MAP hyperemic peak and 24hr NDS (Pearson $p<0.001$, $r=-0.43$). (*=$p<0.05$, ****=$p<0.001$)

Two different methods of inducing CA were performed to mimic various types of CA that occur in real life. Asphyxial CA was induced by asphyxiation (**Fig 2A,** blue tracing) and showed a gradual shutdown of MAP, followed by a large hyperemia. KCl CA was induced with intravenous administration of KCl and produced an immediate shutdown of blood pressure, followed by a lower hyperemia (**Fig 2A**, red tracing). Visually, there was a significant difference in the MAP

profiles during and post an asphyxial and KCl-induced CA. For this study, we chose to focus on the hyperemia which occurred starting from ~11min, which was roughly 2-3min post-ROSC. We simply characterized the hyperemic peak by measuring the peak value of the MAP, which was significantly higher in the asphyxia rats (**Fig. 2B**). Neurological outcome was measured using NDS (**Fig 2C)** for asphyxial and KCl rats at 4hr, 24hr, 48hr, and 72hr post-ROSC. We found that at 4hrs post-ROSC, there was no difference in NDS, while KCL rats had a significantly higher NDS at 24hrs than asphyxial rats ($p<0.05$). However, by 48hrs and 72hrs post-ROSC, the NDS scores were similar between the two groups. 72hr NDS is not shown here as it was similar to the 48hr NDS. Plotting the MAP hyperemic peaks against the 24hr NDS in a scatter plot, we found that there appeared to be a threshold for MAP at around 140 mmHg in which, rats with MAP higher than 140 had variable outcome with many doing poorly, but below 140 mmHg, all the rats had good outcomes, with a Pearson correlation value of $p<0.001$, $r=-0.43$ (**Fig. D**).

KCL CA rats have less astroglial injury while greater hyperemia is associated with greater neuronal death in asphyxia rats

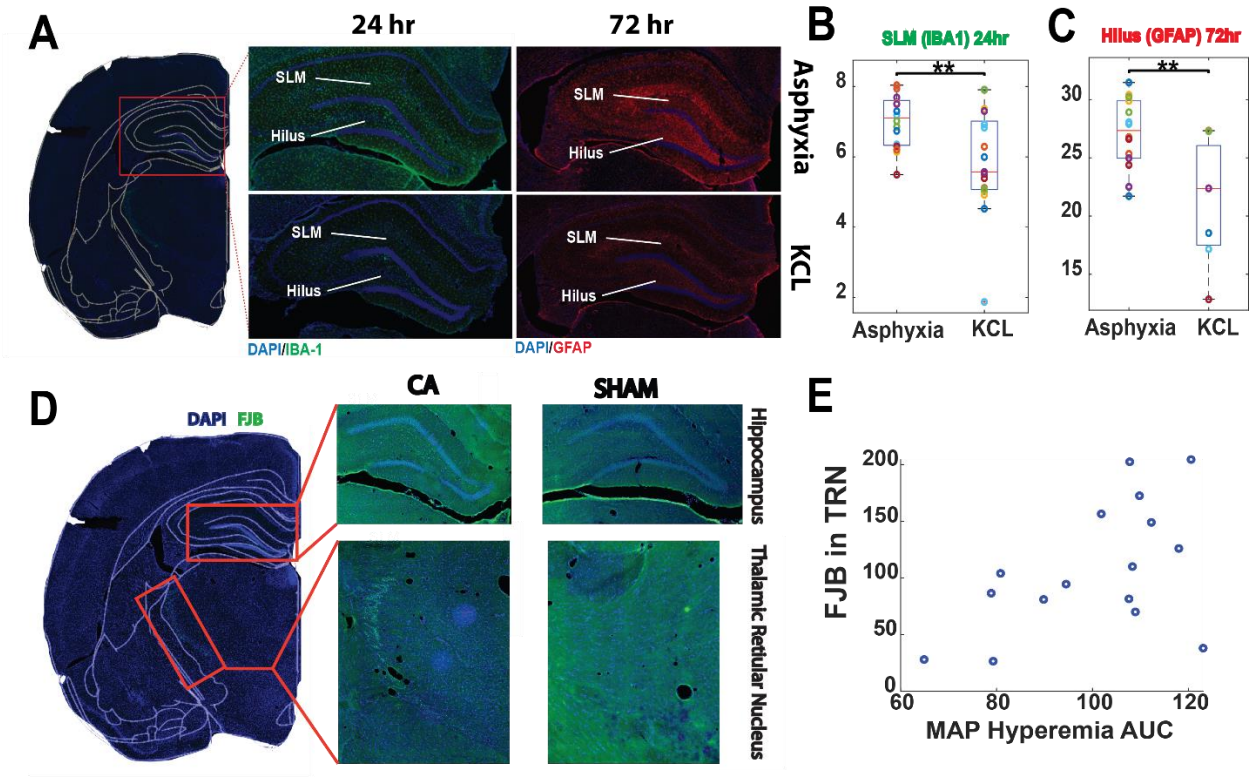

Figure 3. A) Representative images of the hippocampus 24hr and 72hr post-CA. The green shows IBA-1 expression while red shows GFAP. **B)** Unpaired t-test shows greater IBA-1 expression in asphyxial rats than KCL rats at 24hr ($p<0.01$). **C)** Unpaired t-test shows greater GFAP expression in asphyxial rats at 72hr than KCL rats ($p<0.01$). **D)** Representative staining of FJB in hippocampus and TRN in an asphyxial CA and sham rat. FJB is shown in green and DAPI in blue. **E)** Scatterplot of MAP hyperemia AUC vs amount of FJB in the TRN in asphyxial rats (Pearson $p<0.05$, $r=0.51$).

Brain sections of asphyxial and KCL rats of cohort 1 and 2 were stained for astrocyte and microglia activation (with GFAP and IBA-1, respectively) at 24hrs and 72hrs post-ROSC. Expression was most notable in the hippocampus, so this area was the target of our focus in quantification. **Figure 3A** shows expression of microglia and activation in asphyxial and KCL rats in the hippocampus at 24hrs and 72hrs post-ROSC, with subregions SLM and Hilus labeled. Asphyxial rats had significantly greater expression of microglia in the SLM than KCl rats at 24hrs post-ROSC (**Fig. 3B**, $p<0.01$). There was no significant difference between the groups

for astrocytes and microglia expression in the hilus and astrocyte expression in SLM at 24hrs post-ROSC (not shown). However, asphyxial rats greater astrocyte activation at 72hrs post-ROSC than KCL rats in the hilus (**Fig. 3C**, $p<0.01$). There were no significant differences for microglia and astrocyte activation in the SLM at 72hrs and microglia in hilus at 72hrs (data not shown).

Brain tissues of asphyxial and KCL CA rats as well as sham rats were stained with FJB to assess for neuronal death at 24hrs post-ROSC (**Fig. 3D**). Various regions were looked at but the hippocampus and TRN showed the most expression and so were selected to be quantified. It can clearly be seen that there is FJB expression in the asphyxial CA rat in the hippocampus and TRN while there are none in the sham rat. Surprisingly, FJB expression was not different between asphyxial and KCL CA group (not shown). Due to KCL group having not much spread in hyperemia parameters, asphyxial group was the focus of this analysis. We found that greater perfusion during hyperemia (calculated as area under the curve of the MAP) was associated with greater amounts of FJB in the TRN (**Fig. 3E,** $p<0.05$, $r=0.51$). The correlations for hippocampus were not significant.

Greater hyperemic peaks are associated with worse outcome

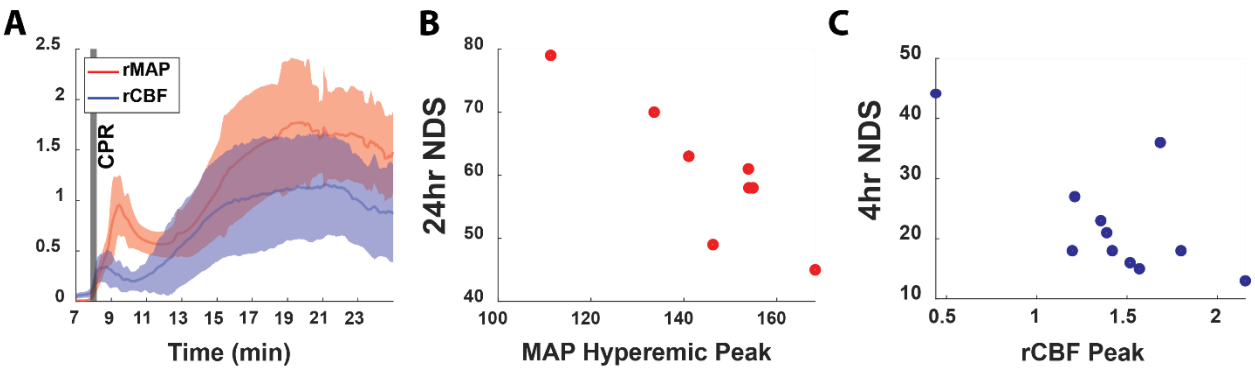

Figure 4. Greater hyperemic peaks are associated with worse outcome. **A)** rMAP (red) and rCBF (blue) traces post-CA. 'r' means normalized to baseline. Solid line is the mean while shaded area is the 1 standard deviation. **B-C)** Scatterplot showing greater MAP and rCBF hyperemic peak is associated with lower NDS (Pearson $p<0.005$, $r=-0.89$ for MAP, and $p<0.05$, $r=-0.68$ for rCBF)**.**

In the asphyxia vs KCL CA groups, none had optical imaging to assess the CBF. As we were assessing neurological outcome, it was important analyze how CBF changed during hyperemia and if it was associated with outcome. Therefore, an additional group of asphyxial CA rats with optical imaging were added to measure cerebral blood flow (CBF) as well as peripheral blood pressure during CA. Qualitatively, CBF appeared to start rising earlier than MAP, although this was not statistically significant (**Fig. 4A**). In general, MAP and CBF rose together into hyperemia, but when CBF came down out of hyperemia, MAP did not show a similarly steep drop. MAP instead gradually decreased out of hyperemia. The relative peak of MAP was significantly greater than the relative peak of CBF, however ($p<0.05$, not shown). The peak values of the MAP hyperemia and rCBF were measured. We found a strong negative correlation between MAP hyperemia peak and 24hr NDS (Pearson $p<0.005$, $r=-0.89$, **Fig. 4B**) and a significant negative correlation between rCBF hyperemia peak and 4hr NDS (**Fig. 4C**). These results suggest that greater hyperemic peaks, cerebrally and peripherally, are associated with worse neurological outcomes. A threshold for MAP hyperemic peak was not noticeable in this group, but it is likely simply underpowered.

Esmolol modulation experiment shows similar pattern with outcome as asphyxia vs KCL-CA

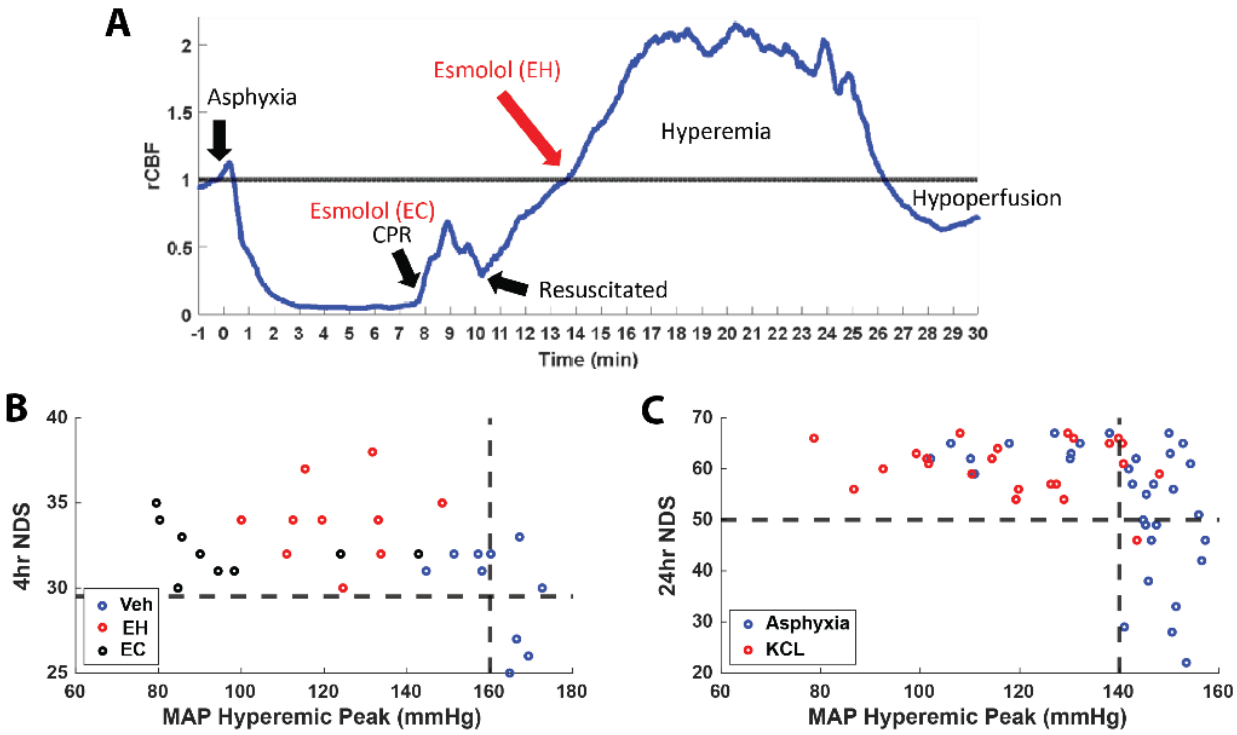

Figure 5. Esmolol modulation experiments show similar pattern with outcome as asphyxia vs KCL-CA. **A)** Tracing of rCBF during the experiment with indications where esmolol was given. **B)** Scatter plot of MAP hyperemic peak and 4hr NDS for Veh, EH, and EC groups. **C)** Scatter plot of MAP hyperemic peak and 24hr NDS for asphyxia and KCL CA groups.

Results from the asphyxia and KCL-induced CA experiments showed that greater hyperemic peaks were associated with worse outcomes and that KCL CA rats had lower hyperemic peaks on average and also better outcomes. To test if this correlation was causal, a cardio-selective beta blocker, esmolol, was infused at two different time points to blunt hyperemia to see if this would improve outcome. **Figure 5A** shows the time course of the experiment and when esmolol would have been infused. **Figure 5B** shows the MAP hyperemic peaks of the vehicle (Veh), esmolol from hyperemia (EH), and esmolol from CPR (EC) groups plotted against 4hr NDS. The esmolol infused groups mimicked the KCL-CA group (**Fig. 5C**) in that they had much lower

hyperemic peaks and also consistently higher NDS scores. These plots show the reproducibility of lower hyperemic peaks being associated with better outcome across different models.

Esmolol blunts MAP, HR, CBF and improves neurological outcome, despite delayed electrocerebral recovery

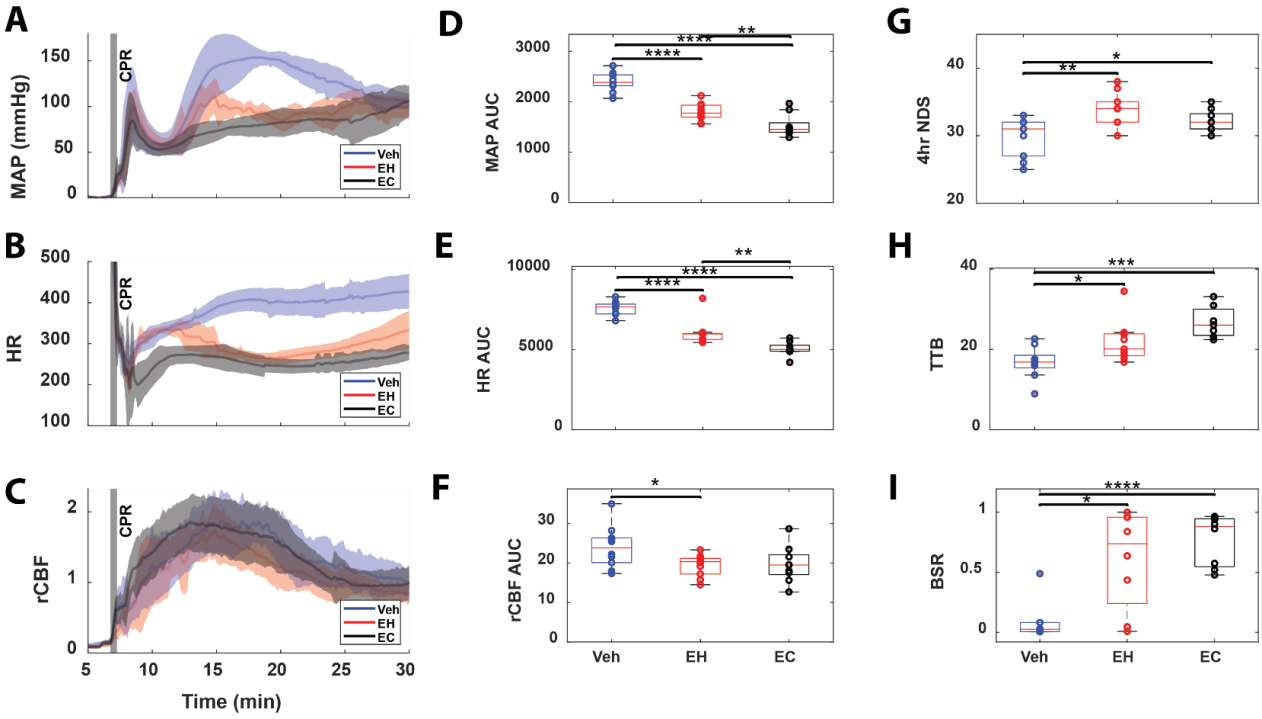

Figure 6. Esmolol blunts MAP, HR, CBF and improves neurological outcome, despite delayed electrocerebral recovery. **A-C)** Traces of MAP, heart rate (HR), and rCBF for each group (Veh, EH, EC) with shaded regions indicating 1 standard deviation and solid line indicating the mean. **D-F)** One-way anova comparison between the three groups for area under the curve (AUC) of MAP, HR, and rCBF, respectively, during hyperemia. **G-I)** One-way anova comparison between the three groups for 4hr NDS, time-to-burst (TTB), and burst suppression ratio (BSR), respectively. (*=p<0.05, **=p<0.01, ***=p<0.005, ****=p<0.001)

To confirm that esmolol worked as desired, we analyzed the MAP, HR, and rCBF traces of each group. MAP of the Veh group showed a noticeable hyperemia whereas in the EH group, as MAP was rising into hyperemia, esmolol blunted it significantly. In the EC group, esmolol was given starting at the beginning of CPR, and so there was not even a rise into hyperemia and the MAP of the entire period was effectively blocked from rising (**Fig. 6A**). Quantifying the area under the curve (AUC) of the hyperemia period showed that Veh group had a significantly greater AUC than EH or EC group ($p<0.001$). The EH group also had a greater AUC than the EC group ($p<0.01$), as expected since esmolol was given earlier in the EC group than the EH group (**Fig. 6D**). The traces of the heart rate (HR) showed the same effect with esmolol(**Fig. 6B**). The rise in HR in Veh group was blunted by esmolol in both EH and EC groups. When the AUC of the hyperemia of the HR traces were quantified, it indeed showed that Veh had the highest HR, followed by EH, then EC ($p<0.001$, $p<0.001$, $p<0.01$, respectively, **Fig. 6E**). For the rCBF traces, it was visually clear as to whether there was significant difference from the esmolol during hyperemia (**Fig. 6C**). However, when the AUC of the hyperemia was measured, the Veh group had significantly higher AUC than the EH group ($p<0.05$), but not the EC group (**Fig 6F**).

To assess if blunting hyperemia with esmolol improved outcome, NDS at 4hr post-ROSC, time-to-burst (TTB), and burst suppression ratio (BSR) at 30-40min post-ROSC were measured. Both esmolol treated groups, EH and EC, had significantly higher 4hr NDS than the Veh group ($p<0.01$, $p<0.05$, **Fig. 6G**). The EC group had the latest TTB, followed by EH group, then Veh group **Fig. 6H**). This is the exact opposite pattern with the MAP and HR AUCs. The two esmolol groups, EH and EC, had significantly higher BSR than Veh as well ($p<0.05$, $p<0.001$, respectively, **Fig. 6I**). These data indicate esmolol reduced hyperemia, improved neurological behavioral outcome, but delayed electrocerebral recovery.

Greater peak metabolism and blood pressure is associated with more neuronal death

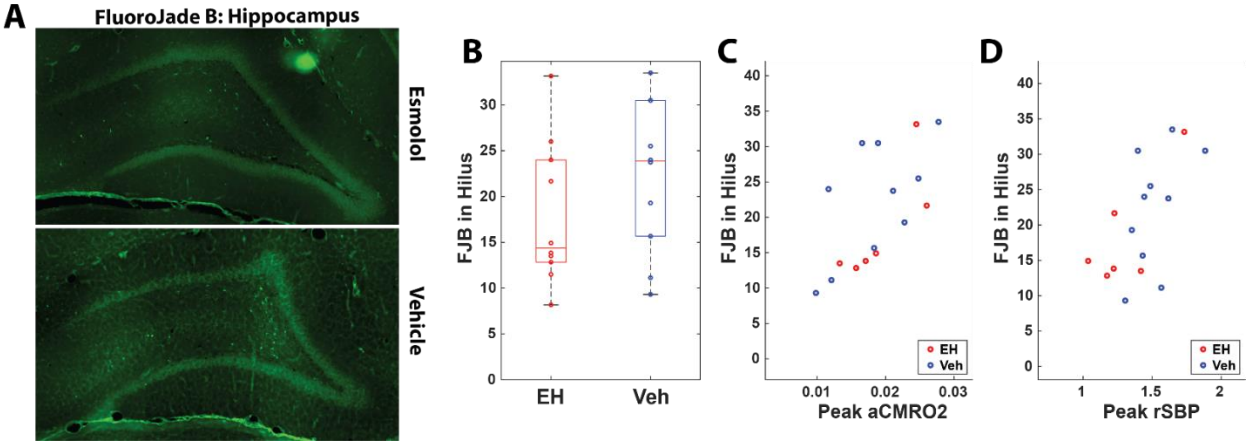

Figure 7. Greater peak metabolism and blood pressure is associated with more neuronal death. **A)** Representative images of Fluorojade-B (FJB, green) stained hippocampal sections for a EH and Veh rat. **B)** Unpaired t-test for FJB between EH and Veh group. **C-D)** Scatter plot of hyperemic peak of absolute CMRO2 (aCMRO2) (Pearson $p<0.008$, $r=-0.636$) and systolic blood pressure normalized to baseline (rSBP). (Pearson $p<0.007$, $r=-0.644$.)

As a histological marker of outcome, we stained the brain sections with Fluorojade-B (FJB), a marker for neuronal death at 4hr post-ROSC. The hippocampus showed FJB, but surprisingly, the expression level was not different between EH and Veh groups, although there appeared to be a trend towards EH group having less FJB than Veh (**Fig. 7A**). Interestingly, we also noticed that a greater hyperemic peak of the absolute CMRO2 (aCMRO2) and the relative systolic blood pressure (rSBP) were correlated with greater expression of the FJB in the hilus of the hippocampus (Pearson $p<0.008$, $r=-0.636$, $p<0.007$, $r=-0.644$, respectively, **Fig. 7C-D**). Unexpectedly, CBF was not correlated with FJB expression.

Esmolol reduces the body and brain's metabolism, which is sustained after infusion is stopped

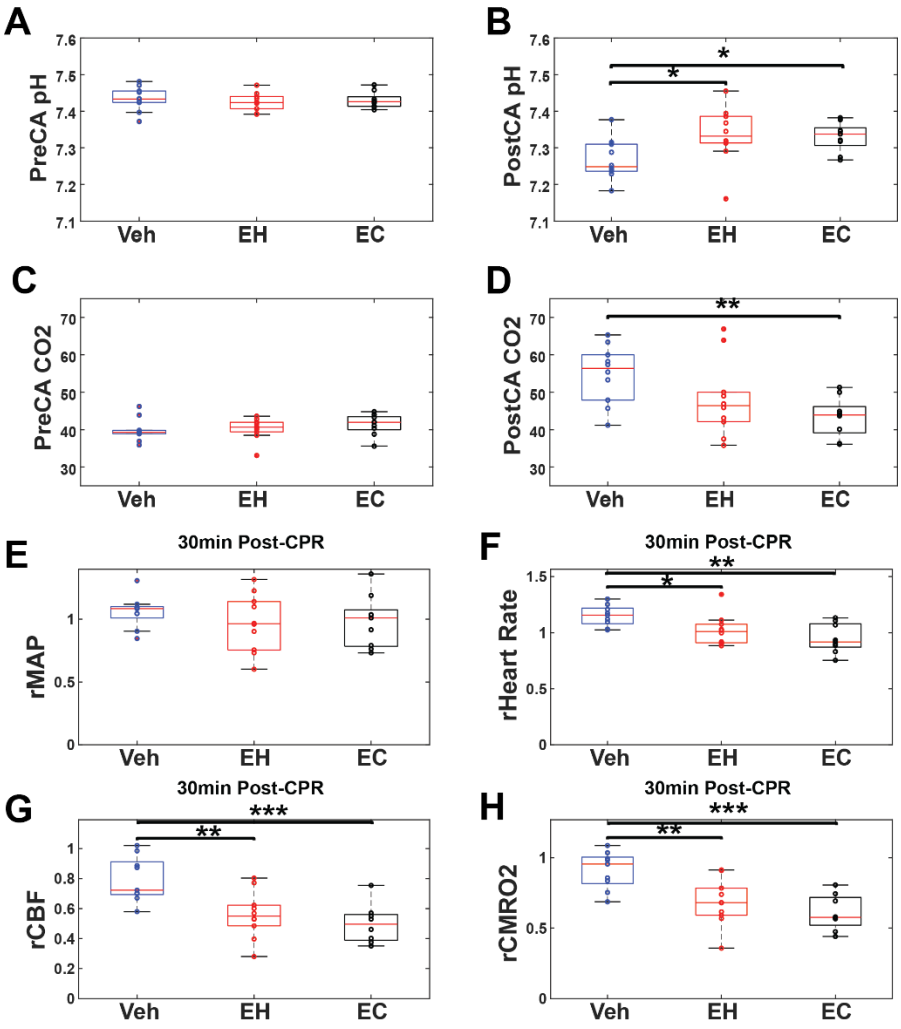

Figure 8. Esmolol reduces the body and brain's metabolism, which is sustained after infusion is stopped. **A-B)** One-way anova comparison between groups (Veh, EH, EC) for pre-CA and post-CA arterial blood pH. **C-D)** One-way anova comparison between groups for pre-CA and post-CA partial pressure of arterial blood CO2 in mmHg. **E-H)** One-way anova comparison between groups for rMAP, rHR, rCBF, rCMRO2, respectively, at 30 min post-CPR with 'r' indicating normalization to baseline. (*=p<0.05, **=p<0.01, ***=p<0.005, ****=p<0.001)

The prior results showed that esmolol had the desired effect of blunting hyperemia and improving outcome. To understand the possible mechanism of improved outcome, we also analyzed the arterial pH and partial pressure of CO2. **Figure 8A** shows pre-CA baseline arterial

blood pH values for each of the groups. The pH for the groups were close to 7.4, a normal physiological pH value. Post-CA, around 10-15min post-ROSC, the arterial blood pH for Veh group was very low, as expected (**Fig. 8B**). However, the EH and EC groups had a higher pH than the Veh group ($p<0.05$), and the pH was closer to 7.4, a normal value. The arterial partial pressure of CO2 at baseline prior to CA is shown in **figure 8C.** All three groups are roughly around 40 mmHg for CO2, which is a normal physiological value. Post-CA, the Veh group has a much higher CO2 compared to pre-CA as expected as seen in **figure 8D**. The Veh group had a higher CO2 level than the two esmolol groups post-CA, although only statistically significant with the EC group ($p<0.01$). Following, we decided to see if there were any sustained effects of esmolol. We measured the levels rMAP, rHR, rCBF, and rCMRO2, at 30min post-ROSC (after infusion of esmolol had been stopped) (**Fig. 8E-H**). 30min post-ROSC, the MAP of the Veh group was not significantly different from the two esmolol groups. However, the rHR, rCBF, and rCMRO2 of the two esmolol groups were significantly lower than the Veh group ($p<0.05$).

Vessel compensates for reduced MAP to maintain CBF in EC group

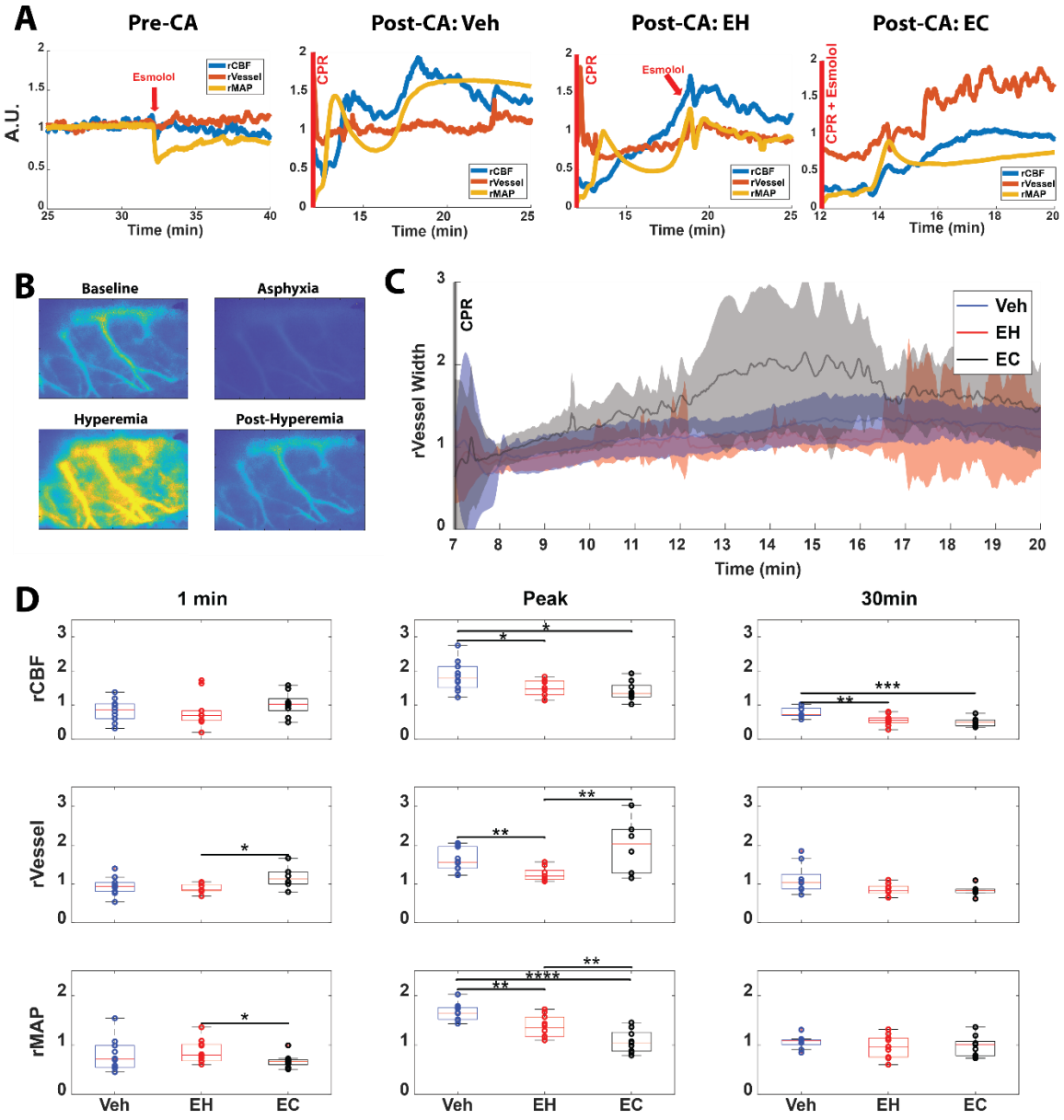

Figure 9. Vessel compensates for very reduced MAP to maintain CBF in EC group. **A)** Representative traces of rCBF, rVessel width (rVessel) and rMAP during pre-CA and Post-CA for each treatment group. **B)** Representative images of speckle flow acquired from LSI showing CBF and vessels during baseline, asphyxia, hyperemia, and post-hyperemia. **C)** Post-CPR traces of vessel width normalized to baseline for each group. Shaded region indicates 1 standard deviation and solid line indicates the mean. **D)** One-way anova comparisons between each group for rCBF, rVessel, and rMAP at 1min post-ROSC, hyperemic peak, and 30 min post-ROSC. (*=p<0.05, **=p<0.01, ***=p<0.005, ****=p<0.001)

Although esmolol had the expected large and significant effect on reducing MAP and HR, the effect on CBF was not similarly as pronounced. We predicted that the vessels must be

compensating and regulating CBF, and thus looked into vessel diameter changes post-ROSC. **Figure 9A** shows traces of rCBF, rMAP, and rVessel (normalized vessel width) of representative rats at pre-CA and post-CA for each of the groups. In the pre-CA tracing, when esmolol is given in a bolus, the MAP drastically drops, but the rCBF does not, as expected. In the vehicle and EH group post-CA, the vessel width did not change much or followed the changes in MAP, along with rCBF. However, in the EC group post-CA, despite the MAP going down, the vessel width was increasing, with a rise in rCBF as well. **Figure 9B** shows representative images of the speckle flow of the optical window during baseline, asphyxia, hyperemia, and post-hyperemia time periods of the experiment. There was a clear increase in the flow and width of the vessels during hyperemia compared to the other time periods. **Figure 9C** shows the traces of the rVessel, rCBF, and rMAP for each of the groups. At a glance, it is clear that the EC group has a much a higher increase in vessel diameter during hyperemia than the other two groups. We measured the rCBF, rVessel, and rMAP at 1min post-ROSC, hyperemic peak, and 30min post-ROSC to see how these parameters responded to hyperemia and to esmolol (**Fig. 9D**). At 1min post-ROSC, only the EC group had a significantly lower MAP ($p<0.05$) since it was the only group to receive esmolol this early. Despite reduced MAP, the vessel width of the EC group increased significantly compared to EH group ($p<0.05$), and the CBF did not significantly change compared to other groups. At the hyperemic peak, the EC group had the lowest MAP, followed by EH, and Veh ($p<0.01$). The EH group did not seem to have much vessel width change as it was close to 1 while the other two groups were significantly higher ($p<0.01$). For CBF, the two esmolol groups had significantly lower CBF than the Veh group ($p<0.05$). At 30min post-ROSC, after esmolol infusion had already been stopped for around 10-15min, there was no difference in the MAP across all groups. The two esmolol groups seemed to have lower vessel width than the Veh group, but was not statistically significant. Lastly, for CBF, the Veh group was significantly higher than the two esmolol groups ($p<0.01$).

Esmolol blocks rise in pulsatility

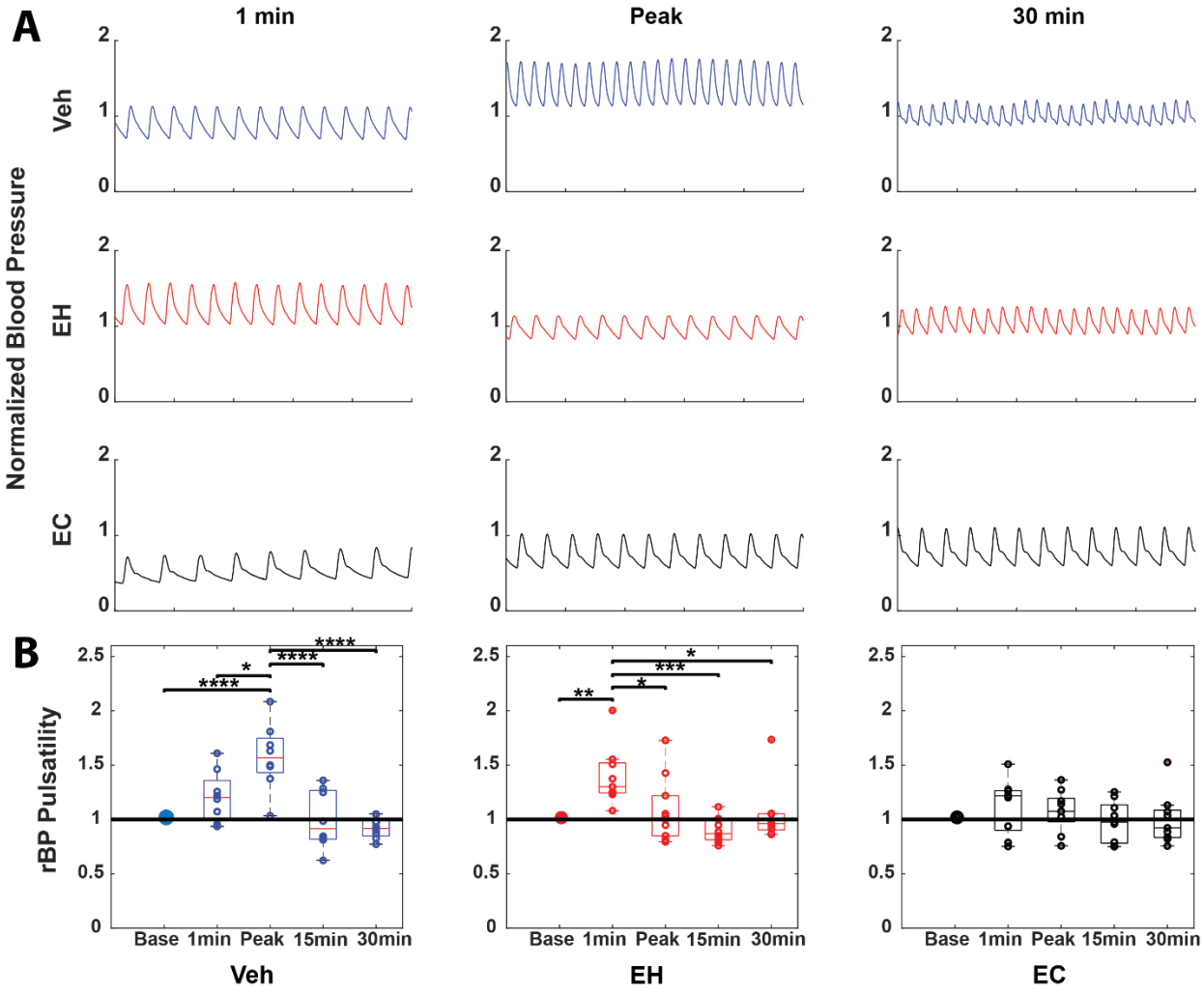

Figure 10. Esmolol blocks rise in pulsatility post-CA. **A)** Traces of pulsatile blood pressure waveforms for each group (Veh, EH, EC) at 1 min post-ROSC, hyperemia, and 30 min post-ROSC. **B)** One-way anova comparisons of blood pressure pulsatility normalized to baseline across time points for Veh, EH, and EC groups respectively. (*=p<0.05, **=p<0.01, ***=p<0.005, ****=p<0.001)

In regards to mechanisms of hyperemia affecting recovery, we decided to look into pulsatility of the blood pressure during hyperemia as increased pulsatility increases the shear stress on the vessels and may injure them. **Figure 10A** shows the pulsatile wave forms of the blood pressure for each group at 1min post-ROSC, hyperemic peak, and 30min post-ROSC. At 1min post-ROSC, qualitatively, it can be seen that the only group that has received esmolol at this point, the EC group, has a smaller pulse amplitude as well as a slower heart rate. At the hyperemic peak, the pulse amplitude and heart rate rises noticeably in the Veh group, but this rise is blunted in the two esmolol groups. At 30min post-ROSC, the pulsatile waveforms did not changed for the esmolol groups, but the amplitude noticeably became smaller in the Veh group. The pulsatile amplitudes, normalized to baseline, were measured as 1min averages at 1min post-ROSC, hyperemic peak, 15min post-ROSC, and 30min post-ROSC (**Fig. 10B**). The pulse amplitude increased over time up to the hyperemic peak and then decreased over time to the 30min time point in the Veh group. In the EH group, the pulse amplitude increased at 1min, as there was no esmolol infused at this time, but then decreased back to baseline by the hyperemic peak and remained at this level until the 30min post-ROSC time point. In the EC group, as esmolol was being infused since CPR, the pulse amplitude did not increase above baseline levels the entire time post-ROSC.

Greater hyperemia is associated with decreased astrocyte activation, vascularity, and increased edema

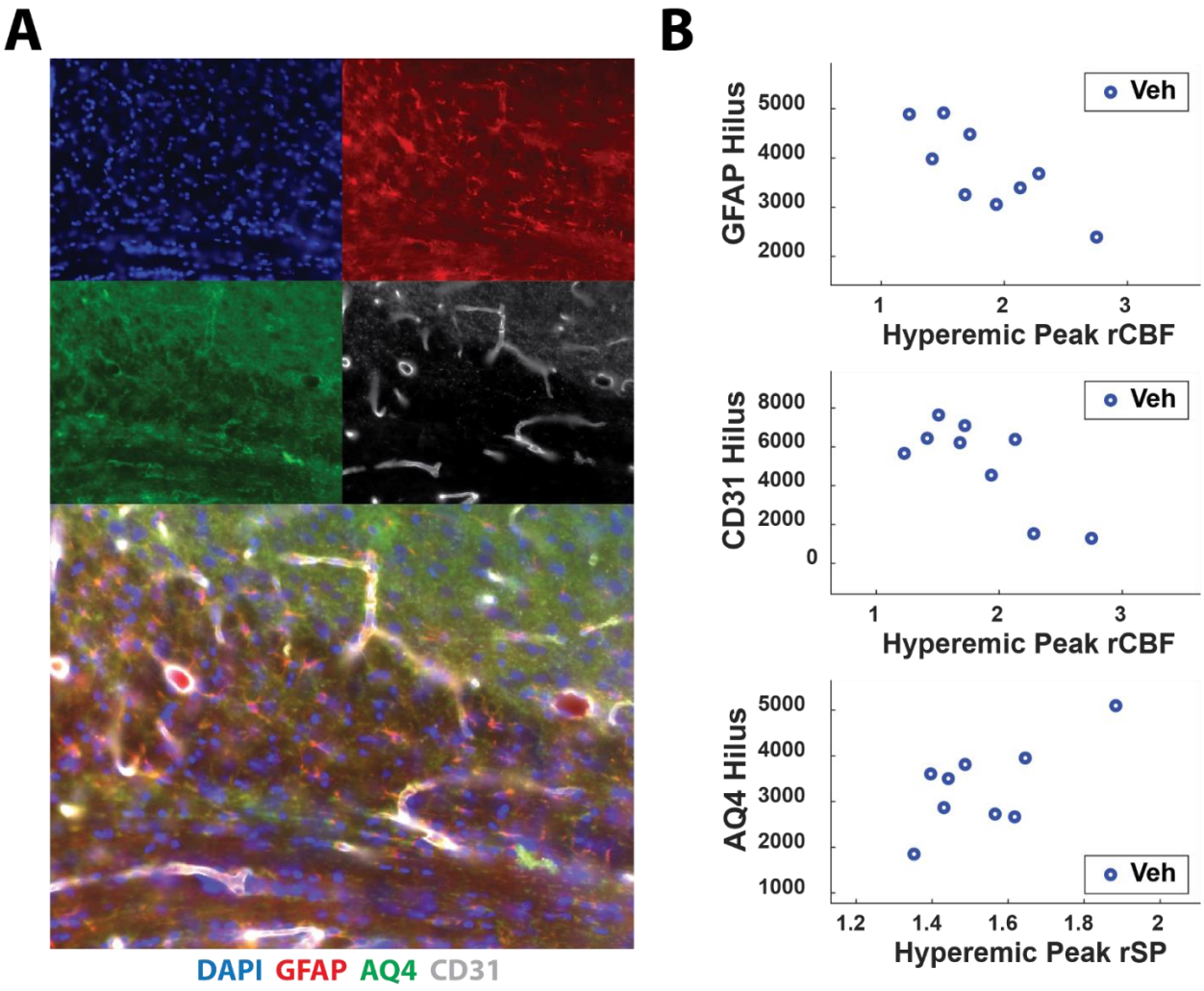

Figure 11. Greater hyperemia is associated with decreased astrocyte activation, vascularity, and increased edema. **A)** Representative image of a rat hippocampus at 60x magnification stained with DAPI (blue), GFAP (red), Aq4 (green), and CD31 (grey). **B)** Scatter plots of rCBF at hyperemic peak compared to fluorescence intensity of GFAP (Pearson $p<0.01$, $r=-0.80$), CD31 (Pearson $p< 0.013$, $r=-0.78$) and rSP at hyperemic peak compared to AQ4 at the hilus (Pearson $p<0.05$, $r=0.69$), respectively.

Finally, the blood brain barrier being impaired and there being edema after cerebral ischemia is well known. Therefore, we looked at some histological markers associated with blood brain barrier such as GFAP for astrocytes and CD31 for endothelial cells. We also looked at the degree of edema using the aquaporin-4 (AQ4) marker (**Fig. 11A**). Surprisingly, there were no significant differences in GFAP, CD31, or AQ4 between Veh and EH groups. The level of

expression of these markers were correlated with the hyperemic peaks of CBF and blood pressure (**Fig. 11B**). Hyperemic peak of rCBF was negatively correlated with the level of GFAP and CD31 in the hilus (Pearson $p<0.01$, $r=-0.80$, Pearson $p<0.013$, $r=-0.78$, respectively). Greater hyperemic peak of blood pressure was associated with more AQ4 in the hilus (Pearson $p<0.05$, $r=0.69$).

Discussion:

Different etiologies of CA have different blood pressure profiles and outcomes post-ROSC

CA does not occur the same way for every patient, which leads to different etiologies of CA clinically. In our study, we modeled two different types of CA: asphyxia-induced and KCL-induced. Asphyxial CAs mimic CAs that occur naturally in humans due to drowning and other forms of suffocation, while KCl CAs may mimic sudden cessation of the heart from drug use, electrical shock, etc. Here, in **Figure 2A**, we saw that CAs of different etiologies also had different blood pressure profiles going into and coming out of CA. Following resuscitation with CPR, in asphyxial CA, we saw a much greater hyperemia peak compared to that in KCL CA (**Fig. 2B**). Not only this, the KCL CA rats had faster neurological recovery compared to asphyxial CA rats (**Fig. 2C**). A different blood pressure profile in addition to a difference in neurological recovery suggests that CAs of different etiologies potentially warrant different approaches in treatment and care.

We found not only that lower hyperemia was associated with better outcome, but that there may be a specific threshold as well (**Fig. 2D**). We found a MAP of 140 mmHg to roughly be the threshold for hyperemia, where animals that had values at or below the threshold all had good neurological outcomes, while those above the threshold had a variable range of outcomes from good to poor. This may point to a threshold for reperfusion injury, in which exceeding this threshold leads to cerebral-autoregulation failure, [124,125,] a leak through an impaired blood-brain-barrier, and brain edema [126–128]. There are also studies that have shown that reactive oxygen species (ROS) accumulates and peaks within 30 min of post-ROSC after CA [43,44]. That may suggest that greater hyperemia may increase circulation of oxygen, thus leading to a burst in ROS, contributing to reperfusion injury and worse outcome. Interestingly, this MAP threshold was only noticeable in the asphyxial CA rats, but not in the KCL CA rats. However, this may simply be due to the fact that all the KCL CA rats had MAP hyperemic peaks around 140mmHg or lower. Therefore, it is possible that KCL CA rats may have the same threshold for outcome, despite not being obvious if seen independently.

As we were investigating neurological outcome, besides peripheral perfusion, it was important to look at CBF as well. We found the CBF had the same pattern of hyperemia like peripheral blood pressure (**Fig. 4A**). The CBF hyperemic peak also similarly correlated negatively with neurological outcome, like MAP (**Fig. 4B-C**). It is well known that cerebral autoregulation is impaired after ischemic injury. This likely explains why CBF rises excessively along with MAP.

Astroglial and neuronal death in different etiologies of CA

Neuronal and astroglial injury, inflammation[129,130], and cell death post-ischemia is known to be a contributing factor of reperfusion injury. As expected, we saw astroglial injury and inflammation

as shown by expression of activated astrocytes and microglia in both asphxyial and KCL CAs. For both, we saw an increase in astrocytic injury over time from 24hr to 72hr post-CA, which suggests that there may be active ongoing astrocytic injury for a period of days following CA. In addition, we saw greater astroglial injury in asphyxial CA rats at both 24hrs and 72hrs post-CA compared to KCL CA rats (**Fig. 3A-C**). Considering that at 24hrs, asphyxial CA rats had a worse NDS score, astrocytic injury may be an important contributing factor for the poorer outcome. Although we do not know why KCL CA rats would have less astrocytic injury, one possible mechanism could be that because they have less hyperemia, inducing less overall reperfusion injury (via less oxygen and ROS or others), which may lead to less activation of astrocytes and microglia. As for neuronal injury, we did not find any differences between the asphyxial and KCl CAs. However, this could be because FJB expression is greatest at 72hr post-injury while we euthanized and stained at 24hr post-injury. There also appeared to be a positive correlation between greater total perfusion during hyperemia with the amount of neuronal death (**Fig. 3E**). Similar to the previous reasoning, it is possible that a greater perfusion causing direct perfusion injury and/or contribution of increased astroglial injury may compromise neuronal survival, thus leading to greater neuronal death.

Esmolol blunts MAP, HR, CBF and improves neurological outcome, despite delayed electrocerebral recovery

Based on the results showing that KCl CA rats that had less hyperemia than asphyxia CA rats had better outcomes, and that hyperemia correlated with outcome as well, we tested to see if the relationship between hyperemia and injury was causal. In this study where we gave esmolol infusions to block hyperemia, we found a similar correlation and pattern that was seen with the asphyxia and KCl CA groups (**Fig.5 B-C**), which suggested that this relationship between hyperemia and outcome is consistent across different models.

Esmolol infusion had the desired effect of reducing BP, HR, and CBF and improving behavioral neurological outcome (**Fig. 6**). However, there was a noted difference in the CBF during hyperemia between EH and EC groups. Although both esmolol groups had lower total CBF during hyperemia than the Veh group, only the EH group was significantly lower (**Fig. 6C**). This could be due to the fact that esmolol improves the ultrastructure integrity of cerebral microvasculature[51], thus improving CBF. Since esmolol reduced the perfusion pressure significantly, the overall CBF dropped, but in the EC group, which received esmolol from onset of CPR, their microvasculature integrity was likely more preserved, leading to slightly improved CBF compared to EH group, that received esmolol later. For outcome, besides NDS, we had two electrocerebral measures to assess recovery. Time-to-burst (TTB) of electrocerebral activity was significantly later in the EC group compared to EH, and Veh, and EH was later than Veh (**Fig. 6H**). This means that the electrocerebral recovery was slower in the esmolol groups. This matches the amount of perfusion pressure in these groups. Lower perfusion pressure appeared to lead to later TTB. This suggests that, whether quickly or slowly, there may be a certain amount of total perfusion necessary to 'start' the brain again. Burst suppression ratio (BSR) was also higher in the two esmolol groups compared to Veh (**Fig. 6I**), meaning that the brain activity was more suppressed. This follows the same logic as for TTB, where lower perfusion led to longer time to resume electrocerebral activity. Traditionally, a delayed electrocerebral recovery is considered to be associated with worse neurological outcome, but in this case, as it may be caused directly by reduced hyperemic perfusion, it may not be the case. Furthermore, the reduced perfusion may induce a hibernative state, and allowing for a more gradual wake up of the brain, rather than forcibly waking it, which may be beneficial.

Although we saw an improvement in NDS in the esmolol groups, we did not find a difference in the histological marker for neuronal death between the EH and Veh groups (**Fig. 7B**). There

was a trend of EH group having less neuronal death, but it was not statistically significant. The lack of difference could be due to the early 4hr time point of the stain, which could have been too early to show the peak amount of neuronal death. However, we found that a greater peak of cerebral metabolism and perfusion pressure during hyperemia was associated with more neuronal death in the hilus of the hippocampus (**Fig. 7C-D**). This further suggests that greater hyperemia is injurious and that having a greater cerebral metabolism may be worse for recovery.

Esmolol reduces the body and brain's metabolism and the effect is sustained

In addition to direct perfusion mediated injury, we sought other potential mechanisms responsible for esmolol's effect on neurological outcome. As hinted at earlier, esmolol seemed to reduce metabolism. Arterial blood analysis showed that the pH and the partial pressure of CO2 (PaCO2) post-CA were more normal in the esmolol groups than the vehicle group (**Fig. 8A-D**). During asphyxia and cardiac arrest, the remaining O2 is consumed, and CO2 is produced. Because CO2 cannot be exhaled, it continues to accumulate. This leads to high levels of PaCO2, making the pH lower, or more acidic. This is seen in the vehicle group which had low pH (~7.25) and high PaCO2 (~57 mmHg). However, in the esmolol groups, the pH was higher and closer to normal, which is 7.35-7.45. This made sense as PaCO2 was also lower and closer to normal, which is 35-45 mmHg. The duration of asphyxia and ventilation settings were kept the same across all rats and groups, so the lower PaCO2 is likely due to decreased production of CO2, rather than reduced clearance of CO2. Since, CO2 production is strongly tied to the metabolic state of the cells, esmolol likely reduced metabolism. Esmolol, a cardio-selective beta blocker acts on the heart to reduce the heart rate and contractility, which reduces

the overall work done by the heart. This helps to explain the reduced CO2, but we found that in addition, the effect of the esmolol was sustained even after infusion was stopped. At 30min post-ROSC, after infusion was stopped, the MAP was not different between groups but the heart rate, CBF, and CMRO2 were lower in the esmolol groups (**Fig. 8E-H**). MAP may not have been different due to vasoconstriction of vessels to maintain blood pressure. But with heart rate, CBF, and CMRO2 being lower in the esmolol groups post-infusion, this further supports that esmolol has a sustained effect on reducing metabolism in the body and brain. This reduced metabolism may potential induce a hibernative state, allowing for a more gradual recovery.

Esmolol may protect the cerebral vasculature and preserve some cerebral autoregulation post-CA

We saw that in Veh groups, the CBF rose with MAP during hyperemia, indicating lack of cerebral autoregulation. This is in line with literature showing that cerebral autoregulation is not intact following ischemic injury[124,125,131–133]. Therefore, when we infused esmolol to blunt MAP, we expected to see a similarly large drop in CBF and disappearance of hyperemia's bell-shaped curve. However, we were surprised to see that CBF did not drop as much as MAP and the hyperemia's bell-shaped curve was still present (**Fig. 6C**). Therefore, we suspected that the cerebral vessels were compensating to maintain CBF and analyzed the changes in cerebral vessel width over the time course of the CA experiment (**Fig. 9C**) and found that the EC group had significant vasodilation compared to the EH and Veh groups. At 1 min post-ROSC, only the EC group was receiving esmolol, and therefore had lower MAP than the other groups. However, the EC group also had increased vessel width indicating vasodilation in response to the reduced MAP (**Fig 9D**). Due to this, the CBF appears to be maintained and is similar to the other groups.

This response of the vessel to the reduced MAP to maintain CBF shows functioning cerebral autoregulation. The interesting part comes during the peak of hyperemia where despite the EH and EC group are receiving esmolol and both have reduced MAP compared to Veh, but only the EC group has a significant vasodilation. A prior study showed that after cardiac arrest, ultrastructure integrity of cerebral microvasculature is impaired, possibly due to epinephrine, but this effect is rescued by bolus esmolol given during CPR[51]. So, the EC group that received esmolol starting from CPR, likely received a protective effect on the vessels, preserving its ability to vasodilate. The EH group, that received esmolol later, roughly 5min post-ROSC, did not seem to be able to vasodilate well in response to the reduced MAP, suggesting that the esmolol must be administered very early, if not at the start of CPR, to show any protective vascular effects. In fact, the EH and Veh group's vessels seemed to lack any autoregulatory function and appeared to just passively dilate and constrict due to perfusion pressure, which also determines the CBF. This is supported by the fact that at the hyperemic peak, the EH group's rMAP, rVessel, and rCBF are roughly ~1, and for the Veh group, they are around ~1.5. The MAP, vessel, and CBF appeared to coupled (moving together). In the EC group, these parameters are not coupled, and in fact the rMAP is below 1, while rVessel is greater than 1, indicating active vasodilation, not passive, to achieve rCBF of ~1.

Esmolol in the EC group may protect vessels by offsetting vasoconstriction that occurs from epinephrine given during CPR or via its effect on cerebral adrenergic system. Epinephrine is an alpha receptor agonist and has been shown to increase vasoconstriction in cerebral microvasculature[134–136], causing capillary stalling (no-reflow), likely due to collapse of the vessel. Landiolol, a selective beta-1 blocker like esmolol, has been shown to block norepinephrine release in the brain, offsetting vasoconstriction produced by norepinephrine, as well as directly causing vasodilation of the cerebral microvasculature through the endothelium hyperpolarization

pathway[49,137]. In the EC group, by preventing the early vasoconstriction post-ROSC, the vessels may not be subjected to potential permanent collapse, preserving its ability to vasodilate later on. In the EH group, due to early vasoconstriction, and possible collapse/injury to vessels, even when esmolol is given later on, the vessels may not be able to achieve much vasodilation.

In addition to esmolol effects on perfusion pressure and vessels, it also seemed to reduce pulsatility (**Fig. 10**). Greater perfusion pressure directly increases shear stress on the vessels[138–140], but a greater pulsatility also increases shear stress and is associated with greater injury after ischemia and reperfusion[111]. After ROSC, pulsatile amplitude rises and peaks during hyperemia and eventually returns to roughly baseline. In EC group, this rise in pulsatility was completely blocked, while in the EH group, pulsatile amplitude rose before esmolol was administered. In addition to rise in perfusion pressure, this rise in pulsatility may be a contributing factor on producing shear stress injury to the vessels, impairing its ability to autoregulate CBF.

Greater hyperemia is associated with decreased astrocyte activation, vascularity, and increased edema

We sought to figure out if esmolol improved the blood-brain barrier integrity and reduced edema. We did not find any difference between EH and Veh groups, but this could be due to the fact that the EH group did not seem to receive much vascular protection. The EC group was not histologically analyzed. However, we expect that it would have greater vascularity and lower edema than the EH and Veh groups. In the Veh group, we found that greater hyperemic peaks of the CBF were correlated with lower levels of astrocyte activation and endothelial cells/vessels, in the hilus of the hippocampus (**Fig 11B-C**). For vessels, if the CBF is high, it could cause injury to the vessels, so it made sense that there was a lower abundance of

vessels. GFAP, a marker of astrocyte activation, is commonly used as a marker for glial injury, or broadly, brain injury. However, astrocyte activation isn't always a harmful process and is sometimes needed to respond to injury appropriately[141]. Studies have shown that after ischemic injury, greater astrocyte activation was associated with greater vascular density, vascular repair/angiogenesis[142]. This process was also impaired without the presence of astrocytes. Considering this, lower astrocyte activation here likely indicates an impaired vascular repair process. Lastly, we found that in the Veh group, greater perfusion pressure was associated with greater aquaporin-4, a water channel commonly used as a marker of edema (**Fig 11D**). This suggests that greater perfusion pressure during hyperemia was associated with greater edema, which makes sense and is supported by the fact that it is well known that there is edema after ischemia-reperfusion.

Conclusion:

In this study, we analyzed various hemodynamic and metabolic parameters during hyperemia post-CA in two naturally different CA models, then tested if hyperemia led to worse outcome, and investigated the possible mechanisms underly hyperemia's role in outcome. While there are many studies investigating blood pressure and perfusion after resuscitation from cardiac arrest, most studies targeted the hypotensive phase that occurs after the hyperemia phase[30–34]. Our study shows for the first time that this very dynamic period within the first 30 min post-resuscitation is associated with outcome with potential implications for precision blood pressure targeted therapies in CA patients. We also show for the first time that esmolol given during CPR may protect vascular function and preserve some cerebral autoregulation. This suggests hyperemia is a large contributor to reperfusion injury and that esmolol treatment at the

beginning of CPR and blunting hyperemia may be potential therapeutic strategy to improve neurological outcome post-CA. In conclusion, this work shows the importance of further investigation into hyperemia as a potential therapeutic target for cardiac arrest and cerebral ischemic injuries.

Limitations:

There were some limitations to these studies that we hope to address in future experiments. Although esmolol was used intending to greatly modulate CBF during hyperemia through modulation of perfusion pressure, the effect was less than expected. A future study should try modulating CBF during hyperemia by targeting not only the heart for perfusion pressure, but the vasculature directly as well. We noticed some cerebral autoregulation post-ROSC in the EC group, but we did not target and identify the limits of autoregulation which would show to what extent autoregulation is intact. We did not assess the blood-brain barrier integrity by directly assessing the extent of edema as well as endothelial injury through morphology. Lastly, this study was limited by the early time points of recovery, assessing at 4hr post-ROSC. Many markers of injury and recovery tend to be more expressed in the days to weeks post-injury, so although we glimpsed at the very early period of recovery, it is uncertain as to whether these treatments would have longer term benefits.

Chapter 4

Hyperemia Following Resuscitation From Cardiac Arrest May Be A Major Contributor to the Burst of ROS During Reperfusion

Authors: Han SW, Yi J, Bazrafkan A, Rafi M, Liu A, Nasouri F, Suayngam K, Avilez A, McCluskey K, Vu M, Wilson RH, Akbari Y

Introduction:

Roughly every 40 seconds, an American will suffer from a cardiac arrest[1], and more than 800,000 people/year suffer from cardiac arrest (CA) in the US[2] and is treated with cardiopulmonary resuscitation (CPR), but in-hospital survival is only around ~15% and out-of-hospital survival is even lower[3], making CA a large burden to society and a public health concern. Despite 40 years of advancements in medicine and care, survival for CA patients have not improved[4]. One of the large contributing factors is the debilitating long-term neurological impairments[5]. Neurological recovery is a major determinant of outcome for CA survivors[6], however, there are no reliable treatments targeting neurological recovery after CA. CA and its recovery is a complex process involving many different body systems.

Patients often have pulmonary dysfunction after cardiac arrest and thus it is common to be mechanically ventilated during post-resuscitation to reduce the work of breathing until the patient can efficiently breath spontaneously. Although patients are recommended to be resuscitated on 100% O2, afterwards, it is recommended that ventilation be adjusted such that the pulse oximeter reads oxyhemoglobin saturation of between 94-96%. Pulse oximeter can read 100% when the PaO2 is between 80-500 mmHg, which is a very wide range[143]. In animal

models, it is shown that high oxygen levels lead to greater production of ROS and is worse for outcome[70,71], the inhaled oxygen levels is suggested to be lowered to the minimum necessary to maintain pulse oximeter reading of >94%. However, the optimal levels of inspired oxygen is still up for debate in humans as clinical data has been inconsistent, with some studies indicating excessively high arterial oxygen concentrations being harmful[144–146], while others did not[147–149]. Production of ROS is a well known contributor of reperfusion injury[44,53,150]. It is possible that the excessive arterial concentrations of oxygen from hyperoxygenation post-ROSC is contributing to the production of ROS and related injury.

Previously, we have shown that hyperemia immediately following return of spontaneous circulation (ROSC) was associated with worse neurological outcome and that blunting hyperemia with a cardio-selective beta blocker, esmolol, improved outcome. We suggested that reducing hyperemia may have improved outcome by reducing direct perfusion injury to the vasculature and tissue. However, the reduced circulation of other substances, such as oxygen, may be a factor as well. In fact, burst of ROS during reperfusion coincides with the timing of hyperemia in an in vitro model[44] and swine model of CA[43], within 30 minutes of reperfusion in both models. Thus, it seems possible that hyperemia is increasing the circulation of oxygen, providing excess oxygen to mitochondria that are dysfunctional following ischemia[53,150,151], to generate the burst of ROS.

As previously mentioned, the current standard of treatment after CA is hyperoxia on 100% oxygen, which may further increase oxygen circulation and worsen ROS mediated injury during reperfusion. Although there is still an ongoing debate regarding normoxia vs hyperoxia following resuscitation from cardiac arrest in human patients, dogs studies have shown a marked

reduction in ROS as well as improved neurological outcome with normoxic ventilation after cardiac arrest compared to hyperoxic ventilation[69–71]. However, these studies did not investigate whether hyperemia was the main cause of the burst of ROS. In this study, we modulated inspired oxygen levels specifically during hyperemia to identify if hyperemia was the major contributor of ROS during reperfusion.

Methods:

Preclinical Rodent Model of CA

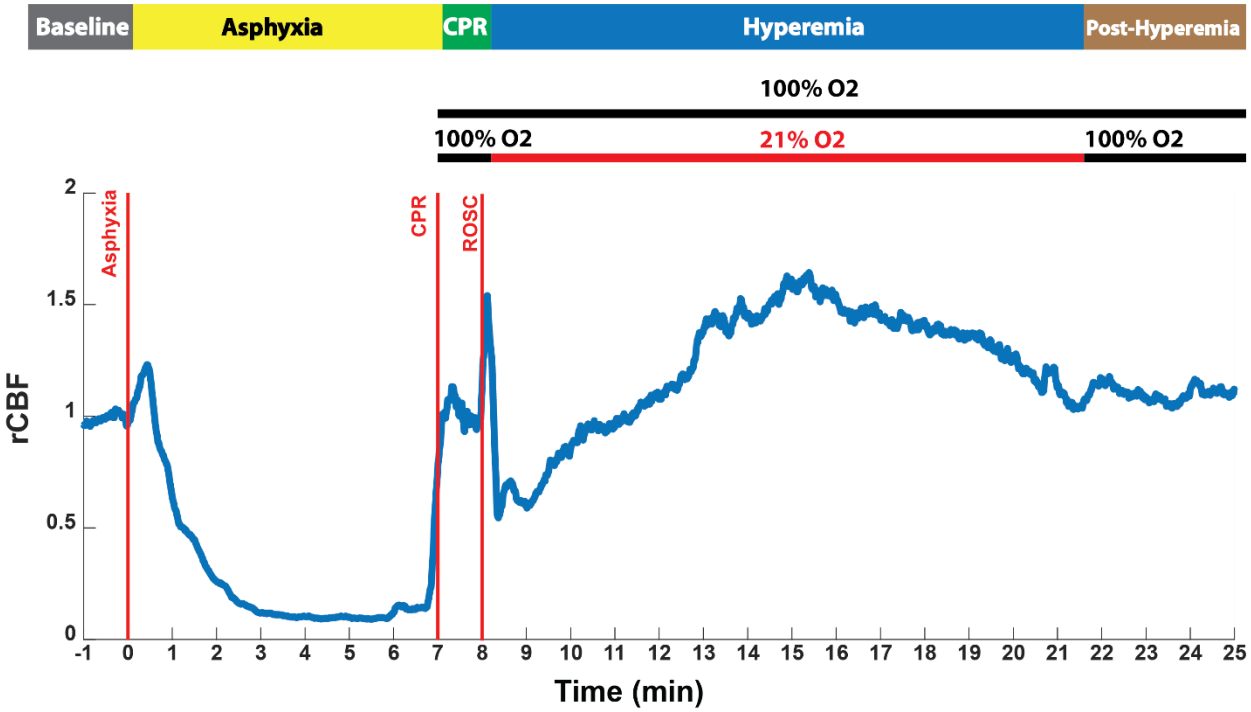

Figure 1. Experimental Timeline showing oxygen modulation during hyperemia post-ROSC (return of spontaneous circulation).

Cohort 1

The animal model of CA and resuscitation used in this study has been described previously by our lab and is summarized in **Figure 1**. In summary, male Wistar rats (Charles River, Canada facility) were endotracheally intubated and received femoral artery and vein cannulation to monitor arterial blood pressure (BP) and allow venous drug delivery, respectively. Recording electrodes were implanted into the frontal left and right hemispheres, left parietal hemisphere,

and in the midline occipital bone. An optical window was created by thinning the right parietal bone with a mechanical hand drill to create a rectangular window. Prior to the start of the experiment, arterial blood gases were measured from the femoral artery to confirm normal blood gas levels at baseline. The animals were on 100% O_2 and the anesthetic (isoflurane) was washed out over a 3 min period. This was followed by administration of a musculo-paralytic agent (vecuronium or rocuronium). After the washout period, CA was induced by turning off the ventilator. Then, 7 min later, CPR was initiated by turning the ventilator back on with 100% O_2, giving epinephrine and sodium bicarbonate, and performing manual chest compressions. Chest compressions were continued until the return of spontaneous circulation (ROSC). Right after ROSC, rats were either continued on 100% O2 or lowered to room air (21% O2, 79% N2) during the duration of hyperemia. Hyperemia was monitored with optical imaging as shown in **Figure 1**. 10-15 min post-ROSC arterial blood gases were measured once again from the femoral artery. The rats were monitored continuously for an additional 4hr until behavioral testing. The animals were kept on 100% O_2 until extubation from the ventilator, which occurred roughly 1hr post-ROSC. Neurological Deficit Scale (NDS), a behavioral test, was used to score neurological function at 4hr and 24hr post-ROSC, with a higher score representing better neurological function[97–99]. Open field behavioral testing was also done at the same time period as NDS. Burst suppression ratio (BSR), a quantification of suppression of AC-ECoG activity, was also used as an outcome measure at 60-80 min post-resuscitation, when the rat was recovering from coma and regaining consciousness. BSR decreases as the rat regains consciousness. Time to burst (TTB) is the time until electrical activity in the brain resumes as measured by the first burst of activity in AC-ECoG signal, and was used as another marker of neurological recovery. The rats were euthanized at 24hr post-ROSC for immunohistochemistry of the brain. The animals' body temperatures were monitored with a rectal probe and maintained at 37 degrees Celsius using a heating pad during the entirety of the experiment.

Data Acquisition and Post-Processing

Post-processing of arterial BP, AC-ECoG, and optical imaging data was performed using MATLAB (The MathWorks, Inc., Natick, MA). In this study, AC-ECoG data was primarily used for the analysis of ECoG burst onset. DC-ECoG data was not analyzed for this study.

Arterial BP

Arterial BP was measured continuously at 191 Hz from an arterial line. Mean arterial pressure (MAP) was calculated using the formula MAP= (systolic blood pressure + 2*diastolic blood pressure)/3.

Optical Imaging

Throughout the experiments, rats with received optical imaging with two diffuse optical imaging technologies: Laser Speckle Imaging (LSI) and multispectral Spatial Frequency Domain Imaging (SFDI). LSI measures blood flow, as previously established in both preclinical and clinical studies [96,111], including investigations into CA[83,101,104]. SFDI [96,106] measures the tissue absorption coefficient (related to hemoglobin concentration and oxygenation[83,105]) and scattering coefficient (related to morphology and distribution of cells and organelles[108]). The combination of LSI and SFDI data can be used to calculate cerebral metabolic rate of oxygen ($CMRO_2$)[109]. In this study, Laser Speckle Imaging data were acquired with a frame rate of 60 Hz and Spatial Frequency Domain Imaging data were acquired with a frame rate of 14 Hz. However, to reduce computational load, we reduced the sampling rate to ~17 data points per min for SFDI and ~39 data points per min LSI, which was enough to capture the dynamic changes during hyperemia.

Data Analysis

LSI Data: relative cerebral blood flow

The Laser Speckle Imaging data was used to compute Speckle Flow Index, a measure of CBF, over a fixed spatial region of interest spanning the majority of the imaging window. Relative cerebral blood flow (rCBF) was normalized to the mean CBF calculated over the one-minute interval immediately prior to the onset of asphyxia.

SFDI Data: Tissue scattering and oxygenation

For SFDI data analysis, custom MATLAB code[83] calculated a best fit of a computational (Monte Carlo) model of light-tissue interaction to the measured data. These model fits provided tissue oxy-hemoglobin concentration (ctHbO2), deoxygenated hemoglobin (ctHb), and scattering maps. The ctHbO2 and ctHb data were combined to calculate tissue oxygenation (StO2) via the formula StO2 = 100*ctHbO2/(ctHbO2+ctHb). Time-resolved ctHbO2, ctHb, StO2, and tissue scattering curves were formulated by averaging the optical property maps over a fixed spatial region of interest (ROI).

LSI + SFDI Data: CMRO2

Time-resolved CMRO2 was calculated using the formalism developed by Boas and Dunn[108,110], combining CBF data from LSI with ctHbO2 and ctHb data from SFDI. For the calculation of

CMRO2, the CBF data were analyzed using an ROI covering the majority of the imaging window (to represent overall perfusion into the brain), while ctHbO2 and ctHb data were analyzed using an ROI over a prominent vein (to more accurately probe the amount of oxygen consumed by the tissue).

Multimodal Parameter Set

For each cohort, a multimodal set of parameters was extracted from the data around the hyperemia phase to analyze several associations. In all cohorts, these parameters included: (i) absolute and relative hyperemic peak post-ROSC; (ii) area under the curve (AUC) of the hyperemia (post-ROSC to 20 min after). These were done for MAP, systolic blood pressure (SBP), cerebral blood flow (CBF), $CMRO_2$, as well as ctHb and ctHbO2.

Statistical Models and Tests

Statistical testing was performed with MATLAB. For each correlation analysis, Spearman correlations were performed when one of the parameters used was not normally distributed. When both parameters used for correlation were normally distributed, Pearson correlation was used. Unpaired or paired T-Tests were used for comparison between two groups while one-way anovas were performed to compare between multiple groups or parameters.

Immunohistochemistry and Quantification

Immunohistochemistry

24 hours after cardiac arrest, animals were subjected to euthanization via sodium pentobarbital and perfused transcardially by injection of 0.9% saline followed by 4% paraformaldehyde (PFA), made at pH 7.6. Animals' brains were post-fixed in 4% PFA for 3 days and then they were transferred into 30% sucrose to cryo-protect. Following that, brains were frozen in optimal cutting temperature (OCT) solution to cryo-cut and sectioned at 30 micrometer thickness coronally. For each animal, three 30 µm tissue sections (Bregma -2.92mm to -3.48mm) which includes the hilus, were chosen from each plate at approximately 360 µm intervals.

For FJB neurodegeneration staining, mounted sections on slides were warmed on a hotplate for 30 minutes at 55°C. In a dipping rack, slides were rehydrated in nanopure water for 5 seconds, dehydrated in an ethanol series, then incubated in: 0.3% Triton X-100 for 3 min, 0.06% $KMnO_4$ for 15 min on an orbital shaker, nanopure water for 1 min, then 0.001% FJB in 0.1% acetic acid with 100µg/mL DAPI for 30 min. Next, sections on slides underwent three washes of nanopure water 1 min each, dried on a hotplate for 10 min at 55°C, cleared in xylenes three times 2 min each, then coverslipped with DPX mounting medium.

For 3-nitrotyrosine (NT3) immunostaining of ROS, free-floating sections were stained at once in 48-well plates to ensure the uniformity of the immunohistochemistry processes for all subjects. Before each of the following steps, sections were washed in new wells of 1xPBS thrice at 5 min each. On the first day of the experiment, sections quenched with 3% H_2O_2 in 1xPBS twice at 10 min each and blocked in blocking buffer (5% normal donkey serum, 1xPBS, and 0.3% Triton x-100) for an hour. The first round of primary antibody incubations was done using Rabbit α NT3 (1:500) [Sigma-Aldrich; #06284MI] and Mouse α GFAP (1:1000) [Sigma; G-3893] antibody diluted in blocking buffer. Plates were left overnight on a shaker at room temperature. On the

second day of immunostaining, sections were incubated in secondary antibodies for direct fluorescence and amplification using Donkey α mouse-Cy3, Donkey α rabbit biotin-conjugated (1:500) [Fisher Scientific; #PI31821], and 100µg/mL DAPI (1:1000) in blocking buffer for one hour—followed by ABC-peroxidase incubation using 10µL/mL of Solution A in 1xPBS with 0.1% Triton X-100 [Vector Laboratories; #PK-6100] for 30 min. NT3 was visualized using tyramide-FITC (1:250) [Akoya Biosciences; #SAT701001EA]. Lastly, sections were mounted on gelatin-covered slides and coverslipped under Vectashield [Vector Laboratories; #H-1900] and stored in 4°C temperature within a dark box.

Cohort 3: Imaging and Quantification

Stained slides were imaged using the Keyence BZ-x800 light microscope. To ensure consistency within imaging runs, all parameters of imaging such as exposure were pre-set for all subjects with a cohort. Imaged sections were stitched together by Keyence software and channels were separated based on different stains. To analyze images, trained members were each assigned to a specific region in which each region was quantified by measuring the fluorescence intensity with ImageJ by least two members. Each person used DAPI staining to identify the region of interest and quantified the mean integrated density of GFAP and NT3 three times after subtracting background. Integrated density values from the three quantifications were averaged, and the resulting values were averaged between quantifiers with three sections per animal.

For FJB quantification, at least two quantifiers counted FJB cells in the hilus and TRN using the Cell Counter Tool in ImageJ. Positive FJB signal was defined as brightly fluoresced GFP signal

compared to tissue background with the same morphology as DAPI-marked cells. Counts were averaged across three sections per animal and then averaged between quantifiers.

Results:

Room air treatment during hyperemia has better behavioral outcome

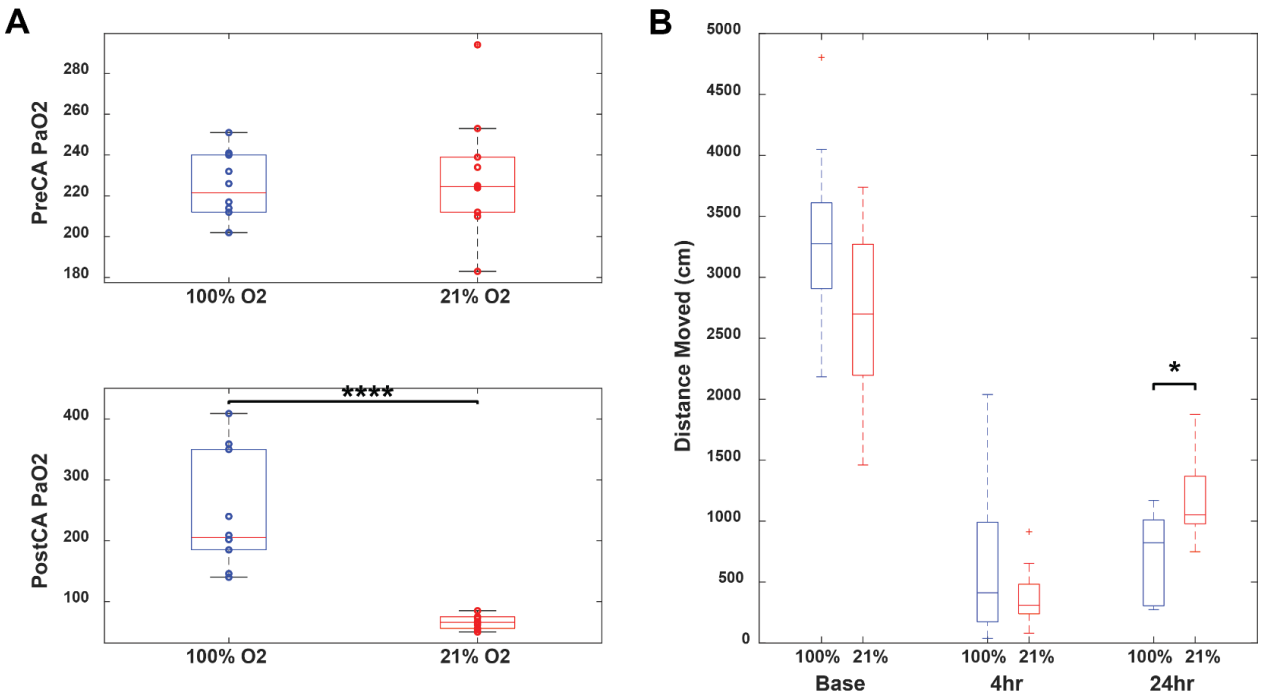

Figure 2. Room air treatment during hyperemia has better behavioral outcome. **A)** Unpaired t-test comparisons of 100% O2 and 21% O2 groups pre-CA and post-CA partial pressure of O2 (mmHg) in arterial blood. **B)** Unpaired t-tests of distanced moved by the rats in each group at baseline, 4hr post-ROSC, and 24hr post-ROSC. (*=p<0.05, **=p<0.01, ***=p<0.005, ****=p<0.001)

Further investigating mechanisms of possible hyperemia related injury, we wondered whether hyperemia itself was causing injury through direct high perfusion pressure, or through increased circulation of harmful substances, such excessive oxygen leading to oxidative injury. We

assessed if hyperemia was exacerbating oxidative injury by increasing the circulation of oxygen by treating a group of rats with room air (21% O2 and 79% N2) during hyperemia, while another group of control rats received 100% O2. **Figure 2A** shows the arterial partial pressure of oxygen (PaO2) in the 100% O2 and 21% O2 groups pre-CA and post-CA. Pre-CA, the PaO2 was not different between the two groups, but was significantly lower in the 21% O2 group post-CA ($p<0.001$). The distance moved by the rats was measured for each group at baseline, 4hr post-ROSC, and 24hr post-ROSC. The 21% O2 group had greater distanced moved than the 100% O2 group ($p<0.05$), indicating better recovery.

21% O2 is sufficient to saturate oxyhemoglobin, and increases O2 metabolism post-CA

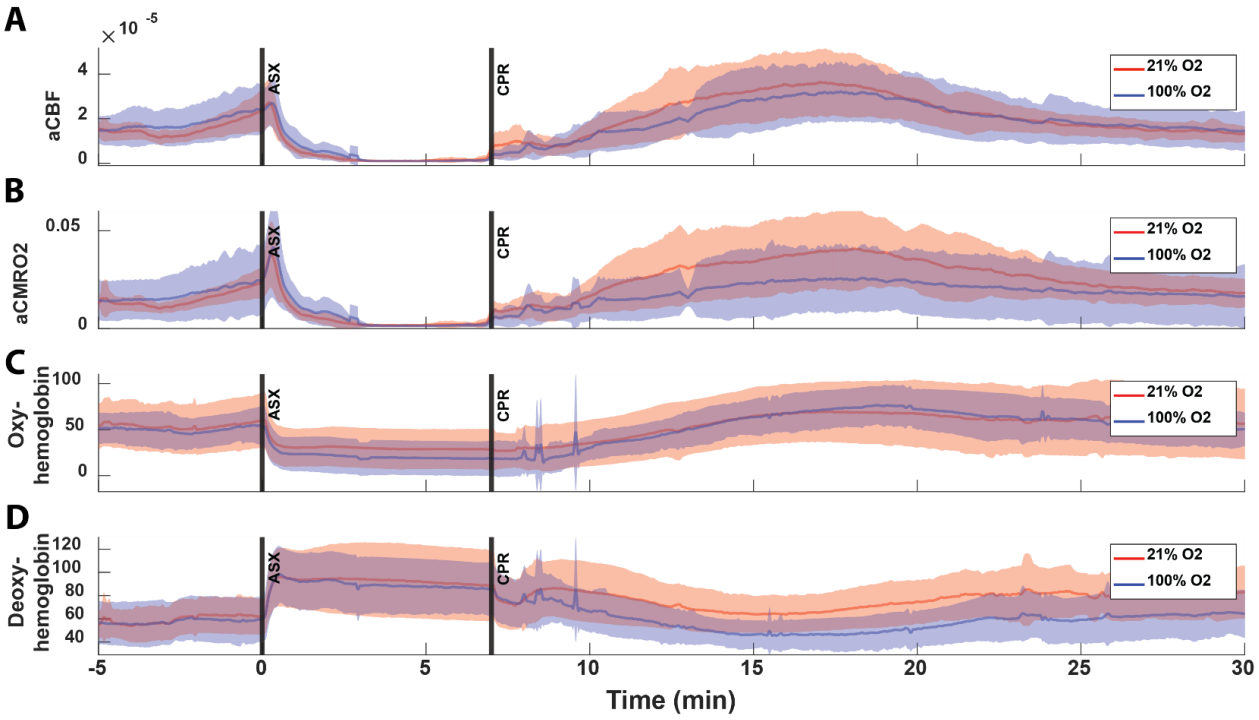

Figure 3. 21% O2 is sufficient to saturate oxyhemoglobin and increases O2 metabolism post-CA. **A-D)** Traces of aCBF, aCMRO2, oxyhemoglobin, and deoxyhemoglobin, respectively, for 21% O2 and 100% O2 groups. Shaded regions indicate 1 standard deviation and solid lines indicate the mean. 'a' in aCBF and aCMRO2 indicate absolute values. ASX indicates start of asphyxia.

Figure 3A-D shows the traces of aCBF, aCMRO2, oxyhemoglobin, and deoxyhemoglobin across the time course of the experiment for both groups. The 21% O2 group appeared to have slightly higher aCBF during hyperemia than 100% O2 group, while aCMRO2 and deoxyhemoglobin levels were noticeably higher in the 21% O2 group. However, the level of oxyhemoglobin were similar post-ROSC between the two groups, indicating that even 21% O2 is enough to have saturated oxyhemoglobins similar to the 100% O2 group.

Room air rats have lower MAP and greater metabolism which is associated with better behavioral outcome

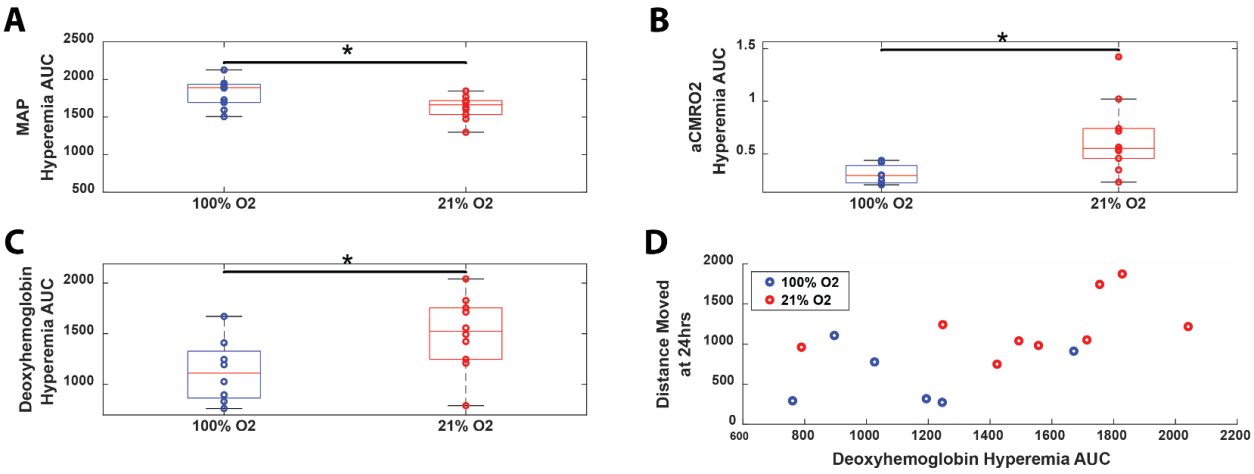

Figure 4. Room air rats have lower MAP and greater metabolism which is associated with better behavioral outcome. **A-C)** unpaired t-test between 100% O2 and 21% O2 groups for area under the curve of MAP, aCMRO2, and deoxyhemoglobin during hyperemia, respectively. (*=p<0.05) **D)** Scatter plot of deoxyhemoglobin AUC during hyperemia vs distance moved at 24hr post-ROSC (Pearson p<0.05, r=0.57).

Interestingly, the 21% O2 group had lower AUC of the MAP hyperemia than the 100% O2 (p<0.05) (**Fig. 4A**). They also had greater aCMRO2 and deoxyhemoglobin AUC of the hyperemia (p<0.05) than the 100% O2 group (**Fig. 4B-C**). Plotting the deoxyhemoglobin

hyperemia AUC against the distance moved at 24hr post-ROSC, we found a positive correlation (Pearson p<0.05, r=-0.57).

Greater cerebral perfusion and metabolism is associated with greater neuronal death in the hippocampus

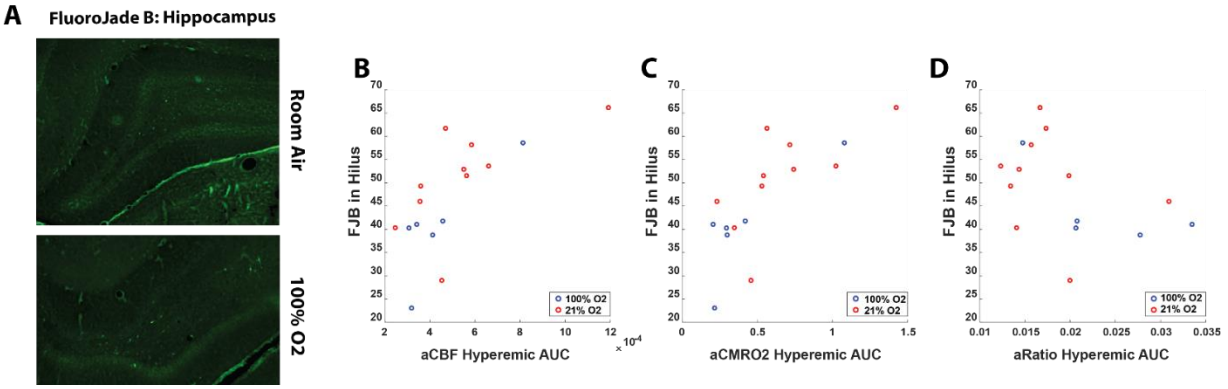

Figure 5. Greater cerebral perfusion and metabolism is associated with greater neuronal death in the hippocampus. **A)** Representative images of the Fluorojade-B (FJB) stained hippocampal sections. **B-D)** Scatter plot of aCBF hyperemic AUC (Pearson p<0.005, r=0.699), aCMRO2 hyperemic AUC (Pearson p<0.001, r=0.759), and aRatio hyperemic AUC (Pearson p<0.05, r=-0.553), respectively, vs the amount of FJB in the hilus region of the hippocampus.

We assessed for neuronal death in the hippocampus, specifically hilus, between the two groups with the FJB stain (**Fig. 5A**). However, we did not find a significant difference between two groups (data not shown). However, in line with the FJB data with the esmolol cohort, we found that greater aCBF hyperemic AUC and aCMRO2 hyperemic AUC were correlated with greater FJB in the hilus (Pearson p<0.005, r=0.699, Pearson p<0.001, r=0.759, respectively, **Fig. 5B-C**). **Figure 5D** shows greater AUC of the aRatio hyperemia being associated with less FJB in the hilus. The 'a' in aRatio indicates absolute values while Ratio is the ratio of CBF/CMRO2, a measure of flow/metabolism coupling, or supply and demand.

Room air treatment reduces amount of ROS in hippocampus post-CA

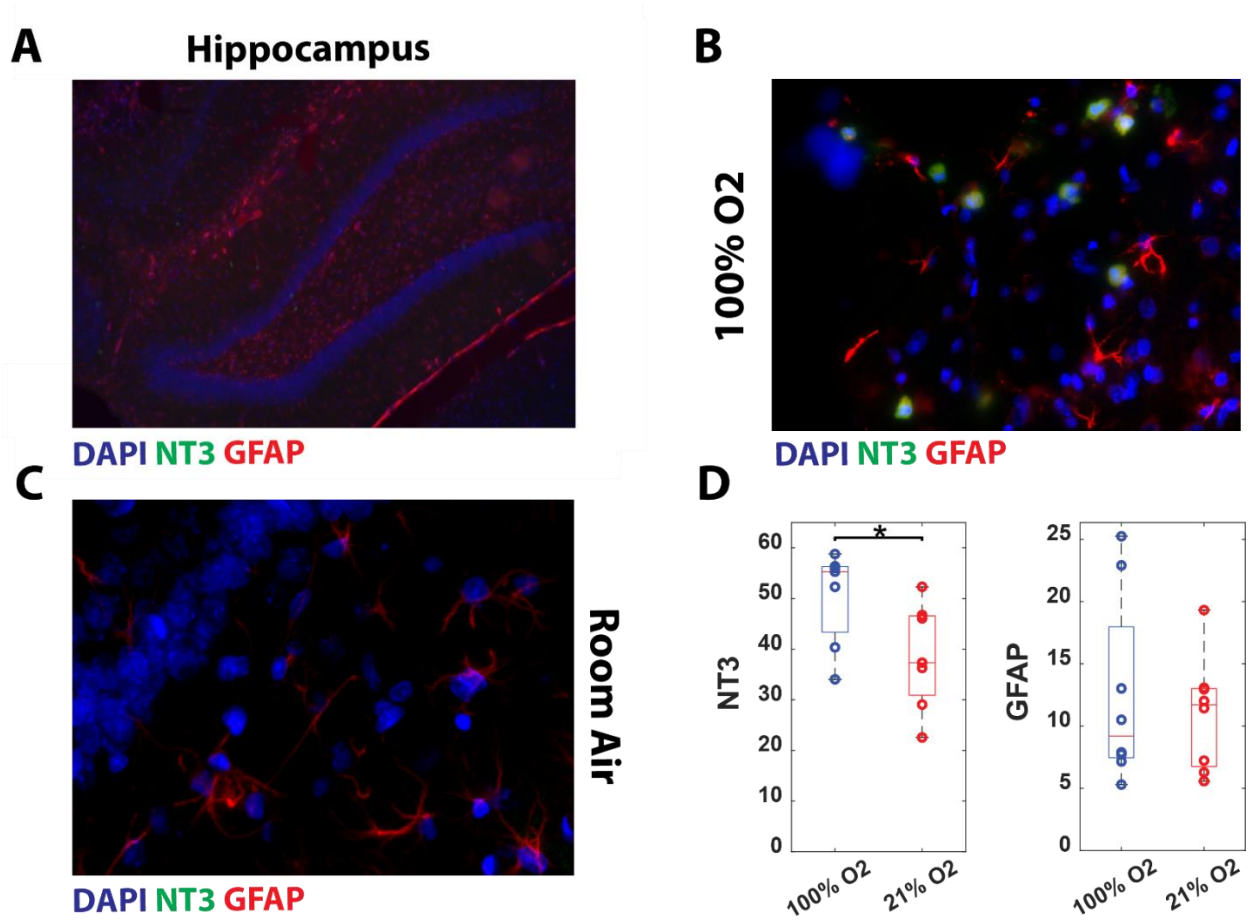

Figure 6. Room air treatment reduces amount of ROS in hippocampus post-CA. **A)** Representative image of the hippocampus stained with DAPI (blue), NT3 (green), and GFAP (red) at 10x magnification. **B-C)** 60x magnification representative images with the same stains for a 100% O2 rat and 21% O2 rat, respectively. **D)** Unpaired t-tests between 100% O2 and 21% O2 groups for the amount of NT3 and GFAP quantified in the hippocampus.

Lastly, we measured the amount of nitrotyrosine-3, a marker of oxidative injury, at 24hr post-ROSC in the two groups, as well as GFAP as a measure of astroglial injury in the hippocampus. **Figure 6A** shows the hippocampus in a representative 21% O2 rat. Although astrocytes were abundant, the NT3 was not so widely visible at 10x magnification. At 60x magnification, we were

able to see NT3 surrounding the nucleus, stained by DAPI, in the 100% O2 group (**Fig. 6B**). In the 21% O2 group, NT3 was more sparse (**Fig. 6C**). Quantification of the fluorescence intensity density showed that the 21% O2 group had lower NT3 levels than the 100% O2 group ($p<0.05$), while the levels of GFAP were similar (**Fig. 6D**).

Discussion:

Room air treatment during hyperemia reduces ROS and improves behavioral outcome

We investigated another potential mechanism of hyperemia-induced reperfusion injury. Production of reactive oxygen species (ROS) and increased oxidative injury is a known contributor of reperfusion injury[44,53,150]. As in-vivo[43] and in-vitro studies have shown that there is a burst of ROS in the first 30 min of ischemia-reperfusion[44], coinciding with the timing of hyperemia, we investigated whether hyperemia was responsible for the burst of ROS. The current standard for CA patients is 100% O2[143], so we tested this by comparing 100% O2 ventilation vs room air (21% O2, 79% N2) ventilation during hyperemia in the production of ROS and eventual outcome. Treatment with room air during hyperemia led to a very significant drop in PaO2 post-CA and an improvement in behavioral outcome (**Fig. 2**) as well as a drop in ROS (**Fig. 6**). This improvement in outcome and ROS is in line with a previous dog study that also did 100% O2 vs room air ventilation post-CA but for a longer period past the hyperemia phase[70]. Reduction of oxygen, the source of ROS, would naturally reduce the amount of ROS. If hyperemia was not responsible for the major portion of ROS production, then room air treatment

only during hyperemia (~15min) would have likely not been enough to result in lowered ROS levels. Instead, the reduction of ROS levels would have likely been directly related to the length of room air treatment. Additionally, the amount of neuronal death was not different between the two groups (**Fig. 5A**), but we found that greater CBF and CMRO2 during hyperemia was associated with more neuronal death, while greater ratio of CBF/CMRO2 was associated with less neuronal death (**Fig. 5B-D**). Greater perfusion and metabolism during hyperemia being associated with more neuronal death shown here is the same as in shown our prior cardiac arrest model using esmolol to block hyperemia. This correlation appears to be consistent across different models.

Room air treatment alters perfusion and metabolism during hyperemia

In the rats with room air treatment, the MAP during hyperemia was significantly lower than the 100% O2 group (**Fig. 4A**), and since the room air rats also had better behavioral outcome, it is in line with our results from a prior study. The room air rats also had the same level of oxyhemoglobin as the 100% O2 rats which indicated that room air was sufficient to have saturated oxyhemoglobins (**Fig. 3C**), despite lower PaO2. Room air rats also had greater deoxyhemoglobin levels post-ROSC, suggesting more oxyhemoglobin was being utilized, and this is reflected by the greater level of cerebral metabolism post-ROSC as well (**Fig. 4B-C**). Increased oxygen metabolism despite lower levels of oxygen seems counterintuitive. However, this had been shown prior in a study of a baseline state in humans[152,153]. That study found that in healthy humans, CMRO2 goes down during hyperoxia and up during hypoxia in an oxygen dose dependent manner. A study suggested that increased oxidative injury from hyperoxia decreases the enzymes necessary for aerobic metabolism, thus resulting in lower CMRO2 in

hyperoxia[154,155]. Interestingly, this was seen in our study in a cardiac arrest model. Furthermore, the level of deoxyhemoglobin during hyperemia was positively correlated with behavioral outcome. This appears to be in conflict with the neuronal death data that had the opposite correlation. However, it should be noted that the room air group also had much lower PaO2, and so increased metabolism would likely lead to even lower PaO2 during hyperemia. The lower PaO2 may be more responsible for the lower ROS production and better behavioral outcome. It could be also that greater cerebral metabolism is associated with better behavioral outcome but is not protective of the most ischemic sensitive regions such as the hippocampus, thus the greater neuronal death.

Conclusion:

In this study, we analyzed various hemodynamic and metabolic parameters during hyperemia post-CA with oxygen modulation during hyperemia and compared the ROS production and neurological outcome afterwards. While there are other studies that showed going down to room air from 100% O2 post-ROSC led to improved outcome and less ROS, our study shows for the first time that a similar effect can be achieved by targeting only the ~15-20min duration of hyperemia. This suggests hyperemia may be the major contributor to the burst of ROS during reperfusion. Extrapolating further, it may possibly suggest that hyperemia increasing circulation of other substances could be a major contributor to reperfusion injury as well. Our study shows for the first time that this very dynamic period within the first 30 min post-ROSC is associated with outcome with potential implications for precision targeted oxygen therapies in CA patients. In conclusion, this work shows the importance of further investigation into increased circulation

of harmful substances during hyperemia as a potential therapeutic target for cardiac arrest and cerebral ischemic injuries.

Limitations:

There were some limitations to these studies that we hope to address in future experiments. For assessing ROS during hyperemia, we did not measure the level of ROS in the blood before and immediately after hyperemia which would have been a more accurate measure of hyperemia's effect on ROS production. Secondly, we did not assess ROS in the a group of rats where hyperemia was blunted. If blocking hyperemia alone also lowered ROS, this would have been more supportive. Lastly, this study was limited by the early time points of recovery, assessing mostly at 4hr and 24hr post-ROSC. Many markers of injury and recovery tend to be more expressed in the days to weeks post-injury, so although we glimpsed at the very early period of recovery, it is uncertain as to whether these treatments would have longer term benefits.

Chapter 5

Discussion

I. Introduction

Despite 40 years of advancements in medicine and care, survival for CA patients have not improved[4]. One of the large contributing factors is the debilitating long-term neurological impairments[5]. Neurological recovery is a major determinant of outcome for CA survivors[6], however, there are no reliable treatments targeting neurological recovery after CA. CA and its recovery is a complex process involving many different body systems. In this discussion, we will review current post-cardiac arrest care, current developments in treatments, and use of beta-blockers for care.

II. Post-Cardiac Arrest Care

Throughout history of post-CA care, it has transitioned from a cookie-cutter approach to a more systematic, individualized method which has shown to improve the chance of patient survival and better chance at improved quality of life[156,157]. Appropriate post-CA care has the potential to reduce early mortality caused by hemodynamic instability and later morbidity and mortality from multiorgan failure and brain injury[158,159]. The following methods of care have been taken mostly from the American Heart Association's Post-Cardiac Arrest Care, published in the journal, Circulation[35,143].

Hypothermia and Hyperthermia

Current recommendations still indicate the use of therapeutic temperature management (TTM), which is cooling patients to between 32-34 degrees Celsius for the first 24 hours post-resuscitation. However, there are no concrete guidelines on specific indications, populations,

timing, duration, and methods for induction, maintenance, and reversal of hypothermia. Perhaps because of this, recent large clinical studies have shown no benefits to survival between normothermia and hypothermia in CA patients[7,160]. However, there are essentially no patients in which TTM would be harmful or contraindicated for[72] in the hospital setting. In the pre-hospital setting, routine cooling of patients after resuscitation with rapid infusion of cold intravenous fluids are recommended against due to increased risk of pulmonary edema and rearresting[161]. Fever after CA and in other conditions needing intensive care has been associated with worse neurologic injury for comatose patients[162,163]. The intervention to prevent fever is relatively benign thus it is recommended to be performed against the potential worsening of brain injury[72].

Pulmonary

Patients often have pulmonary dysfunction after cardiac arrest and thus it is common to be mechanically ventilated during post-resuscitation to reduce the work of breathing until the patient can efficiently breath spontaneously. Although patients are recommended to be resuscitated on 100% O2, afterwards, it is recommended that ventilation be adjusted such that the pulse oximeter reads oxyhemoglobin saturation of between 94-96%. Pulse oximeter can read 100% when the PaO2 is between 80-500 mmHg, which is a very wide range. Since, at least, in animal models and in our data, it is shown that high oxygen levels lead to greater production of ROS and is worse for outcome, the inhaled oxygen levels is suggested to be lowered to the minimum necessary to maintain pulse oximeter reading of >94%. However, the optimal levels of inspired oxygen is still up for debate in humans as clinical data has been inconsistent.

Vasopressor Drugs

Vasopressors are drugs that increase blood flow and pressure. These may be given after resuscitation to support or maintain adequate blood pressure and flow, especially in CA patients

who have low blood pressures. There are many types of these drugs, such as those that increase heart rate, increase heart contractility, cause vasoconstriction, and those that cause vasodilation. Many of these drugs are adrenergic targeting and are not selective to the heart, producing many unwanted side effects such as increasing metabolism, blood glucose, and lactate. In some cases, these adrenergic drugs may cause a mismatch of the heart oxygen demand and delivery and worsen ischemia of the heart. Therefore, it is important for providers to be aware of which drugs to use appropriately depending on the patient's condition[164]. After CA, patients are often hemodynamically unstable[165] and can have another CA or multiorgan failure from poor perfusion[165,166]. Furthermore, ischemia/reperfusion after CA can cause temporary stunning of the heart[167] and metabolic acidosis and loss of sympathetic tone can cause vasodilation[165,166], worsening hypotension. Giving routine intravenous fluids or vasoactive drugs for patients with myocardial dysfunction has not been shown to be harmful or beneficial, but giving them to maintain a MAP of >65 is suggested to be reasonable for maintaining cardiac output and organ perfusion.

III. Current Developments for Treatments for Reperfusion Injury

In CA, the first line of treatment is to rapidly regain blood flow. In cases of coronary artery disease, angioplasty or thrombolysis are recommended to restore blood flow[168]. However, this sudden restoration of blood flow can lead to further injury and cell death due to various intracellular cascades being activated[169]. This is mainly associated with regulated cell death due to a burst of reactive oxygen species (ROS), loss of ionic homeostasis, mitochondrial dysfunction, and inflammation[170]. However, despite reperfusion injury being described almost 40 years ago, there are still no pharmacological treatments for reperfusion injury[171,172]. This portion of the discussion will review the current developments in potential treatments for reperfusion injury.

Therapeutic Peptides

Peptides are popular as potential therapeutic molecules due to their favorable pharmacokinetic profile, good solubility, low toxicity, and high modifiability allowing for better stability/binding affinity[173]. Therefore, bioactive peptides that target processes of apoptosis, necroptosis, inflammation, and autophagy in reperfusion injury have been studied[174]. Clinical trials have been disappointing, but now is leading towards further research into aspects of reperfusion injury besides infarct size such as microvascular injury. Moving forward, other things to kept in mind are improvements in specificity of targeting the ischemic regions with the drugs to reduce side effects and using a cocktail of drugs to target different pathways and cell types[175].

Ischemic Preconditioning

Ischemic preconditioning is a short period of ischemia followed by brief reperfusion before another prolonged interval of ischemia. This has been shown to be sufficient to decrease organ ischemic-reperfusion injury in clinical and experimental studies[176], despite the protective mechanism not being fully understood. It is thought that this might delay the ATP depletion rate during ischemia and subsequent ischemic episodes and that periodic reperfusion could flush out catabolites that accumulate during ischemia[177]. Although these experimental studies have shown some benefit, the benefits in the clinical setting are controversial[178].

Remote Ischemic Conditioning

Remote ischemic conditioning is known promising method to reduce ischemic-reperfusion injury in studies[179]. This is where a reversible short-term ischemia with reperfusion in one organ or tissue leads to gaining of resistance to another remote organ or tissue to ischemia-reperfusion injury[180]. For example, performing brief ischemia and reperfusion episodes introduced in a limb gives systemic resistance to other organs and tissues. The mechanism of this is also not fully understood. However, it is thought that a protective signal is sent from the site of original

ischemia-reperfusion to other organs via systemic, neuronal, and/or humoral mechanisms. One systematic meta-analysis and review showed the remote ischemic conditioning improved myocardial infarct size[181].

Therapies Modulating Neuroinflammation

Inflammatory response promotes cellular injury in the acute injury setting, but also aids in restoration of cellular functions during the recovery phase. This is a major challenge for clinical applications[182]. Drugs targeting microglia such as minocycline are able to inhibit microglial activation, reduce the amount of neuronal apoptosis[183], reduced free radicals[184], and infarct size[185]. Clinical studies showed it may be effective[186], but one study also showed that it did not have any efficacy for stroke[187]. Several trials have also targeted blocking leukocyte adhesion and transmigration to reduce inflammation after stroke, which seemed effective pre-clinically, but were not clinically[182]. Immunomodulation therapy is very attractive, but due to the dual nature of neuroinflammation, more research is still needed to produce positive results.

Nitric Oxide

Nitric Oxide (NO) is a potent vasodilator that can regulate blood flow. Inhaled NO gas can play an important role in alleviating ischemia-reperfusion injury in many organs, including the brain[188]. Inhaled NO at the beginning of ischemia reduced infarct volume and neurological function. It also selectively vasodilated vessels in the ischemic tissue[189]. In cerebral ischemia, NO increased CBF in the ischemic tissue, reducing total ischemic volume. Although, NO inhaled at the beginning of ischemia seemed beneficial, NO inhaled during reperfusion was detrimental[190].

Mitochondrial Transplantation

Mitochondrial transplantation is a method of injecting healthy mitochondria into damaged organs. Recent studies showed that healthy mitochondria may be able to replace damaged mitochondria[191,192], which may protect against further injury[151]. In ischemia-reperfusion injury, mitochondrial electron transport chain is dysfunctional, there is excess ROS production, apoptotic pathways are activated, mitochondrial shape and fission/fusion dynamics are altered[193,194]. Therefore, mitochondrial targeting therapies are on the rise. These therapies involve intraarterial, intravenous, or direct injection of healthy isolated mitochondria into tissue of interest[195]. All animal studies improved ischemia-reperfusion injury in the targeted tissues, but showed no improvements in functional outcomes. Although, this approach seems promising pre-clinically, it still needs further investigation for clinical feasibility.

III. Beta-Blockers

Cardioprotection

After ischemia and reperfusion following cardiac arrest, there is potentially lethal myocardial damage which may lead to congestive heart failure, thus increasing overall long-term morbidity and mortality risk[196]. Usage of beta blockers for post-cardiac arrest treatments to protect the heart have been studied for a long time. Before reperfusion injury was well-understood, beta-1 blockade therapy during cardiac arrest showed inconsistent efficacy[197,198], with some showing higher incidence of cardiogenic shock. With the introduction of percutaneous coronary interventions, coronary reperfusion could be definitively assessed. Around 20 years ago, a study showed that a beta-1 blocker, esmolol, given at the onset of reperfusion in canines after cardiac arrest, improved infarct size and outcome[199]. Similar reports with other beta blockers, such as metoprolol[200], showed improved outcomes and infarct size. Giving beta blockers shortly before reperfusion showed reduced infarct size in rodent models as well as in in human patients[201],

with longer term maintenance of left ventricular ejection fraction and systolic function[202]. Studies with beta blockade for reperfusion injury has consistently shown throughout history to be cardioprotective and has been extensively studied. In fact, esmolol's effect on reducing infarct size was found to be through the beta-2 adrenergic receptor signaling pathway[203], which is anti-apoptotic, despite being a beta-1 specific drug.

Neuroprotection

In cardiac arrest, there is global ischemia, which involves the highly ischemic-sensitive brain. The benefits of beta blockers in cerebral ischemia-reperfusion has been studied but not as extensively as for cardioprotection. As we saw in our data, others have reported beta-1 blockade leading to significant vasodilation of cerebral pial arterioles during ischemia-reperfusion[51,137], as well as retained integrity of vascular ultrastructure [51]. These animal studies also showed increased neurological outcome and survival as well[49–51] for ischemia-reperfusion. Furthermore, beta-blockade showed reduction of brain swelling[204]. Our data also supports the improve neurological outcome as well, but adds to the literature a potential mechanism of reperfusion injury that is mediated greatly by hyperemia.

V. Impact

So far, treatments for reperfusion injury following CA is very lacking and applications for beta blockade treatments clinically are difficult due to inconsistent guidelines on how to implement the treatments, such as timing, duration, dose, etc. Additionally, the population that suffers from CA is very wide and diverse including young to the elderly, and different etiologies of cardiac arrest such as coronary artery disease, drug overdose, drowning, and others which are all different in cause and lead to difference in hemodynamic profiles. Furthermore, it is difficult to implement pre-treatments prior CA since CA occurrence is often unpredictable. Therefore, finding a window of opportunity where treatment would still be efficacious after CA is important.

Reperfusion certainly fits the bill, but reperfusion does have a set duration of time and thus simply indefinitely treating with beta blockers after resuscitation may not be practical. Instead, finding the period of time during reperfusion when the greatest amount of injury occurs, and specifically targeting that time period would be best. This would reduce potential complications of hemodynamic instability, especially for elderly patients that may not tolerate long durations of beta blockade treatment. In this dissertation, we showed that hyperemia may be that specific period of reperfusion that could be targeted to reduce the majority of injury following resuscitation from CA with a hemodynamic goal based off of the mean arterial pressure to guide the treatment on an individual basis. Further research is necessary to optimize the method of treatment (intravenous infusion vs bolus vs intramuscular injection) to make it more practical as well as account for the diverse range of different etiologies of CA, the patients' age, as well as other physiological factors to push it to the next level of clinical implementation. However, nonetheless, this work emphasizes the potential of hyperemia period as a therapeutic target for ischemia-reperfusion injury.

References

1. Tsao CW, Aday AW, Almarzooq ZI, et al. Heart Disease and Stroke Statistics-2023 Update: A Report From the American Heart Association. Circulation 2023;147(8):e93–621.

2. Virani SS, Alonso A, Benjamin EJ, et al. Heart Disease and Stroke Statistics-2020 Update: A Report From the American Heart Association. Circulation 2020;141(9):e139–596.

3. Girotra S, Tang Y, Chan PS, Nallamothu BK, American Heart Association Get With The Guidelines–Resuscitation Investigators. Survival After In-Hospital Cardiac Arrest in Critically Ill Patients: Implications for COVID-19 Outbreak? Circ Cardiovasc Qual Outcomes 2020;13(7):e006837.

4. Kutsogiannis DJ, Bagshaw SM, Laing B, Brindley PG. Predictors of survival after cardiac or respiratory arrest in critical care units. CMAJ 2011;183(14):1589–95.

5. Allen BS, Buckberg GD. Studies of isolated global brain ischaemia: I. Overview of irreversible brain injury and evolution of a new concept - redefining the time of brain death. Eur J Cardiothorac Surg 2012;41(5):1132–7.

6. Laver S, Farrow C, Turner D, Nolan J. Mode of death after admission to an intensive care unit following cardiac arrest. Intensive Care Med 2004;30(11):2126–8.

7. Dankiewicz J, Cronberg T, Lilja G, et al. Hypothermia versus Normothermia after Out-of-Hospital Cardiac Arrest. N Engl J Med 2021;384(24):2283–94.

8. Lai C-Y, Tsai S-H, Lin F-H, et al. Survival rate variation among different types of hospitalized traumatic cardiac arrest: A retrospective and nationwide study. Medicine (Baltimore) 2018;97(28):e11480.

9. Wolbinski M, Swain AH, Harding SA, Larsen PD. Out-of-hospital Cardiac Arrest Patient Characteristics: Comparing ventricular arrhythmia and Pulseless Electrical Activity. Heart Lung Circ 2016;25(7):639–44.

10. Attin M, Tucker RG, Carey MG. In-Hospital Cardiac Arrest: An Update on Pulseless Electrical Activity and Asystole. Crit Care Nurs Clin North Am 2016;28(3):387–97.

11. Fukuda T, Ohashi-Fukuda N, Matsubara T, et al. Association of initial rhythm with neurologically favorable survival in non-shockable out-of-hospital cardiac arrest without a bystander witness or bystander cardiopulmonary resuscitation. Eur J Intern Med 2016;30:61–7.

12. Hartings JA, Shuttleworth CW, Kirov SA, et al. The continuum of spreading depolarizations in acute cortical lesion development: Examining Leão's legacy. J Cereb Blood Flow Metab 2017;37(5):1571–94.

13. Ayata C, Lauritzen M. Spreading depression, spreading depolarizations, and the cerebral vasculature. Physiol Rev 2015;95(3):953–93.

14. Chang JC, Shook LL, Biag J, et al. Biphasic direct current shift, haemoglobin desaturation and neurovascular uncoupling in cortical spreading depression. Brain 2010;133(Pt 4):996–1012.

15. Piilgaard H, Lauritzen M. Persistent increase in oxygen consumption and impaired neurovascular coupling after spreading depression in rat neocortex. J Cereb Blood Flow Metab 2009;29(9):1517–27.

16. Dohmen C, Sakowitz OW, Fabricius M, et al. Spreading depolarizations occur in human ischemic stroke with high incidence. Ann Neurol 2008;63(6):720–8.

17. Strong AJ, Anderson PJ, Watts HR, et al. Peri-infarct depolarizations lead to loss of perfusion in ischaemic gyrencephalic cerebral cortex. Brain 2007;130(Pt 4):995–1008.

18. Chen S-P, Qin T, Seidel JL, et al. Inhibition of the P2X7-PANX1 complex suppresses spreading depolarization and neuroinflammation. Brain 2017;140(6):1643–56.

19. Menyhárt Á, Zölei-Szénási D, Puskás T, Makra P, Bari F, Farkas E. Age or ischemia uncouples the blood flow response, tissue acidosis, and direct current potential signature of spreading depolarization in the rat brain. Am J Physiol Heart Circ Physiol 2017;313(2):H328–37.

20. Sato S, Kawauchi S, Okuda W, Nishidate I, Nawashiro H, Tsumatori G. Real-time optical diagnosis of the rat brain exposed to a laser-induced shock wave: observation of spreading depolarization, vasoconstriction and hypoxemia-oligemia. PLoS ONE 2014;9(1):e82891.

21. Dreier JP. The role of spreading depression, spreading depolarization and spreading ischemia in neurological disease. Nat Med 2011;17(4):439–47.

22. Urbach A, Baum E, Braun F, Witte OW. Cortical spreading depolarization increases adult neurogenesis, and alters behavior and hippocampus-dependent memory in mice. J Cereb Blood Flow Metab 2017;37(5):1776–90.

23. Wilson RH, Crouzet C, Lee DE, et al. Spreading depolarization and repolarization during cardiac arrest as an ultra-early marker of neurological recovery in a preclinical model. BioRxiv 2019;

24. Hosseini M, Wilson RH, Crouzet C, Amirhekmat A, Wei KS, Akbari Y. Resuscitating the globally ischemic brain: TTM and beyond. Neurotherapeutics 2020;17(2):539–62.

25. Chen S-P, Ay I, Lopes de Morais A, et al. Vagus nerve stimulation inhibits cortical spreading depression. Pain 2016;157(4):797–805.

26. Momose-Sato Y, Sato K, Mochida H, Yazawa I, Sasaki S, Kamino K. Spreading depolarization waves triggered by vagal stimulation in the embryonic chick brain: optical evidence for intercellular communication in the developing central nervous system. Neuroscience 2001;102(2):245–62.

27. Morais A, Liu T-T, Qin T, et al. Vagus nerve stimulation inhibits cortical spreading depression exclusively through central mechanisms. Pain 2020;161(7):1661–9.

28. Lindemann J, Rakers C, Matuskova H, Simon BJ, Kinfe T, Petzold GC. Vagus nerve stimulation reduces spreading depolarization burden and cortical infarct volume in a rat model of stroke. PLoS ONE 2020;15(7):e0236444.

29. Sekhon MS, Gooderham P, Menon DK, et al. The burden of brain hypoxia and optimal mean arterial pressure in patients with hypoxic ischemic brain injury after cardiac arrest. Crit Care Med 2019;47(7):960–9.

30. Roberts BW, Kilgannon JH, Hunter BR, et al. Association between elevated mean arterial blood pressure and neurologic outcome after resuscitation from cardiac arrest: results from a multicenter prospective cohort study. Crit Care Med 2019;47(1):93–100.

31. Kilgannon JH, Roberts BW, Jones AE, et al. Arterial blood pressure and neurologic outcome after resuscitation from cardiac arrest*. Crit Care Med 2014;42(9):2083–91.

32. Fritz C, Kimmoun A, Vanhuyse F, et al. High Versus Low Blood-Pressure Target in Experimental Ischemic Prolonged Cardiac Arrest Treated with Extra Corporeal Life Support. Shock 2017;47(6):759–64.

33. Berg RA, Sutton RM, Reeder RW, et al. Association Between Diastolic Blood Pressure During Pediatric In-Hospital Cardiopulmonary Resuscitation and Survival. Circulation 2018;137(17):1784–95.

34. Wang C-H, Chang W-T, Huang C-H, Tsai M-S, Liu S-H, Chen W-J. Cerebral Blood Flow-Guided Manipulation of Arterial Blood Pressure Attenuates Hippocampal Apoptosis After Asphyxia-Induced Cardiac Arrest in Rats. J Am Heart Assoc 2020;9(13):e016513.

35. Callaway CW, Donnino MW, Fink EL, et al. Part 8: Post-Cardiac Arrest Care: 2015 American Heart Association Guidelines Update for Cardiopulmonary Resuscitation and Emergency Cardiovascular Care. Circulation 2015;132(18 Suppl 2):S465-82.

36. Zimmer R, Lang R, Oberdörster G. Post-ischemic reactive hyperemia of the isolated perfused brain of the dog. Pflugers Arch 1971;328(4):332–43.

37. Krep H, Böttiger BW, Bock C, et al. Time course of circulatory and metabolic recovery of cat brain after cardiac arrest assessed by perfusion- and diffusion-weighted imaging and MR-spectroscopy. Resuscitation 2003;58(3):337–48.

38. Iordanova B, Li L, Clark RSB, Manole MD. Alterations in Cerebral Blood Flow after Resuscitation from Cardiac Arrest. Front Pediatr 2017;5:174.

39. Sekhon MS, Ainslie PN, Griesdale DE. Clinical pathophysiology of hypoxic ischemic brain injury after cardiac arrest: a “two-hit” model. Crit Care 2017;21(1):90.

40. Busl KM, Greer DM. Hypoxic-ischemic brain injury: pathophysiology, neuropathology and mechanisms. NeuroRehabilitation 2010;26(1):5–13.

41. Patil KD, Halperin HR, Becker LB. Cardiac arrest: resuscitation and reperfusion. Circ Res 2015;116(12):2041–9.

42. Niizuma K, Yoshioka H, Chen H, et al. Mitochondrial and apoptotic neuronal death signaling pathways in cerebral ischemia. Biochim Biophys Acta 2010;1802(1):92–9.

43. Idris AH, Roberts LJ, Caruso L, et al. Oxidant injury occurs rapidly after cardiac arrest, cardiopulmonary resuscitation, and reperfusion. Crit Care Med 2005;33(9):2043–8.

44. Becker LB. New concepts in reactive oxygen species and cardiovascular reperfusion physiology. Cardiovasc Res 2004;61(3):461–70.

45. Oyama Y, Blaskowsky J, Eckle T. Dose-dependent Effects of Esmolol-epinephrine Combination Therapy in Myocardial Ischemia and Reperfusion Injury. Curr Pharm Des 2019;25(19):2199–206.

46. Bessho R, Chambers DJ. Myocardial protection with oxygenated esmolol cardioplegia during prolonged normothermic ischemia in the rat. J Thorac Cardiovasc Surg 2002;124(2):340–51.

47. Danura T, Takeda Y, Shiraishi K, et al. Quantitative evaluation of the neuroprotective effects of a short-acting β-adrenoceptor antagonist at a clinical dose on forebrain ischemia in gerbils: effects of esmolol on ischemic depolarization and histologic outcome of hippocampal CA1. J Neurosurg Anesthesiol 2013;25(3):292–8.

48. Geissler HJ. Reduction of myocardial reperfusion injury by high-dose beta-blockade with esmolol. Thorac Cardiovasc Surg 2002;50(6):367–72.

49. Goyagi T, Horiguchi T, Nishikawa T, Tobe Y, Masaki Y. Neuroprotective effects of selective β-1 adrenoceptor antagonists, landiolol and esmolol, on transient forebrain ischemia in rats; a dose-response study. Brain Res 2012;1461:96–101.

50. Ruggeri L, Nespoli F, Ristagno G, et al. Esmolol during cardiopulmonary resuscitation reduces neurological injury in a porcine model of cardiac arrest. Sci Rep 2021;11(1):10635.

51. Li Z, Yuan W, Li J, et al. Selective beta-blocker esmolol improves cerebral cortex microcirculation in a swine ventricular fibrillation model. J Cell Biochem 2019;120(3):3679–88.

52. Hess ML, Manson NH. Molecular oxygen: friend and foe. The role of the oxygen free radical system in the calcium paradox, the oxygen paradox and ischemia/reperfusion injury. J Mol Cell Cardiol 1984;16(11):969–85.

53. Sanderson TH, Reynolds CA, Kumar R, Przyklenk K, Hüttemann M. Molecular mechanisms of ischemia-reperfusion injury in brain: pivotal role of the mitochondrial membrane potential in reactive oxygen species generation. Mol Neurobiol 2013;47(1):9–23.

54. Rodrigo R, Fernández-Gajardo R, Gutiérrez R, et al. Oxidative stress and pathophysiology of ischemic stroke: novel therapeutic opportunities. CNS Neurol Disord Drug Targets 2013;12(5):698–714.

55. Koh JY, Suh SW, Gwag BJ, He YY, Hsu CY, Choi DW. The role of zinc in selective neuronal death after transient global cerebral ischemia. Science 1996;272(5264):1013–6.

56. Frederickson CJ, Cuajungco MP, Frederickson CJ. Is zinc the link between compromises of brain perfusion (excitotoxicity) and Alzheimer's disease? J Alzheimers Dis 2005;8(2):155–60; discussion 209.

57. Gazaryan IG, Krasinskaya IP, Kristal BS, Brown AM. Zinc irreversibly damages major enzymes of energy production and antioxidant defense prior to mitochondrial permeability transition. J Biol Chem 2007;282(33):24373–80.

58. Medvedeva YV, Weiss JH. Intramitochondrial Zn2+ accumulation via the Ca2+ uniporter contributes to acute ischemic neurodegeneration. Neurobiol Dis 2014;68:137–44.

59. Ji SG, Medvedeva YV, Wang H-L, Yin HZ, Weiss JH. Mitochondrial zn2+ accumulation: A potential trigger of hippocampal ischemic injury. Neuroscientist 2019;25(2):126–38.

60. Yin HZ, Wang H-L, Ji SG, et al. Rapid intramitochondrial zn2+ accumulation in CA1 hippocampal pyramidal neurons after transient global ischemia: A possible contributor to mitochondrial disruption and cell death. J Neuropathol Exp Neurol 2019;78(7):655–64.

61. Albensi BC, Igoechi C, Janigro D, Ilkanich E. Why do many NMDA antagonists fail, while others are safe and effective at blocking excitotoxicity associated with dementia and acute injury? Am J Alzheimers Dis Other Demen 2004;19(5):269–74.

62. Starkov AA, Chinopoulos C, Fiskum G. Mitochondrial calcium and oxidative stress as mediators of ischemic brain injury. Cell Calcium 2004;36(3–4):257–64.

63. Hoyte L, Barber PA, Buchan AM, Hill MD. The rise and fall of NMDA antagonists for ischemic stroke. Curr Mol Med 2004;4(2):131–6.

64. Huang X, Hussain B, Chang J. Peripheral inflammation and blood-brain barrier disruption: effects and mechanisms. CNS Neurosci Ther 2021;27(1):36–47.

65. Ma A, Qi S, Chen H. Antioxidant therapy for prevention of inflammation, ischemic reperfusion injuries and allograft rejection. Cardiovasc Hematol Agents Med Chem 2008;6(1):20–43.

66. Escribano-Lopez I, Diaz-Morales N, Iannantuoni F, et al. The mitochondrial antioxidant SS-31 increases SIRT1 levels and ameliorates inflammation, oxidative stress and leukocyte-endothelium interactions in type 2 diabetes. Sci Rep 2018;8(1):15862.

67. Akbari Y, Mulder M, Razmara A, Geocadin R. Cool Down the Inflammation: Hypothermia as a Therapeutic Strategy for Acute Brain Injuries. In: Immunological Mechanisms and Therapies in Brain Injuries and Stroke. 2014.

68. Akbari Y, Mulder M, Razmara A, Geocadin R. Cool Down the Inflammation: Hypothermia as a Therapeutic Strategy for Acute Brain Injuries. In: Immunological Mechanisms and Therapies in Brain Injuries and Stroke. 2014.

69. Balan IS, Fiskum G, Hazelton J, Cotto-Cumba C, Rosenthal RE. Oximetry-guided reoxygenation improves neurological outcome after experimental cardiac arrest. Stroke 2006;37(12):3008–13.

70. Vereczki V, Martin E, Rosenthal RE, Hof PR, Hoffman GE, Fiskum G. Normoxic resuscitation after cardiac arrest protects against hippocampal oxidative stress, metabolic dysfunction, and neuronal death. J Cereb Blood Flow Metab 2006;26(6):821–35.

71. Liu Y, Rosenthal RE, Haywood Y, Miljkovic-Lolic M, Vanderhoek JY, Fiskum G. Normoxic ventilation after cardiac arrest reduces oxidation of brain lipids and improves neurological outcome. Stroke 1998;29(8):1679–86.

72. Berg KM, Cheng A, Panchal AR, et al. Part 7: systems of care: 2020 american heart association guidelines for cardiopulmonary resuscitation and emergency cardiovascular care. Circulation 2020;142(16_suppl_2):S580–604.

73. Skrifvars MB, Åneman A, Ameloot K. Individualized blood pressure targets during postcardiac arrest intensive care. Curr Opin Crit Care 2020;26(3):259–66.

74. Roberts BW, Kilgannon JH, Hunter BR, et al. Association Between Early Hyperoxia Exposure After Resuscitation From Cardiac Arrest and Neurological Disability: Prospective Multicenter Protocol-Directed Cohort Study. Circulation 2018;137(20):2114–24.

75. Wang C-H, Chang W-T, Huang C-H, et al. The effect of hyperoxia on survival following adult cardiac arrest: a systematic review and meta-analysis of observational studies. Resuscitation 2014;85(9):1142–8.

76. Pilcher J, Weatherall M, Shirtcliffe P, Bellomo R, Young P, Beasley R. The effect of hyperoxia following cardiac arrest - A systematic review and meta-analysis of animal trials. Resuscitation 2012;83(4):417–22.

77. Patel JK, Kataya A, Parikh PB. Association between intra- and post-arrest hyperoxia on mortality in adults with cardiac arrest: A systematic review and meta-analysis. Resuscitation 2018;127:83–8.

78. Llitjos J-F, Mira J-P, Duranteau J, Cariou A. Hyperoxia toxicity after cardiac arrest: What is the evidence? Ann Intensive Care 2016;6(1):23.

79. Crouzet C, Wilson RH, Bazrafkan A, et al. Cerebral blood flow is decoupled from blood pressure and linked to EEG bursting after resuscitation from cardiac arrest. Biomed Opt Express 2016;7(11):4660–73.

80. Kirkman MA, Smith M. Brain Oxygenation Monitoring. Anesthesiol Clin 2016;34(3):537–56.

81. Manole MD, Foley LM, Hitchens TK, et al. Magnetic resonance imaging assessment of regional cerebral blood flow after asphyxial cardiac arrest in immature rats. J Cereb Blood Flow Metab 2009;29(1):197–205.

82. Li Y-Q, Liao X-X, Lu J-H, et al. Assessing the early changes of cerebral glucose metabolism via dynamic (18)FDG-PET/CT during cardiac arrest. Metab Brain Dis 2015;30(4):969–77.

83. Wilson RH, Crouzet C, Torabzadeh M, et al. High-speed spatial frequency domain imaging of rat cortex detects dynamic optical and physiological properties following cardiac arrest and resuscitation. Neurophotonics 2017;4(4):045008.

84. Hartings JA, Strong AJ, Fabricius M, et al. Spreading depolarizations and late secondary insults after traumatic brain injury. J Neurotrauma 2009;26(11):1857–66.

85. Dreier JP, Woitzik J, Fabricius M, et al. Delayed ischaemic neurological deficits after subarachnoid haemorrhage are associated with clusters of spreading depolarizations. Brain 2006;129(Pt 12):3224–37.

86. Østergaard L, Dreier JP, Hadjikhani N, Jespersen SN, Dirnagl U, Dalkara T. Neurovascular coupling during cortical spreading depolarization and -depression. Stroke 2015;46(5):1392–401.

87. Leo AAP. Pial circulation and spreading depression of activity in the cerebral cortex. Journal of neurophysiology 1944;7(6):391–6.

88. Farkas E, Bari F, Obrenovitch TP. Multi-modal imaging of anoxic depolarization and hemodynamic changes induced by cardiac arrest in the rat cerebral cortex. Neuroimage 2010;51(2):734–42.

89. Takano T, Tian G-F, Peng W, et al. Cortical spreading depression causes and coincides with tissue hypoxia. Nat Neurosci 2007;10(6):754–62.

90. Sukhotinsky I, Dilekoz E, Moskowitz MA, Ayata C. Hypoxia and hypotension transform the blood flow response to cortical spreading depression from hyperemia into hypoperfusion in the rat. J Cereb Blood Flow Metab 2008;28(7):1369–76.

91. Richter F, Bauer R, Lehmenkühler A, Schaible H-G. The relationship between sudden severe hypoxia and ischemia-associated spreading depolarization in adult rat brainstem in vivo. Exp Neurol 2010;224(1):146–54.

92. Hartings JA, Andaluz N, Bullock MR, et al. Prognostic value of spreading depolarizations in patients with severe traumatic brain injury. JAMA Neurol 2020;77(4):489–99.

93. Lee DE, Lee LG, Siu D, et al. Neural Correlates of Consciousness at Near-Electrocerebral Silence in an Asphyxial Cardiac Arrest Model. Brain Connect 2017;7(3):172–81.

94. Dreier JP, Major S, Foreman B, et al. Terminal spreading depolarization and electrical silence in death of human cerebral cortex. Ann Neurol 2018;83(2):295–310.

95. Azadian M, Tian G, Bazrafkan A, et al. Overnight caloric restriction prior to cardiac arrest and resuscitation leads to improved survival and neurological outcome in a rodent model. Front Neurosci 2020;14:609670.

96. Wilson RH, Crouzet C, Torabzadeh M, et al. High-speed quantitative optical imaging of absolute metabolism in the rat cortex. Neurophotonics 2021;8(2):025001.

97. Yli-Hankala A, Edmonds HL, Jiang YD, Higham HE, Zhang PY. Outcome effects of different protective hypothermia levels during cardiac arrest in rats. Acta Anaesthesiol Scand 1997;41(4):511–5.

98. Kang Y-J, Tian G, Bazrafkan A, et al. Recovery from Coma Post-Cardiac Arrest Is Dependent on the Orexin Pathway. J Neurotrauma 2017;34(19):2823–32.

99. Koenig MA, Jia X, Kang X, Velasquez A, Thakor NV, Geocadin RG. Intraventricular orexin-A improves arousal and early EEG entropy in rats after cardiac arrest. Brain Res 2009;1255:153–61.

100. Li C, Narayan RK, Wu P-M, et al. Evaluation of microelectrode materials for direct-current electrocorticography. J Neural Eng 2016;13(1):016008.

101. Kim B, Park I, Lee JH, Kim S, Lee MJ, Jo YH. Effect of electrical vagus nerve stimulation on cerebral blood flow and neurological outcome in asphyxial cardiac arrest model of rats. Neurocrit Care 2019;30(3):572–80.

102. Crouzet C, Nguyen JQ, Ponticorvo A, Bernal NP, Durkin AJ, Choi B. Acute discrimination between superficial-partial and deep-partial thickness burns in a preclinical model with laser speckle imaging. Burns 2015;41(5):1058–63.

103. Dunn AK, Bolay H, Moskowitz MA, Boas DA. Dynamic imaging of cerebral blood flow using laser speckle. J Cereb Blood Flow Metab 2001;21(3):195–201.

104. Wang Q, Miao P, Modi HR, Garikapati S, Koehler RC, Thakor NV. Therapeutic hypothermia promotes cerebral blood flow recovery and brain homeostasis after resuscitation from cardiac arrest in a rat model. J Cereb Blood Flow Metab 2019;39(10):1961–73.

105. Cuccia DJ, Bevilacqua F, Durkin AJ, Ayers FR, Tromberg BJ. Quantitation and mapping of tissue optical properties using modulated imaging. J Biomed Opt 2009;14(2):024012.

106. Mazhar A, Cuccia DJ, Rice TB, et al. Laser speckle imaging in the spatial frequency domain. Biomed Opt Express 2011;2(6):1553–63.

107. Dreier JP, Lemale CL, Kola V, Friedman A, Schoknecht K. Spreading depolarization is not an epiphenomenon but the principal mechanism of the cytotoxic edema in various gray matter structures of the brain during stroke. Neuropharmacology 2018;134(Pt B):189–207.

108. Dunn AK, Devor A, Dale AM, Boas DA. Spatial extent of oxygen metabolism and hemodynamic changes during functional activation of the rat somatosensory cortex. Neuroimage 2005;27(2):279–90.

109. Wilson RH, Crouzet C, Torabzadeh M, et al. Cerebral perfusion and metabolism coupling during a critical time window provides rapid assessment of cardiac arrest severity and prognosis in a preclinical model. BioRxiv 2019;

110. Dunn AK, Devor A, Bolay H, et al. Simultaneous imaging of total cerebral hemoglobin concentration, oxygenation, and blood flow during functional activation. Opt Lett 2003;28(1):28–30.

111. Crouzet C, Wilson RH, Lee D, et al. Dissociation of cerebral blood flow and femoral artery blood pressure pulsatility after cardiac arrest and resuscitation in a rodent model: implications for neurological recovery. J Am Heart Assoc 2020;9(1):e012691.

112. Clark LR, Nation DA, Wierenga CE, et al. Elevated cerebrovascular resistance index is associated with cognitive dysfunction in the very-old. Alzheimers Res Ther 2015;7(1):3.

113. Yew B, Nation DA, Alzheimer's Disease Neuroimaging Initiative. Cerebrovascular resistance: effects on cognitive decline, cortical atrophy, and progression to dementia. Brain 2017;140(7):1987–2001.

114. Robertson AD, Tessmer CF, Hughson RL. Association between arterial stiffness and cerebrovascular resistance in the elderly. J Hum Hypertens 2010;24(3):190–6.

115. Khan S, Milot M, Lecompte-Collin J, Plamondon H. Time-dependent changes in CRH concentrations and release in discrete brain regions following global ischemia: effects of MK-801 pretreatment. Brain Res 2004;1016(1):48–57.

116. Global brain ischemia in Mongolian gerbils: assessing the level of anastomosis in the cerebral circle of Willis - PubMed [Internet]. [cited 2021 May 6];Available from: https://pubmed.ncbi.nlm.nih.gov/23377268/

117. Liu S, Dai Q, Hua R, et al. Determination of Brain-Regional Blood Perfusion and Endogenous cPKCγ Impact on Ischemic Vulnerability of Mice with Global Ischemia. Neurochem Res 2017;42(10):2814–25.

118. Human Cardiovascular Control - Loring B. Rowell, Professor of Physiology and Biophysics Loring B Rowell - Google Books [Internet]. [cited 2021 May 6];Available from: https://books.google.com/books?hl=en&lr=&id=EWSLdmqFx-8C&oi=fnd&pg=PA3&dq=Rowell+LB.+Human+Cardiovascular+Control.+New+York,+NY:+Oxford+University+Press%3B+1993:268.&ots=gcXRz42CrJ&sig=6NZycxBqRsWPCNGMNxx8pQ4FpMw#v=onepage&q&f=false

119. Brett SE, Ritter JM, Chowienczyk PJ. Diastolic blood pressure changes during exercise positively correlate with serum cholesterol and insulin resistance. Circulation 2000;101(6):611–5.

120. Zaza A, Rosen M. An Introduction to Cardiac Electrophysiology. CRC Press; 2000.

121. Windmüller O, Lindauer U, Foddis M, et al. Ion changes in spreading ischaemia induce rat middle cerebral artery constriction in the absence of NO. Brain 2005;128(Pt 9):2042–51.

122. Mozaffarian D, Benjamin EJ, Go AS, et al. Heart Disease and Stroke Statistics-2016 Update: A Report From the American Heart Association. Circulation 2016;133(4):e38-360.

123. Tóth ZE, Mezey E. Simultaneous visualization of multiple antigens with tyramide signal amplification using antibodies from the same species. J Histochem Cytochem 2007;55(6):545–54.

124. Kirschen MP, Morgan RW, Majmudar T, et al. The association between early impairment in cerebral autoregulation and outcome in a pediatric swine model of cardiac arrest. Resuscitation Plus 2020;4:100051.

125. van den Brule JMD, van der Hoeven JG, Hoedemaekers CWE. Cerebral Perfusion and Cerebral Autoregulation after Cardiac Arrest. Biomed Res Int 2018;2018:4143636.

126. Fuller ZL, Faro JW, Callaway CW, Coppler PJ, Elmer J, University of Pittsburgh Post-Cardiac Arrest Service. Recovery among post-arrest patients with mild-to-moderate cerebral edema. Resuscitation 2021;162:149–53.

127. Hayman EG, Patel AP, Kimberly WT, Sheth KN, Simard JM. Cerebral edema after cardiopulmonary resuscitation: A therapeutic target following cardiac arrest? Neurocrit Care 2018;28(3):276–87.

128. Rud J, May TL, Riker RR, Seder DB. Early cerebral edema after cardiac arrest and its ramifications. Resuscitation 2020;154:112–4.

129. Li G, LeiQian, Gu P, Fan D. Dexmedetomidine post-conditioning attenuates cerebral ischemia following asphyxia cardiac arrest through down-regulation of apoptosis and neuroinflammation in rats. BMC Anesthesiol 2021;21(1):180.

130. Wu CY-C, Couto E Silva A, Citadin CT, et al. Palmitic acid methyl ester inhibits cardiac arrest-induced neuroinflammation and mitochondrial dysfunction. Prostaglandins Leukot Essent Fatty Acids 2021;165:102227.

131. Nishizawa H, Kudoh I. Cerebral autoregulation is impaired in patients resuscitated after cardiac arrest. Acta Anaesthesiol Scand 1996;40(9):1149–53.

132. Lee JK, Brady KM, Mytar JO, et al. Cerebral blood flow and cerebrovascular autoregulation in a swine model of pediatric cardiac arrest and hypothermia. Crit Care Med 2011;39(10):2337–45.

133. Lidington D, Wan H, Bolz S-S. Cerebral autoregulation in subarachnoid hemorrhage. Front Neurol 2021;12:688362.

134. Ristagno G, Tang W, Huang L, et al. Epinephrine reduces cerebral perfusion during cardiopulmonary resuscitation. Crit Care Med 2009;37(4):1408–15.

135. Oghifobibi OA, Toader AE, Nicholas MA, et al. Resuscitation with epinephrine worsens cerebral capillary no-reflow after experimental pediatric cardiac arrest: An in vivo multiphoton microscopy evaluation. J Cereb Blood Flow Metab 2022;42(12):2255–69.

136. Ristagno G, Sun S, Tang W, Castillo C, Weil MH. Effects of epinephrine and vasopressin on cerebral microcirculatory flows during and after cardiopulmonary resuscitation. Crit Care Med 2007;35(9):2145–9.

137. Asano N, Hishiyama S, Ishiyama T, Kotoda M, Matsukawa T. Effects of β1-adrenergic receptor blockade on the cerebral microcirculation in the normal state and during global brain ischemia/reperfusion injury in rabbits. BMC Pharmacol Toxicol 2020;21(1):13.

138. O'Neil MP, Fleming JC, Badhwar A, Guo LR. Pulsatile versus nonpulsatile flow during cardiopulmonary bypass: microcirculatory and systemic effects. Ann Thorac Surg 2012;94(6):2046–53.

139. Barić D. Why pulsatility still matters: a review of current knowledge. Croat Med J 2014;55(6):609–20.

140. Avolio A, Kim MO, Adji A, et al. Cerebral haemodynamics: effects of systemic arterial pulsatile function and hypertension. Curr Hypertens Rep 2018;20(3):20.

141. Patabendige A, Singh A, Jenkins S, Sen J, Chen R. Astrocyte activation in neurovascular damage and repair following ischaemic stroke. Int J Mol Sci 2021;22(8).

142. Williamson MR, Fuertes CJA, Dunn AK, Drew MR, Jones TA. Reactive astrocytes facilitate vascular repair and remodeling after stroke. Cell Rep 2021;35(4):109048.

143. Peberdy MA, Callaway CW, Neumar RW, et al. Part 9: post-cardiac arrest care: 2010 American Heart Association Guidelines for Cardiopulmonary Resuscitation and Emergency Cardiovascular Care. Circulation 2010;122(18 Suppl 3):S768-86.

144. Kilgannon JH, Jones AE, Shapiro NI, et al. Association between arterial hyperoxia following resuscitation from cardiac arrest and in-hospital mortality. JAMA 2010;303(21):2165–71.

145. Janz DR, Hollenbeck RD, Pollock JS, McPherson JA, Rice TW. Hyperoxia is associated with increased mortality in patients treated with mild therapeutic hypothermia after sudden cardiac arrest. Crit Care Med 2012;40(12):3135–9.

146. Elmer J, Scutella M, Pullalarevu R, et al. The association between hyperoxia and patient outcomes after cardiac arrest: analysis of a high-resolution database. Intensive Care Med 2015;41(1):49–57.

147. Nelskylä A, Parr MJ, Skrifvars MB. Prevalence and factors correlating with hyperoxia exposure following cardiac arrest – an observational single centre study. Scand J Trauma Resusc Emerg Med 2013;21(1):35.

148. Bellomo R, Bailey M, Eastwood GM, Nichol A, Pilcher D. Study of Oxygen in Critical Care G (2011) Arterial hyperoxia and in-hospital mortality after resuscitation from cardiac arrest.

149. Rachmale S, Li G, Wilson G, Malinchoc M, Gajic O. Practice of excessive F(IO(2)) and effect on pulmonary outcomes in mechanically ventilated patients with acute lung injury. Respir Care 2012;57(11):1887–93.

150. Han F, Da T, Riobo NA, Becker LB. Early mitochondrial dysfunction in electron transfer activity and reactive oxygen species generation after cardiac arrest. Crit Care Med 2008;36(11 Suppl):S447-53.

151. McCully JD, Cowan DB, Pacak CA, Toumpoulis IK, Dayalan H, Levitsky S. Injection of isolated mitochondria during early reperfusion for cardioprotection. Am J Physiol Heart Circ Physiol 2009;296(1):H94–105.

152. Lajoie I, Tancredi FB, Hoge RD. The impact of inspired oxygen levels on calibrated fMRI measurements of M, OEF and resting CMRO2 using combined hypercapnia and hyperoxia. PLoS ONE 2017;12(3):e0174932.

153. Xu F, Liu P, Pascual JM, Xiao G, Lu H. Effect of hypoxia and hyperoxia on cerebral blood flow, blood oxygenation, and oxidative metabolism. J Cereb Blood Flow Metab 2012;32(10):1909–18.

154. Bogaert YE, Rosenthal RE, Fiskum G. Postischemic inhibition of cerebral cortex pyruvate dehydrogenase. Free Radic Biol Med 1994;16(6):811–20.

155. Richards EM, Fiskum G, Rosenthal RE, Hopkins I, McKenna MC. Hyperoxic reperfusion after global ischemia decreases hippocampal energy metabolism. Stroke 2007;38(5):1578–84.

156. Hypothermia after Cardiac Arrest Study Group. Mild therapeutic hypothermia to improve the neurologic outcome after cardiac arrest. N Engl J Med 2002;346(8):549–56.

157. Bernard SA, Gray TW, Buist MD, et al. Treatment of comatose survivors of out-of-hospital cardiac arrest with induced hypothermia. N Engl J Med 2002;346(8):557–63.

158. Safar P. Resuscitation from clinical death: pathophysiologic limits and therapeutic potentials. Crit Care Med 1988;16(10):923–41.

159. Neumar RW, Nolan JP, Adrie C, et al. Post-cardiac arrest syndrome: epidemiology, pathophysiology, treatment, and prognostication. A consensus statement from the International Liaison Committee on Resuscitation (American Heart Association, Australian and New Zealand Council on Resuscitation, European Resuscitation Council, Heart and Stroke Foundation of Canada, InterAmerican Heart Foundation, Resuscitation Council of Asia, and the Resuscitation Council of Southern Africa); the American Heart Association Emergency Cardiovascular Care Committee; the Council on Cardiovascular Surgery and Anesthesia; the Council on Cardiopulmonary, Perioperative, and Critical Care; the Council on Clinical Cardiology; and the Stroke Council. Circulation 2008;118(23):2452–83.

160. Holgersson J, Meyer MAS, Dankiewicz J, et al. Hypothermic versus Normothermic Temperature Control after Cardiac Arrest. NEJM evid 2022;

161. Kim F, Nichol G, Maynard C, et al. Effect of prehospital induction of mild hypothermia on survival and neurological status among adults with cardiac arrest: a randomized clinical trial. JAMA 2014;311(1):45–52.

162. Badjatia N. Hyperthermia and fever control in brain injury. Crit Care Med 2009;37(7 Suppl):S250-7.

163. Bohman L-E, Levine JM. Fever and therapeutic normothermia in severe brain injury: an update. Curr Opin Crit Care 2014;20(2):182–8.

164. De Backer D, Biston P, Devriendt J, et al. Comparison of dopamine and norepinephrine in the treatment of shock. N Engl J Med 2010;362(9):779–89.

165. Laurent I, Monchi M, Chiche J-D, et al. Reversible myocardial dysfunction in survivors of out-of-hospital cardiac arrest. J Am Coll Cardiol 2002;40(12):2110–6.

166. Müllner M, Domanovits H, Sterz F, et al. Measurement of myocardial contractility following successful resuscitation: quantitated left ventricular systolic function utilising non-invasive wall stress analysis. Resuscitation 1998;39(1–2):51–9.

167. Weaver WD, Cobb LA, Copass MK, Hallstrom AP. Ventricular defibrillation -- a comparative trial using 175-J and 320-J shocks. N Engl J Med 1982;307(18):1101–6.

168. Gallego-Colon E, Bonaventura A, Vecchié A, Cannatà A, Fitzpatrick CM. Cardiology on the cutting edge: updates from the European Society of Cardiology (ESC) Congress 2020. BMC Cardiovasc Disord 2020;20(1):448.

169. Davidson SM, Adameová A, Barile L, et al. Mitochondrial and mitochondrial-independent pathways of myocardial cell death during ischaemia and reperfusion injury. J Cell Mol Med 2020;24(7):3795–806.

170. de Groot H, Rauen U. Ischemia-reperfusion injury: processes in pathogenetic networks: a review. Transplant Proc 2007;39(2):481–4.

171. Hausenloy DJ, Yellon DM. Preconditioning and postconditioning: new strategies for cardioprotection. Diabetes Obes Metab 2008;10(6):451–9.

172. Braunwald E, Kloner RA. Myocardial reperfusion: a double-edged sword? J Clin Invest 1985;76(5):1713–9.

173. Lee AC-L, Harris JL, Khanna KK, Hong J-H. A comprehensive review on current advances in peptide drug development and design. Int J Mol Sci 2019;20(10).

174. Wu D, Wang J, Wang H, Ji A, Li Y. Protective roles of bioactive peptides during ischemia-reperfusion injury: From bench to bedside. Life Sci 2017;180:83–92.

175. Fernandez Rico C, Konate K, Josse E, Nargeot J, Barrère-Lemaire S, Boisguérin P. Therapeutic Peptides to Treat Myocardial Ischemia-Reperfusion Injury. Front Cardiovasc Med 2022;9:792885.

176. Serafín A, Roselló-Catafau J, Prats N, Xaus C, Gelpí E, Peralta C. Ischemic preconditioning increases the tolerance of Fatty liver to hepatic ischemia-reperfusion injury in the rat. Am J Pathol 2002;161(2):587–601.

177. Murry CE, Jennings RB, Reimer KA. Preconditioning with ischemia: a delay of lethal cell injury in ischemic myocardium. Circulation 1986;74(5):1124–36.

178. Chu MJJ, Vather R, Hickey AJR, Phillips ARJ, Bartlett ASJR. Impact of ischemic preconditioning on outcome in clinical liver surgery: A systematic review. BioMed Research International 2015;2015:1–13.

179. Liu Z, Gong R. Remote ischemic preconditioning for kidney protection: GSK3β-centric insights into the mechanism of action. Am J Kidney Dis 2015;66(5):846–56.

180. Naito H, Nojima T, Fujisaki N, et al. Therapeutic strategies for ischemia reperfusion injury in emergency medicine. Acute Med Surg 2020;7(1):e501.

181. Blusztein DI, Brooks MJ, Andrews DT. A systematic review and meta-analysis evaluating ischemic conditioning during percutaneous coronary intervention. Future Cardiol 2017;13(6):579–92.

182. Jurcau A, Simion A. Neuroinflammation in cerebral ischemia and ischemia/reperfusion injuries: from pathophysiology to therapeutic strategies. Int J Mol Sci 2021;23(1).

183. Plane JM, Shen Y, Pleasure DE, Deng W. Prospects for minocycline neuroprotection. Arch Neurol 2010;67(12):1442–8.

184. Morimoto N, Shimazawa M, Yamashima T, Nagai H, Hara H. Minocycline inhibits oxidative stress and decreases in vitro and in vivo ischemic neuronal damage. Brain Res 2005;1044(1):8–15.

185. Matsukawa N, Yasuhara T, Hara K, et al. Therapeutic targets and limits of minocycline neuroprotection in experimental ischemic stroke. BMC Neurosci 2009;10:126.

186. Padma Srivastava MV, Bhasin A, Bhatia R, et al. Efficacy of minocycline in acute ischemic stroke: a single-blinded, placebo-controlled trial. Neurol India 2012;60(1):23–8.

187. Kohler E, Prentice DA, Bates TR, et al. Intravenous minocycline in acute stroke: a randomized, controlled pilot study and meta-analysis. Stroke 2013;44(9):2493–9.

188. Siriussawakul A. Role of nitric oxide in hepatic ischemia-reperfusion injury. WJG 2010;16(48):6079.

189. Terpolilli NA, Kim S-W, Thal SC, et al. Inhalation of nitric oxide prevents ischemic brain damage in experimental stroke by selective dilatation of collateral arterioles. Circ Res 2012;110(5):727–38.

190. Charriaut-Marlangue C, Bonnin P, Gharib A, et al. Inhaled nitric oxide reduces brain damage by collateral recruitment in a neonatal stroke model. Stroke 2012;43(11):3078–84.

191. Cipolat S, Martins de Brito O, Dal Zilio B, Scorrano L. OPA1 requires mitofusin 1 to promote mitochondrial fusion. Proc Natl Acad Sci USA 2004;101(45):15927–32.

192. Liu C-S, Chang J-C, Kuo S-J, et al. Delivering healthy mitochondria for the therapy of mitochondrial diseases and beyond. Int J Biochem Cell Biol 2014;53:141–6.

193. Willmes C. Mitochondria - A Powerful Therapeutic Target. Trends Mol Med 2020;26(1):1–2.

194. Murphy MP. How mitochondria produce reactive oxygen species. Biochem J 2009;417(1):1–13.

195. Hayashida K, Takegawa R, Shoaib M, et al. Mitochondrial transplantation therapy for ischemia reperfusion injury: a systematic review of animal and human studies. J Transl Med 2021;19(1):214.

196. Huang M-H, Poh K-K, Tan H-C, Welt FGP, Lui CY. Therapeutic synergy and complementarity for ischemia/reperfusion injury: β1-adrenergic blockade and phosphodiesterase-3 inhibition. Int J Cardiol 2016;214:374–80.

197. First International Study of Infarct Survival Collaborative Group. Randomised trial of intravenous atenolol among 16,027 cases of suspected acute myocardial infarction : ISIS-1. Lancet 1986;

198. THE MIAMI TRIAL RESEARCH GROUP. Metoprolol in acute myocardial infarction (MIAMI). A randomised placebo-controlled international trial. Eur Heart J 1985;6(3):199–226.

199. Geissler HJ, Davis KL, Buja LM, et al. Esmolol and cardiopulmonary bypass during reperfusion reduce myocardial infarct size in dogs. Ann Thorac Surg 2001;72(6):1964–9.

200. Ibanez B, Cimmino G, Prat-González S, et al. The cardioprotection granted by metoprolol is restricted to its administration prior to coronary reperfusion. Int J Cardiol 2011;147(3):428–32.

201. Ibanez B, Macaya C, Sánchez-Brunete V, et al. Effect of early metoprolol on infarct size in ST-segment-elevation myocardial infarction patients undergoing primary percutaneous coronary intervention: the Effect of Metoprolol in Cardioprotection During an Acute Myocardial Infarction (METOCARD-CNIC) trial. Circulation 2013;128(14):1495–503.

202. Pizarro G, Fernández-Friera L, Fuster V, et al. Long-term benefit of early pre-reperfusion metoprolol administration in patients with acute myocardial infarction: results from the METOCARD-CNIC trial (Effect of Metoprolol in Cardioprotection During an Acute Myocardial Infarction). J Am Coll Cardiol 2014;63(22):2356–62.

203. Huang MH, Nguyen V, Wu Y, Rastogi S, McConnell BK. Synergistic Infarct Size Reduction by Combination Therapy with Milrinone and Esmolol at Early Reperfusion during Acute Myocardial Infarction.

204. Song D, Xu J, Du T, et al. Inhibition of brain swelling after ischemia-reperfusion by β-adrenergic antagonists: correlation with increased K+ and decreased Ca2+ concentrations in extracellular fluid. Biomed Res Int 2014;2014:873590.